To the Graduate Council:

I am submitting herewith a dissertation written by Yue Wu entitled "Investigation of Magnetic Field Dependent Electroluminescence and Charge Injection in Organic Light Emitting Diodes." I have examined the final electronic copy of the dissertation for form and content and recommend that it be accepted in partial fulfillment of the requirements for the degree of Doctor of Philosophy, with a major in Polymer Engineering.

Bin Hu
Major Professor

We have read this dissertation
And recommend its acceptance:

Jimmy Mays

Roberto S. Benson

Kevin M. Kit

Accepted for the Council:

Carolyn R. Hodges

Vice Provost and Dean
of the Graduate School

(Original signatures are on file with official student records.)

Investigation of Magnetic Field Dependent Electroluminescence and Charge Injection in Organic Light Emitting Diodes

A Dissertation

Presented for the

Doctor of Philosophy

Degree

The University of Tennessee, Knoxville

Yue Wu

Aug 2007

Dedicated To My Parents

&

My Wife Weihua Zhu and My Oncoming Daughter Annie Zhu Wu

ACKNOWLEDGEMENTS

I am deeply thankful to my advisor, Dr. Bin Hu, for his irreplaceable guidance and valuable suggestions about my research work and dissertation. He provided a comfortable and flexible research environment throughout my years in graduate school. I acquired lots of practical and theoretical knowledge from him. Without his guidance and support, I could not have completed this thesis. I would also like to sincerely thank my committee members for their kind help, including Dr. Roberto Benson, Dr. Kevin M. Kit, and Dr. Jimmy Mays.

I owe a large debt of gratitude to Dr. Jane Howe in Oak Ridge National Laboratory, who provided the TEM facility and gave cheerfully of her time and expertise.

I especially thank my parents in China for their great support and encouragements to me all the years. Particular thanks are given to my wife, Weihua Zhu, for her great understanding and selfless assistance.

I would like thank Dr. Hongwei Zhang, Dr. Tianzi Huang and other friends in Dr. Mays's group for their assistance in polymer synthesis and characterization. I also want to thank Dr. Ke An, Dr. Kai Xiao, Dr. Chengjun Sun in Oak Ridge National Laboratory. Dr. Ke An helped me to build a Labview program to better control the magnetic field. Dr. Kai Xiao helped me a lot in the film thickness measurements. Without their helps, I would not finish my research smoothly. Another big thank-you goes to Carl Menako, Zhihua Xu, Liang Yan, Ming Shao, Jaime Sullivan for their kind help in both my study and my personal life.

ABSTRACT

After 20 years of development, conjugated polymers have been extensively applied in organic light emitting diodes (OLED), solar cells, transistors, and chemical or bio-sensors. Recently it is discovered that magnetic field can tune the electroluminescence intensity and conductivity in OLEDs, leading to the development of organic magneto-optoelectronics. However, the underlying mechanisms are still unclear.

In this dissertation, we investigated a wide range of conjugated polymers and low molecular weight molecules and proposed that the magnetic field effect on electroluminescence and magnetoresistance arise from the magnetic field enhanced polaron pair dissociation and reduced triplet-charge reaction. The final magnetic field effects are determined by the sum of the two contributions.

The magnetic field effect on polaron pair dissociation can be tuned by varying the spin-orbital coupling of the organic semiconductor. Stronger spin-orbital coupling leads to the reduction of magnetic field effect on both electroluminescence and magnetoresistance. Phosphorescent dye doping can also tune the magnetic field effects through energy transfer process and intermolecular interaction.

Triplet-charge reaction can be largely controllable by manipulating the bipolar injection. It has found that unbalanced bipolar injection enhance the triplet-charge injection, leading to more positive magnetoresistance and more negative magnetic field effect on electroluminescence. Balanced bipolar injection reduces triplet charge reaction, resulting in more negative magnetoresistance and more positive magnetic filed effect on

electroluminescence. The triplet-charge reaction can also be morphologically tuned. In poly(9,9-dioctylfluorenyl-2,7-diyl) (PFO) based OLEDs, low energy crystalline domains can be induced in PFO amorphous matrix by either high boiling point solvent or annealing treatments. The low energy domains can both spatially confine both excitons and charges to enhance the triplet-charge reaction. Consequently the enhanced triplet-charge reaction reduces the magnitude of magnetic field effects

Our study successfully built a bridge between the magnetic field effects and the spin dependent excitonic processes in OLEDs. Scientifically, the excitonic processes, e.g. intersystem crossing, triplet-charge reaction, can be investigated by simply measuring the magnetic responses. Technically, this tunable magnetic field effects have the potential to be used to in new generation smart screens, magnetic sensors.

TABLE OF CONTENTS

1. INTRODUCTION 1

1.1 Development history of organic semiconductors 2

1.2 Operation principle of organic light emitting diodes (OLED) 3

1.2.1 Charge injection 4

1.2.1.1 Charge injection barriers 5

1.2.1.2 Charge injection models 5

1.2.2 Charge transport 7

1.2.2.1 Low mobility in organic semiconductors 7

1.2.2.2 Basic space-charge-limited current theory 9

1.2.2.3 Comparison between charge injection and charge transport 10

1.2.3 Recombination 10

1.2.3.1 The nature of polaron 11

1.2.3.2 Formation of excitons 13

1.2.4 Exciton decay 17

1.2.5 Summary of electroluminescence processes 18

1.3 Determination of light emission efficiency of OLEDs 20

1.4 Magnetic field effect on excitonic processes 22

1.4.1 Magnetic filed effect on triplet-triplet annihilation (TTA) 23

1.4.2 Magnetic field effect on intersystem crossing 24

1.4.3 Magnetic field effect on exciton dissociation 25

1.4.4 Magnetic field effect on triplet-charge reaction 27
1.4.5 Magnetic field effect on light emitting efficiency. 27
1.5 Research objective 28
1.6 Outline of thesis 29
2 MAGNETIC FIELD EFFECT ON ELECTROLUMINESCENCE AND MAGNETORESISTANCE IN ORGANIC LIGHT EMITTING DIODES 31
2.1 Introduction 31
2.2 Experimental 32
2.2.1 Organic semiconductor materials 32
2.2.2 Device fabrication 33
2.2.2.1 Substrate cleaning 33
2.2.2.2 Deposition of organic layer 35
2.2.2.3 Deposition of electrodes 37
2.2.3 Devices characterization 38
2.3 Universality of MR and MFE 39
2.4 Similar magnetic field effects between electroluminescence and resistance 41
2.5 Opposite magnetic field effect on electroluminescence and resistance 43
2.6 The relationship between magnetic field effect on electroluminescence and resistance 44
2.7 Mechanisms for MR and MFE 45
2.7.1 Failure of triplet-triplet annihilation (TTA) mechanism 45
2.7.2 Magnetic field enhanced singlet polaron pairs 45
2.7.3 Magnetic field enhanced reaction yield 46

2.8 Possible mechanisms 48
2.8.1 Determination of magnetic field effects on polaron pair or exciton states .. 48
2.8.2 Excited states related magnetic field effect on electroluminescence and magnetoresistance 49
2.8.3 Mechanism for magnetic field effect on electroluminescence 51
2.8.4 Mechanism for magnetoresistance 52
2.9 Summary 53
3 SPIN-ORBITAL COUPLING EEFECT ON MAGNETORESISTANCE AND MAGNETIC FIELD DEPENDENT ELECTROLUMINESCENCE 55
3.1 Introduction 55
3.2 Experimental 56
3.3 Realization of working OLED at both forward and reverse biases 57
3.4 Identification of the recombination zones 57
3.5 Bias dependent magnetoresistance 59
3.5.1 Balancing degree of charge injection 59
3.5.2 Spin –orbital coupling effect 60
3.6 Enhancement of spin-orbital coupling by using a heavier metal electrode 62
3.7 Reduction of spin-orbital coupling by separating MEH-PPV from the metal electrode 66
3.8 Internal spin-orbital coupling effect 66
3.9 Summary 69

4 TUNABLE MAGNETIC FIELD DEPENDENT ELECTROLUMINESCENCE AND MAGNETORESISTANCE IN FLUORESCENT POLYMER/PHOSPHORESCENT DYE COMPOSITES 70
4.1 Introduction 70
4.2 Experimental 71
4.3 Tunable magnetoresistance in $Ir(ppy)_3$ doped polymer composite 72
4.4 Charge transport channel effects on magnetoresistance 74
4.5 Energy transfer effects on magnetoresistance 76
4.5.1 Energy transfer-dependent magnetic field effect on electroluminescence 77
4.5.2 Energy transfer-dependent magnetoresistance 79
4.6 Intermolecular spin-orbital interaction 80
4.6.1 Energy transfer system 80
4.6.2 Non-energy transfer system 81
4.7 Magnetic field effect on photocurrent 84
4.8 Possible mechanism for the dye-doping-tunable magnetic field effect on EL and magnetorsistance 85
4.9 Summary 87
5 BIPOLAR INJECTION EFFECTS ON MFE AND MR 88
5.1 Introduction 88
5.2 Experimental 89
5.3 Modification of bipolar injection by changing bias polarity 90
5.3.1 Enhanced interfacial resistance 91
5.3.2 Modified bipolar injection 92

5.4 Modification of bipolar injection by reducing electron injection 94
5.5 Modification of bipolar injection effect by reducing hole injection 96
5.6 Investigation of possible change of the triplet-charge reaction constant 97
5.7 bipolar injection effects on MFE 99
5.7.1 Bipolar injection effects on MFE in a hole transport material..... 100
5.7.2 Bipolar injection effects on MFE in an electron transport material..... 100
5.8 Summary 103
6 MORPHOLOGY EFFECTS ON MAGNETIC FIELD DEPENDENT ELECTROLUMINESCENCE AND MAGNTORESISTANCE 105
6.1 Introduction..... 105
6.2 Experimental 106
6.3 Spectroscopic evidences for the formation of crystalline structure in solvent treated PFO films 107
6.4 Microscopic evidences for the formation of crystalline structure in solvent treated PFO films 110
6.5 Evidences for crystalline structures in annealed PFO films 111
6.6 Application of a phosphorescent dye as a probe to clarify exciton-confinement characteristic of the crystalline domains..... 113
6.6.1 Energy transfer in PFO/$Ir(ppy)_3$ composites..... 114
6.6.2 Quenching rate in PFO/$Ir(ppy)_3$ composite films 116
6.7 Morphology dependent magnetoresistance and magnetic field effect on electroluminescence..... 118
6.8 Morphology dependent magnetic field effect on photocurrent..... 121

6.9 Summary 123

7 Conclusions 125

LIST OF REFERENCES 129

VITA 12948

LIST OF FIGURES

Figure 1.1 P_z orbital sticking up out of the molecular plane and forming delocalized π-electron bonding in a typical poly (p-phenylene vinylene) (PPV) type backbone . 1

Figure 1.2 A typical structure of an OLED..... 3

Figure 1.3 The operation principle of an OLED. It can be divided into four steps: charge injection, charge transport, charge recombination, and light generation..... 4

Figure 1.4 Complete picture of trapping sites for disordered molecular materials. The deep tail sites act as continuous, pseudo-exponential trap distributions. Chemical impurities or structural defects form relatively discrete, isoelectronic trapping levels in the carrier energy gap 8

Figure 1.5 Illustration of the energies involved in a molecular ionization process 12

Figure 1.6 Band structure of a positive polaron and three possible optical transitions below the V_b-C_b transition 13

Figure 1.7 Vector representation of the triplet state and singlet state..... 15

Figure 1.8 Visualization of spin-orbital coupling..... 16

Figure 1.9 Schematic representation of spin rephrasing (a) and spin flip (b)..... 16

Figure 1.10 Schematic representation of spin configurations for ground state, singlet excited state, and triplet excited state 18

Figure 1.11 The formation of electroluminescence and the evolution scheme of excited species. e, h are electron and hole; ^{1}PP and ^{3}PP are singlet and triplet polaron pairs; k_{isc} is intersystem crossing rate in polaron pair states; P_1 and P_3 are the

formation rate of generate singlet and triplet polaron pairs; S_1 and T_1 are singlet and triplet exciton; k'_{isc} is intersystem crossing rate in the exciton states; TTA represents triplet-triplet annihilation; S_0 is singlet ground state. 19

Figure 1.12 The scheme for generation of photoluminescence and photocurrent. S_1, T_1 are singlet and triplet excitons, respectively; S_0 is ground state; ISC and TTA represent intersystem crossing and triplet-triplet annihilation, respectively. 26

Figure 2.1 Procedures for device fabrication and characterization..... 32

Figure 2.2 Chemical structures of some organic semiconductors used in experiments ... 34

Figure 2.3 Basic single-layer OLED..... 35

Figure 2.4 Formation of polymer thin film by spin coating 36

Figure 2.5 Thermal evaporation of molecule based thin films 37

Figure 2.6 Setup for the magnetic field dependent electroluminescence, photocurrent and magnetoresistance measurements 38

Figure 2.7 Magnetoresistances in typical single-layer OLEDs 40

Figure 2.8 Magnetic field effect on electroluminescence in typical single-layer OLEDs 40

Figure 2.9 Magnetic field effect on electroluminescence and magnetoresistance in the ITO/PmPV/Al device..... 42

Figure 2.10 Magnetic field effect on electroluminescence and magnetoresistance in the ITO/MEH-PPV/Al device..... 43

Figure 2.11 Magnetic field effect on photoluminescence and photocurrent in the ITO/PmPV/Al device..... 49

Figure 2.12 Voltage dependent magnetoresistance 50

Figure 2.13 Proposed magnetic field effect on the intersystem crossing between singlet and triplet polaron pairs 52
Figure 2.14 The principle for the formation of negative and positive magnetoresistance 53
Figure 3.1 (a)EL-current-voltage characteristics of ITO/MEHPPV/Al OLED at forward and reverse biases. (b) Device structure and definition of forward and reverse bias. 58
Figure 3.2 (a) Schematic electron-hole recombination zones in ITO/MEHPPV/Al at forward and reverse biases. (b)Forward and reverse EL spectra from ITO/MEHPPV/Al OLED. 58
Figure 3.3 Magnetoresistances from MEH-PPV OLEDs with Al cathode at forward and reverse biases 60
Figure 3.4 Magnetoresistances from MEH-PPV OLEDs with Al cathode at forward and reverse biases 63
Figure 3.5 Electroluminescence-voltage-current characteristics for ITO/MEH-PPV/Au OLED at both forward and reverse bias. REL, FEL represents the electroluminescence at reverse bias and forward bias, respectively. 0G, 1500G is the magnetic field strength 64
Figure 3.6 Forward and reverse electroluminescence and photoluminescene spectra from ITO/MEHPPV/Al OLED 64
Figure 3.7 Magnetic field effect on EL and magnetoresistance from the MEHPPV OLED with gold electrode at forward and reverse biases 65

Figure 3.8 Magnetoresistances from double-layer MEHPPV/PMMA (dots) and single-layer MEHPPV (circles) OLEDs with ITO and Au electrodes. Inset shows the MFEs with/out the PMMA layer 67

Figure 3.9 Magnetic field effect on electroluminescence and magnetoresistance for Alq_3 and $Ir(ppy)_3$ based OLEDs..... 68

Figure 4.1 Magentoresistance as a function of magnetic field. x is the weight concentration of $Ir(ppy)_3$ dopant in the composite OLED of ITO/$Ir(ppy)_3$(xwt%)+PVK/Al..... 73

Figure 4.2 MFE from composite at constant voltage (dots) and current (circles). x is the weight concentration of $Ir(ppy)_3$ dopant in the composite OLED of ITO/$Ir(ppy)_3$(xwt%)+PVK/Al..... 73

Figure 4.3 Schematic transport channels for the PVK $Ir(ppy)_3$ composite (a)parallel connection and (b) series connection..... 75

Figure 4.4 (a) Magnetoresistance and (b) magnetic field effect on EL at constant voltage (dots) and current (circles), respectively, in double-layer OLEDs of ITO/PVK(xnm)/$Ir(ppy)_3$(80nm)/Al. x is the thickness of PVK layer..... 75

Figure 4.5 Normalized emission spectra and absorption spectra for PVK and $Ir(ppy)_3$... 77

Figure 4.6 Intersystem crossing and (Förster T_F and Dexter T_D) energy transfer in the PVK + $Ir(ppy)_3$ composite. K_{ISC}-1 and K_{ISC}-2 are magnetic field independent and independent intersystem crossing in PVK matrix and $Ir(ppy)_3$ dopant, respectively 78

Figure 4.7 Voltage-dependent magnetocurrent and EL intensity in PVK/ (1wt%)$Ir(ppy)_3$ composite LED. The magnetoresistance was measured at the field of 150 mT... 79

Figure 4.8 Electroluminescence spectra of pristine PVK, pristine $Ir(ppy)_3$, and PVK + (x%)$Ir(ppy)_3$ composite LEDs. (b) Fluorescence- and phosphorescence-based MFEs from PVK matrix and $Ir(ppy)_3$ dopant in the dilute PVK + (0.3wt%)$Ir(ppy)_3$ composite. The MFEs from pristine PVK and $Ir(ppy)_3$ are also shown as reference. 81

Figure 4.9 Normalized emission spectra and absorption spectra for PmPV and $Ir(ppy)_3$ 82

Figure 4.10 Magnetic field effect on electroluminescence in ITO/PmPV/Al based on the PmPV/$Ir(ppy)_3$ composites. x% represents the concentration of $Ir(ppy)_3$ in PmPV 83

Figure 4.11 Magnetoresistances from PMPV + (x%)$Ir(ppy)_3$ composite OLEDs 84

Figure 4.12 Photocurrent as a function of magnetic field in the composite OLEDs of ITO/$Ir(ppy)_3$(xwt%)+PVK/Al under the light illumination of 0.1 mW/cm^2 at 330 nm 85

Figure 4.13 Formation of built-in electric field due to the dissociation of electron-hole pairs in $Ir(ppy)_3$+PVK composite OLED..... 86

Figure 5.1 Structure of ITO/MEH-PPV/PMMA/Au OLED. Varying the thickness of PMMA layer changes the bipolar injection, hence, the ratio of electrons and holes 90

Figure 5.2 Forward magnetoresistance as a function of magnetic field for the double-layer ITO/MEHPPV/PMMA(xnm)/Au OLEDs 91

Figure 5.3 Reverse magnetoresistance as a function of magnetic field for the double-layer ITO/MEHPPV/PMMA(xnm)/Au OLEDs 92

Figure 5.4 Band diagrams for reverse (a) and forward (b) charge injection in the double-layer ITO/MEH-PPV/PMMA/Au OLED. Dots and circles are electrons and holes 93

Figure 5.5 Band diagram for the ITO/PVK/PMMA/Al OLED 95

Figure 5.6 Magnetoresistance as a function of magnetic field for the ITO/PVK/PMMA(xnm)/Al double-layer OLEDs 95

Figure 5.7 Band diagram for the OLED of ITO/ PMMA / Alq_3/Al 96

Figure 5.8 Magnetoresistance as a function of magnetic field for the ITO/ PMMA(xnm)/Alq_3/Al double-layer OLEDs..... 97

Figure 5.9 Magnetoresistance as a function of magnetic field for the ITO/ PMMA(xnm)/$Ir(ppy)_3$/Al double-layer OLEDs 98

Figure 5.10 Magnetic field dependent electroluminescence for the ITO/PVK/PMMA(xnm)/Al OLEDs 101

Figure 5.11 Magnetic field effects on electroluminescence at voltage mode and current mode for ITO/PVK/PMMA(xnm)/Al OLEDs..... 101

Figure 5.12 Magnetic field effects on electroluminescence at voltage mode and current mode for ITO/PMMA(xnm)/Alq_3/Al OLEDs 102

Figure 6.1 Photoluminescence spectra of PFO films spin-cast from combined ODCB(x%)/chloroform solvent. The emission gradually changes from amorphous PFO to crystalline PFO 108

Figure 6.2 Absorption spectra of $Ir(ppy)_3$(0.1%)/PFO films spin-cast from combined ODCB(x%)/chloroform solvent..... 109

Figure 6.3 Fluorescent efficiency for the PFO films spin-cast from mixed ODCB/$CHCl_3$ solvents 110

Figure 6.4 TEM microscopic images and inverted electron diffraction patterns. a $CHCl_3$-based PFO film. b ODCB(2%)/$CHCl_3$-based PFO film 111

Figure 6.5 Absorption spectra of chloroform-based films before and after annealing at 80°C, 100°C for 100 minutes..... 112

Figure 6.6 PL spectra of chloroform-based films before and after annealing at 100°C for 100 minutes..... 113

Figure 6.7 Possible energy transfer in PFO/$Ir(ppy)_3$ composites 115

Figure 6.8 TEM image for PFO/0.1wt% $Ir(ppy)_3$ composite film..... 115

Figure 6.9 Relative fluorescence quenching as a function of $Ir(ppy)_3$ concentration for the $Ir(ppy)_3$(0.1%)/PFO films spin-cast from $CHCl_3$ (stars) and mixed ODCB(2%)/$CHCl_3$ (dots) 117

Figure 6.10 Schematic morphology-dependent exciton emission and energy transfer processes in (a) PFO and (b) dye/PFO composite films..... 117

Figure 6.11 Magnetoresistance as a function of magnetic field in three types of PFO based single-layer ITO/PFO/Al OLEDs..... 118

Figure 6.12 Visualization of the crystalline domains enhanced triplet-charge reaction 119

Figure 6.13 Magnetic field dependent electroluminescence in the three types of PFO based single-layer ITO/PFO/Al OLEDs..... 120

Figure 6.14 Magnetic field effect on photocurrent for ITO/PFO/Al photovoltaics..... 121

Figure 6.15 Formation of photocurrent in ITO/PFO/Al devices. Photocurrent has two contributions: polaron dissociation (1) and triplet-charge reaction (2) 123

1. INTRODUCTION

Conjugated high-molecular-weight polymers or low molecular-molecular-weight molecules have alternating single-double carbon-carbon bonds in their structures. The carbons on the backbones are sp2 hybridized, leaving one unhybridized p_z orbital sticking up out of the molecular plane and overlapping shoulder by shoulder to form delocalized π-electron bonding[1,2], as shown in Figure 1.1[3]. The delocalized π electrons form valence and conduction bands, respectively, through bonding and anti bonding configurations. The difference between the highest occupied molecular orbitals (HOMO, top of valance band) and the lowest unoccupied molecular orbital (LUMO, bottom of the conduction band) determines the width of energy gap and the color of light emission for a conjugated organic materials[4]. As a result, conjugated organic molecules can be treated as soluble semi-conductive materials to fabricate a wide range of semiconductor devices with attractive mechanical and optoelectronic properties[1,2,4].

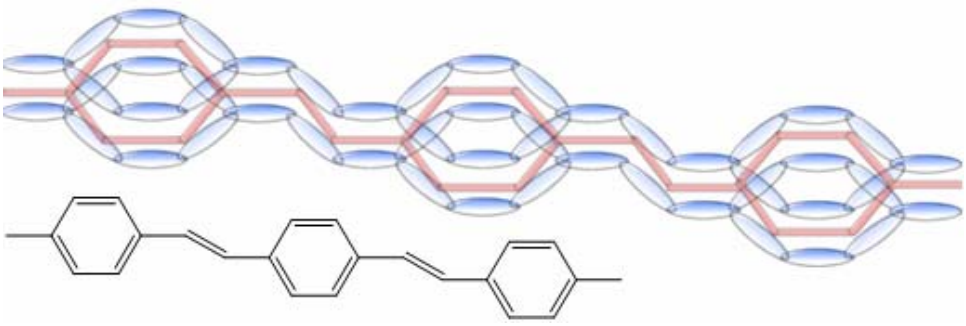


Figure 1.1 P_z orbital sticking up out of the molecular plane and form delocalized π-electron bonding in a typical poly (p-phenylene vinylene) (PPV) type backbone

1.1 Development history of organic semiconductors

Organic Electroluminescence (EL) was first reported in 1960s from an anthracence based device[5] . Because of limited understanding of intrinsic electronic processes, decent EL can only be observed at a very high voltage, usually several hundred volts, in those primary organic devices. After a long and slow development[6,7] till late 1980s, Tang and Slyke[8] in Kodak demonstrated a low-voltage (several volts) drivable organic light emitting diode (OLED) of small molecule tris-(8-hydroxylquinoline) aluminum (Alq_3) with transparent indium tin oxide (ITO) and Mg/Al alloy as anode and cathode, respectively. The sandwich design: the emitting layer located between a high-work-function ITO anode and a low-work-function metal cathode has built a solid foundation for later development of organic optoelectronic devices. In parallel with the development of small molecule-based OLEDs, polymer EL was discovered in 1990 by Cambridge University, based on the semi-conductive polymer: poly (p-phenylene vinylene) (PPV)[9]. However, the PPV film has to be thermally converted from its precursor due to its insolubility in common organic solvents. In 1991, Heeger group successfully synthesized the soluble PPV derivative, poly(2-methoxy-5-(2'-ethyl-hexoxy)-p-phenylene vinylene) (MEH-PPV) which can form excellent thin film simply by using spin coating technique without further thermo-conversion as required in case of PPV[10]. They also spin cast the MEH-PPV onto poly (ethylene terephthalate) (PET) plastic substrate and fabricated a flexible OLED. At that stage the organic semiconductors are limited to only fluorescent materials, which have lower light emitting efficiencies due to the limited formation of singlets under electrical excitation. Baldo et al. then developed an electro-phosphorescent

OLED by doping Alq_3 with PtOEP molecules and improved the external and internal quantum efficiency to 4% and 23%, respectively[11,12], taking advantage of the radiative emission from triplets. Their work initiated the research of using triplet for light emitting applications[13,14].

After a decade development of OLEDs, the efficiencies have been dramatically enhanced and the longevity was largely improved. In addition, a wide range of organic semiconductors have been synthesized with every emitting colors in the entire visible spectrum. Furthermore, organic semiconductors have also been successfully explored in the applications of organic thin film transistors[15,16], photovoltaic cells[17,18], memory devices[19,20], and organic sensors[21].

1.2 Operation principle of organic light emitting diodes (OLED)

A typical structure of an OLED comprises of a light-emitting layer and two electrodes (anode and cathode) as shown in Figure 1.2[8]. A transparent ITO is usually used as an anode for hole injection, while a thin layer of a low workfuction metal (or alloy) such as Ca, Al or Mg/Al is commonly used as a cathode for electron injection.

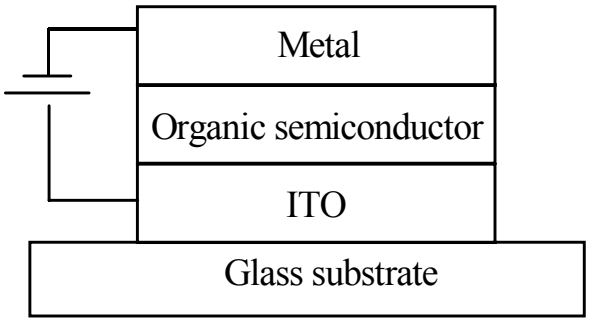


Figure 1.2 Typical structure of an OLED

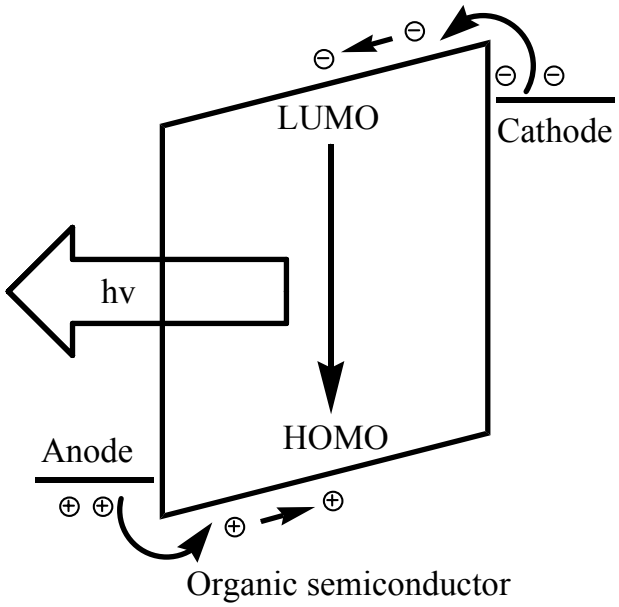


Figure 1.3 The operation principle of an OLED. It can be divided into four steps: charge injection, charge transport, charge recombination, and light generation

The operation principle of a typical OLED can be described in Figure 1.3. Basically, it can be divided into four steps: 1. injection of electrons from cathode and holes from anode; 2. charge transport; 3. charge recombination; 4. radiative decay to generate light emission.

1.2.1 Charge injection

Operation of an OLED requires both hole and electron injection since intrinsic organic semiconductors possess very limited charge carriers. Holes are injected into HOMO of an organic semiconductor from a high work function anode (positively biased electrode) while electrons are injected from low work-function metal cathode (negatively biased electrode) to its LUMO.

1.2.1.1 Charge injection barriers

Usually, the energy barrier for hole injection is estimated to be the difference in energy levels between the work-function anode and HOMO of organic semiconductor, $B_h = HOMO_{organic} - \Phi_{anode}$. Accordingly the electron injection barrier is estimated by the energy difference between cathode work-function and LUMO of the organic semiconductor, $B_e = \Phi_{cathode} - LUMO_{organic}$. However, the actual height of injection barrier, especially the barrier for electron injection, may be different to the above simplified estimation based on the electrode work-function and the energy levels of the organic semiconductors, due to the presence of interfacial layers and surface states in an organic semiconductor film[22]. The effective energy barrier for charge injection can be determined by internal photoemission spectroscopy[23].

1.2.1.2 Charge injection models

Due to the existence of injection barriers, sufficient electrical field is required for electrons and holes to either surmount over or tunnel through those barriers and inject into organic layer by either thermionic emission or tunneling processes, respectively. According to thermionic emission theory the injected current can be calculated by

$$J = J_0(e^{qV_F/nk_bT} - 1) \qquad \text{Equation 1.1}$$

where q is the electron charge, n the ideality factor, V_F applied voltage, and k_B the Boltzman constant[24].

According to Fowler-Nordheim tunneling theory, electrons tunnel through the energy the barrier and injection current can be calculated by

$$J = (C/\phi_B)(V/d)^2 \exp[-B\phi_B^{1.5}/(V/d)] \qquad \text{Equation 1.2}$$

where $C = q^3/8\pi h$, $B = 8\pi(2m^*)^{1/2}/3hq$, V is the applied bias, d is the thickness of the organic film, and m* is the relative effective mass[25,26].

Marks[27] successfully applied Fowler-Nordheim tunneling theory to fit the current-voltage characteristics of ITO/PPV/metal devices at high field range. The obtained barrier heights are consistent with the expected value based on the metal work-functions and the HOMO of PPV[27]. Parker thoroughly studied MEH-PPV based OLEDs with a wide range of metal electrodes and concluded that both electron and hole are injected through Fowler-Nordheim process[28,29]. The calculated injection barriers are basically consistent with the expected value. Gmeiner and coworkers successfully applied Schottky thermionic emission theory to fit the ITO/PPV/Al devices by considering the OLED as a serials circuit of resistive and capacitive components[30]. Friend used thermionic emission theory and tunneling theory to interpret current-voltage characteristics of ladder poly(p-phenylene)s based on OLED for low field and high field range, respectively[31].

Nevertheless, neither thermionic emission theory nor Fowler-Nordheim tunneling theory can fully describe the current-voltage behavior at full range for a typical OLED[10,29] without considering build-up of charge in the region near electrode, low charge transport mobility of organic semiconductors, or existence of traps in organic films. The later two effects are directly related to bulk effects in an OLED. Therefore, it is not sufficient to describe current-voltage characteristic in an OLED by only considering injection effects including both thermionic emission and tunneling processes.

Therefore, the bulk effects will be introduced in next section to better understand the current-voltage behavior in an OLED.

1.2.2 Charge transport

In inorganic semiconductor crystals, the strong interaction between constituting atoms and the long range order lead to the delocalization of electronic states. The mobility of charges can be 100 to 10^4 $cm^2V^{-1}s^{-1}$, much higher than their organic counterparts[32]. The transport of the free charge carriers can be described by classical band theories[33]. However, in organic solids, the mobility of charge is quite low due to their intra- or inter-intra-molecular interaction and the existence of traps. Thus the space charge limited current theory needs to be used to describe the charge transport behavior in low-mobility materials[34].

1.2.2.1 Low mobility in organic semiconductors

In organic semiconductors, intra-molecular interaction is mainly covalent, but the intermolecular interaction is typically due to weak van der Waals force[35]. Different from inorganic semiconductors, the charge transport in organic semiconductors usually occurs through hopping between molecular sites in small molecular semiconductor based devices or between different polymer segments in polymer based devices[36,37]. Besides, the chemical impurities and structural defects inevitably exist in organic semiconductor thin films and act as different types of charge traps inside organic films which further reduce the charge carrier mobility. A complete picture of trapping sites for disordered materials has been given as shown in figure 1.4[25]. Brutting and coworkers[22] have

determined the depth of the traps to be from 0.1ev to 0.8ev, using a thermally stimulated current (TSC) measurement. Those traps further reduce the charge transport mobility.

Usually charge transport behaviors in those low mobility organic semiconductor films show space-charge-limited characteristics, which has been confirmed by several groups[25,35,38] .

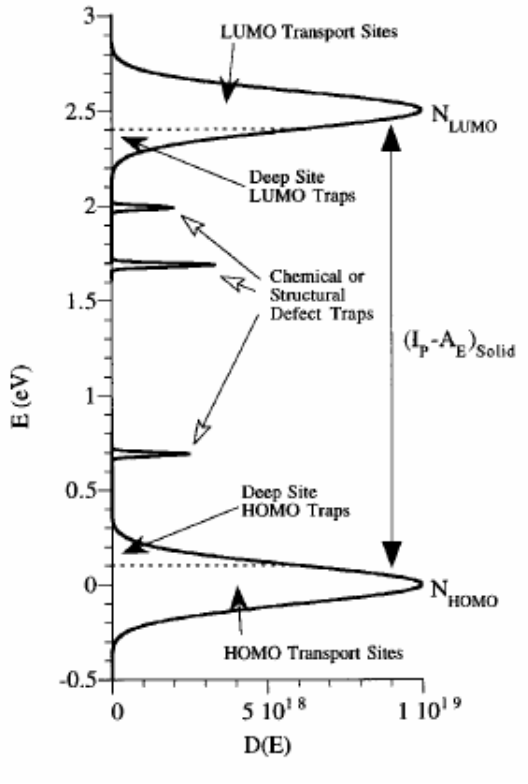


Figure 1.4 Complete picture of trapping sites for disordered molecular materials. The deep tail sites act as continuous, pseudo-exponential trap distributions. Chemical impurities or structural defects form relatively discrete, isoelectronic trapping levels in the carrier energy gap (reference 25).

1.2.2.2 Basic space-charge-limited current theory

According to the space-charge-limited current (SCLC) theory[34], the relationship between the electrical field and the local charge density can be expressed by the Poisson equation,

$$\frac{dF}{dx} = \frac{q}{\varepsilon_0 \varepsilon_r}(p_c(x) + p_t(x)) \qquad \text{Equation 1-3}$$

Where q is the electron charge, ε_0 is the permittivity of free space, ε_r is the dielectric constant of the organic film, x is the distance form film edge and p_c and p_t are free charge and trapped charge respectively.

The current density can be calculated by

$$J = q\mu(F)F(x)P_c(x) \qquad \text{Equation 1.4}$$

where μ(F) is the field dependent mobility, x is the depth.

Combined with equation 1.3 and 1.4, current-voltage characteristic can be described by the following differential equation.

$$\frac{dF(x)}{dx} = \frac{J}{\varepsilon_0 \varepsilon_r \mu(F)F(x)} + \frac{q}{\varepsilon_0 \varepsilon_r} p_t(x) \qquad \text{Equation 1.5}$$

The boundary condition is F(x=0)=0 and the applied voltage $V = \int_0^d F(x)dx$, where d is the film thickness. $p_t(x)$ is the distribution of trapped charges. By solving the above differential equation, current-voltage characteristics can be described in different systems with different space charge distributions, e.g. discrete trap distribution and continuous exponential[39,40]. Detailed calculation and more complicated behaviors are beyond this dissertation, which can be referred in the references[41,42].

1.2.2.3 Comparison between charge injection and charge transport

In an OLED, it is difficult to disentangle charge injection limited current-voltage characteristics from that of transported limited. Depending on charge injection height, charge carrier mobility and trap distribution, current-voltage characteristics can be either injection limited or bulk limited, or even both. Generally, when charge carriers supplied by electrode, under electrical field, outnumber those can be transported through the organic film in unit time, the current is bulk limited and the space-charge-limited current theory can be applied to express the current-voltage characteristics. Otherwise the injection process, either thermionic or tunneling process, would be the dominating process. Empirically the bulk limited behavior is expected when the charge injection barrier height is less than 0.2ev[35]. However, even in the case of charge injected limited, space charge effects still need to be considered to better describe current-voltage behavior. For example, build-up of space charge may alter the local electrical field near an organic film/electrode interface and vary the effective height of a charge injection barrier[43].

1.2.3 Recombination

After electron and hole are injected into conduction band (CB) and valence band (VB), respectively, negative and positive polarons will be formed in organic semiconductor molecules or chains. Under electrical field, they migrate to opposite electrodes till they meet each other. This process is referred to as electron-hole recombination.

1.2.3.1 The nature of polaron

Electron injection can be considered as reduction of organic semiconductor molecules or segments while hole injection can be considered as oxidation of the molecules (extract an electron from the semiconductor). During redox process, the molecules are ionized accompanied with a change in equilibrium geometry. In other words, the ionized state (after redox process) of an organic molecule usually has different equilibrium geometry from that in ground state (before redox process). For example, Baughman reported that biphenyl in $Rb^{+}(biphenyl)^{-}$ complex has a benzenoid-like structure in ground and a quinoid-like structure in ionized state[44].

During ionization, the energy change involved in the transition of chemical geometry from ground state (A) to ionized state (C) can be illustrated in Figure 1.5[45]. After gaining energy $E_{IP\text{-}V}$, the molecule vertically transits from stable ground state A to ionized state B without chemical geometry change since electronic motions are much faster than nuclear motion (Frank-Cordon principle)[46]. Then the molecule in ionized state relaxes to lowest energy level of ionized state by releasing a relaxation energy E_{rel}, accompanied by a chemical geometry change. This process can also be considered as an alternative way. First the molecule distorts to the geometry same as the one in ionized state (A-D). This process requires a distortion energy E_{dis}. Then it vertically transits to the equilibrium ionized state C by obtaining an energy $E_{IP\text{-}d}$[45]. Therefore the relaxation in ionized state and distortion in ground state lead to an upward shift $\Delta\varepsilon$ of the highest occupied molecular orbital (HOMO, top edge of the valence band) and downward shift $\Delta\varepsilon$ of the lowest unoccupied molecular orbital (LUMO, bottom of conduction band) as shown in-

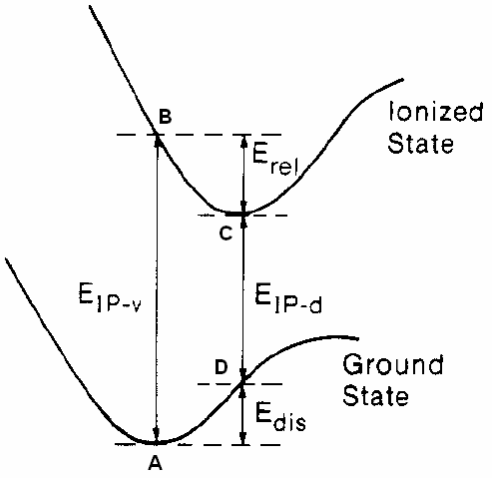


Figure 1.5 Illustration of the energies involved in a molecular ionization process

Figure 1.6. The formed charge associated with a lattice distortion is named a polaron. In chemical terminology, the polaron is a radical ion with a lattice distortion.

The presence of polarons can be proven by electron-spin-resonance (ESR) studies[47,48,49] since a polaron has spin quantum number of 1/2 and optical absorption measurements[50,51,52] because of the presence of two additional energy levels in the energy gap and three possible transitions (ω1, ω2, ω3) as shown in Figure 1-6[47]. Yakushi[50] indeed observed three additional transitions located at 0.7, 1.4, 2.1ev within V_b-C_b transition 3.2ev in a doped polypyrrole system in an optical absorption measurement.

Similarly, in OLED processes, a positively charged polaron forms after hole injection (losing an electron) while a negatively charged polaron forms after electron injection (obtaining an electron)[53,54,55]. In this dissertation, the positive and negative polaron are sometimes also conveniently called hole and electron, respectively.

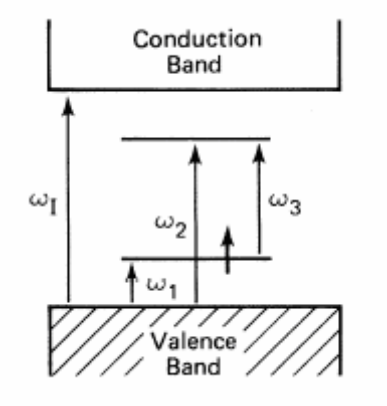


Figure 1.6 Band structure of a positive polaron and three possible optical transitions below the V_b-C_b transition

1.2.3.2 Formation of excitons

After charge injection, the formed positive polarons and negative polarons move towards opposite electrodes until they collide with each other to form coulombically bind polaron pairs (P^+P^-). Each polaron has a spin ½, either spin down or spin up. Therefore in a polaron pair, there are four possible spin configurations: one singlet (S) and three triplets (T_+, T_0, T_-) (Figure 1.7). Singlet/triplet polaron pairs further internally convert to singlet/triplet excitons. Statistically the ratio of formed singlet and triplet exciton would be 1:3[56]. However, in conjugated polymer based OLEDs, the exact value of singlet/ triplet ratio r_{ST} is still in controversy[57,58], due to their possible different formation cross sections and existence of intersystem crossing between singlet and triplet excitons.

Formation cross section of singlet and triplet excitons

Although the spin states during forming excitons do not change, the cross section of forming singlet excitons (σ_S) might be different from that of forming triplet excitons (σ_T). The singlet/triplet ratio can be calculated by equation 1-6

$$r_{ST} = \frac{\sigma_S}{3\sigma_T}$$ Equation 1-6

If the cross sections of forming singlet and triplet exciton are same, $\sigma_S = \sigma_T$, then the singlet ratio r_{ST} will be 1:3, obeying the simple spin statistics. However, it is known that the singlet exciton is ionic while the triplet exciton has a large covalent character[59]. Since both parent negative and positive polarons are ionic, the most likely outcomes of polaron recombination are ionic products, favoring formation of ionic singlet excitons[60]. Hence, it is very possible that $\sigma_S > \sigma_T$, leading to r_{ST} >1/3. Indeed, Wohlgenannt experimentally determined that the singlet/triplet ratio can vary from about 0.6 to 1.6 depending on optical gaps of different materials[60]. Y. Cao [61] observed very efficient electroluminescence in an OC1C10-PPV/PBD composite based devices and the singlet triplet/ratio r_{ST} was determined to be 1[62]. Burin[63] and Shuai[62] theoretically calculated the singlet/triplet ratio and found the ratio is possible to be larger than 1/3.

Intersystem crossing between singlet and triplet excitons

Besides, the singlets and triplets can mutually convert to each other through an intersystem crossing. For organic semiconductors, singlet-triplet intersystem conversion rate can be determined by hyperfine interaction and spin-orbital coupling. Hyperfine interaction is the interaction between nuclear spin and electron spin. Because the proton dipole moment in the hyperfine interaction is much weaker than the electron orbital dipole involved in the spin-orbital coupling, spin-orbital coupling is essentially the determining factor for intersystem crossing. To better understand the spin-orbital coupling effect, a Bohr model was used to describe the motions of the electrons in-

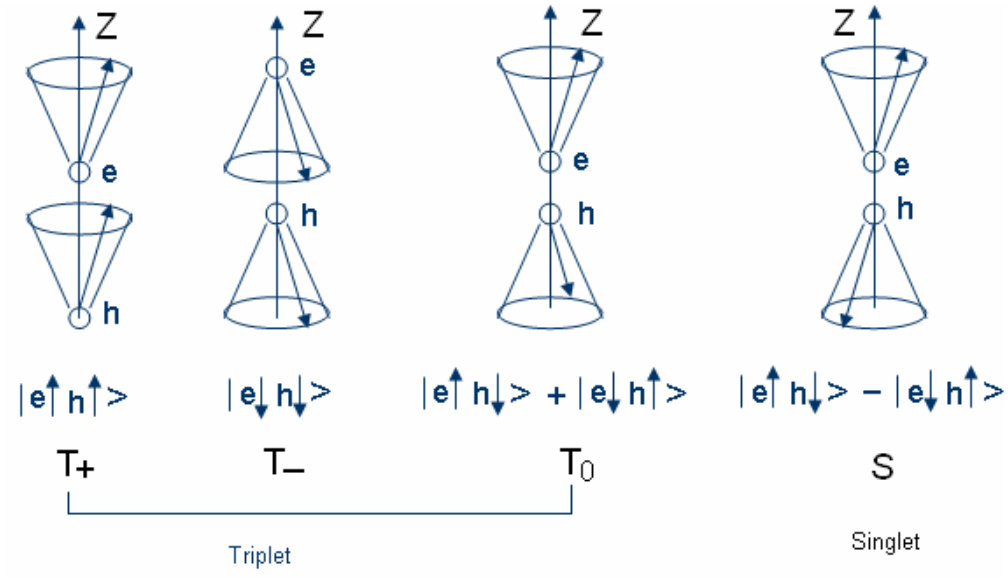


Figure 1.7 Vector representation of the triplet state and singlet state

molecules. The electron has both an orbital motion surround a nuclear and a spin motion, as shown in Figure 1.8. The spin motion of an electron generate a magnetic moment μ which interacts with magnetic field B generated by the orbital motion. The spin orbital coupling is proportional to the atomic number of the nuclear. Heavier atoms have stronger spin-orbital coupling.

Now let us discuss how the spin-orbital coupling leads to the transition between singlets and triplets. A singlet exciton has anti-parallel spin configuration with 180^o out of phase while the triplet has parallel configuration. As shown in Figure 1.9, once the electron and hole experience a slight different magnetic field B_z with direction parallel to the axis z, the velocities of the electron and hole become different because they experience different torques due to magnetic field B_z. Consequently, their phase difference changes and it is no longer 180^o out of phase. The singlet exciton gains a triplet characteristic. If the phase gets same, then the singlet exciton completely-

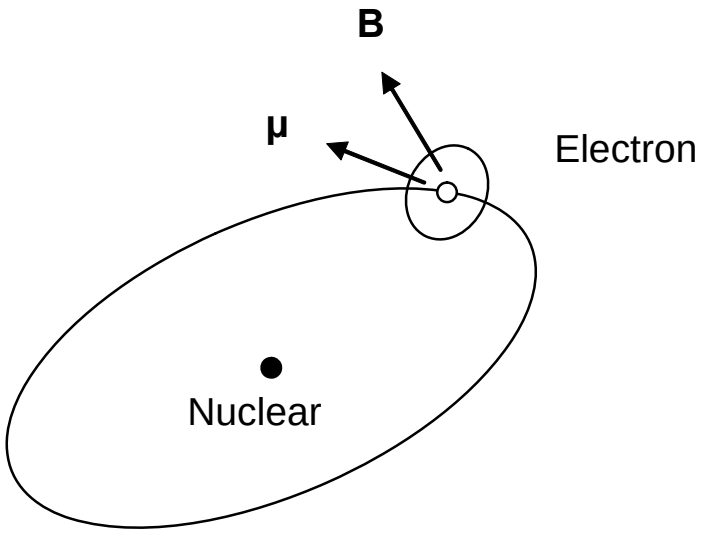


Figure 1.8 Visualization of spin-orbital coupling

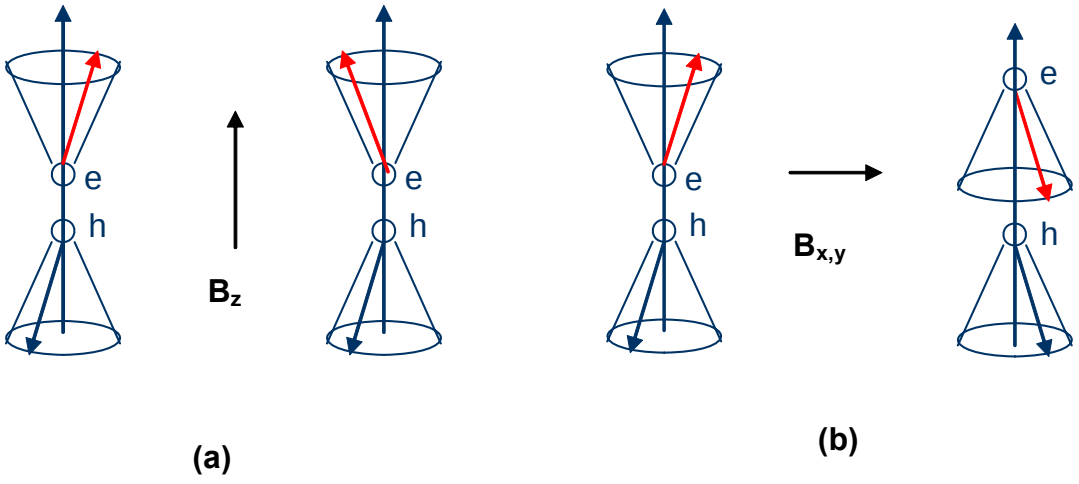


Figure 1.9 Schematic representation of spin rephrasing (a) and spin flip (b)

converts to a triplet exciton. It is called rephrases process. If the direction of the magnetic field $B_{x,y}$ perpendicular to the axis z, a spin flip would occur, leading to a transition from singlet exciton to triplet exciton. This is called spin flip process. Similarly, it is also possible for a triplet to convert to a singlet exciton.

Besides, it is known that two triplet excitons can also generate one singlet through triplet-triplet annihilation (TTA) process[64], which further changes the singlet/triplet ratio

1.2.4 Exciton decay

The Pauli principle requires that any ground state configuration must be a ground singlet, thus the two electrons in any orbital are spin anti-parallel paired as can be visualized as in Figure 1.10. In excited states, the two electrons are in different orbital (HOMO and LUMO) and they may have either parallel or anti-parallel spin configurations (Figure 1.10). For a singlet exciton, they have an anti-parallel spin configuration while a triplet exciton has a parallel configuration. Since molecules in the ground state have a singlet spin configuration, the transition from singlet exciton to singlet ground is allowed, leading to a radiative decay and giving off light emission (fluorescence). However, the transition from triplet exciton to singlet ground state in fluorescent materials is forbidden due to their different spin configuration. Therefore the triplet excitons decay non-radiatively to generate heat without light emission. Since only singlet exciton can generate light emission, any process causing the loss of singlet exciton needs to be suppressed for light emitting application. Such processes basically include intersystem crossing from singlet to triplet exciton, exciton-exciton fusion, and exciton migration to quenching sites (charges or defects).

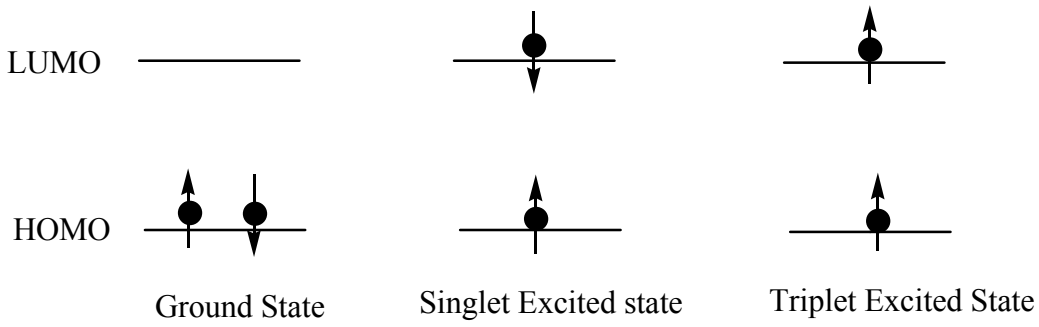


Figure 1.10 Schematic representation of spin configurations for ground state, singlet excited state, and triplet excited state

1.2.5 Summary of electroluminescence processes

In summary, the full view of electroluminescence can described as Figure 1.11. Firstly negative and positive polarons forms in the organic films close to the electrodes. Then under electrical field, they migrate through hopping process to meet each other and form polaron pairs which either dissociate back to free polarons or further relax into excitons including both singlet and triplet excitons. Only singlet exciton can decay radiatively to generate light in fluorescent materials. Singlet and triplet excitons can also convert to each other through intersystem crossing, and triplet can also react with another triplet exciton to generate one singlet exciton though TTA process. The fluorescence from TTA comes out later than the fluorescence directly from singlet excitons; therefore it is also called delayed electroluminescence.

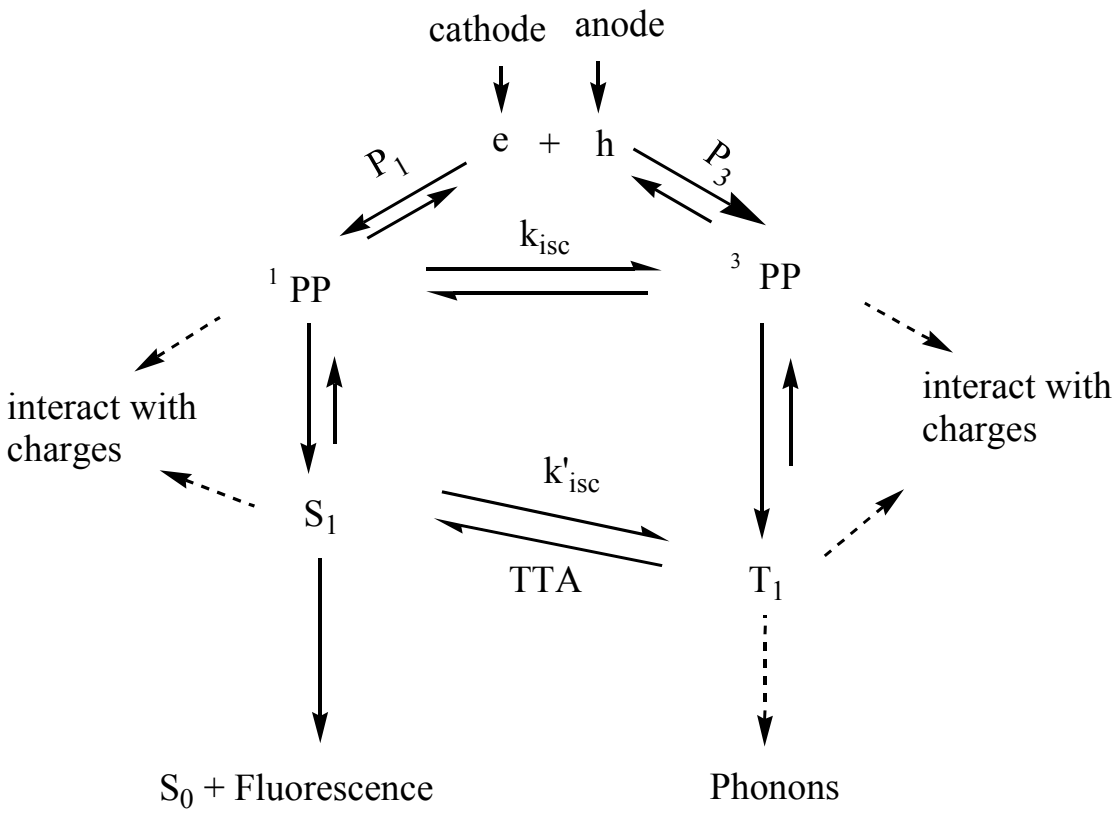


Figure 1.11 The formation of electroluminescence and the evolution scheme of excited species. e, h are electron and hole; ^{1}PP and ^{3}PP are singlet and triplet polaron pairs; kisc is intersystem crossing rate in polaron pair states; P_1 and P_3 are the formation rate of generate singlet and triplet polaron pairs; S_1 and T_1 are singlet and triplet exciton; k'_{isc} is intersystem crossing rate in the exciton states; TTA represents triplet-triplet annihilation; S_0 is singlet ground state.

1.3 Determination of light emission efficiency of OLEDs

For the application of light emitting, the quantum efficiency η of an OLED is one of the most important parameters. A lot of efforts have been put to understand and solve the limited factors for the device efficiency.

The quantum efficiency η has been defined as the number of generated photons per 100 electrons and it can be given by

$$\eta = \gamma \chi_{st} q \,, \qquad \text{Equation 1-7}$$

where γ is exciton formation fraction of electron-hole recombination, $\chi_{st} = \frac{r_{ST}}{r_{ST}+3}$ is the singlet exciton fraction, q is the efficiency of radiative decay[1]. The exciton formation fraction γ and radiative decay efficiency q can be optimized by balancing electron and hole injection and optimized OLED device design. To enhance the balance of electron and hole injection can be fulfilled by inserting a thin hole-transport-electron-blocking layer between anode and a thin electron-transport-hole-blocking layer between emitting layer and cathode. This two additional layers on one hand optimize the effective barriers for both electron and hole injection and balance the number of injected electrons and holes. On the other hand, they are also able to confine the injected electrons and holes inside the emitting layers, facilitating the recombination process and enhancing emission efficiency. Besides balancing charge injection and increasing semiconductor purity also reduce the non-radiative decay e.g. exciton-charge reaction and enhance the radiative decay q.

Essentially, singlet exciton fraction χ_{ST} is the most critical issue which determines the final efficiency limit of an OLED. How to control and take advantage of the χ_{ST} constantly attracts the interests from both industrial and academic fields. Mainly, there are three ways to manipulate the fraction χ_{ST}: utilize phosphorescent materials; control spin orientation of injected charge carriers including both electrons and holes; tune the intersystem crossing between singlets and triplets. Utilizing phosphorescent materials is the most straightforward. Due to the strong spin-orbital coupling, the transitions from triplet excited states to singlet ground state are allowed, consequently both singlet and triplet can be harvested to generate light emission and the quantum efficiency could reach 100%. However, the phosphorescent materials, especially blue phosphorescent polymers, are still challenging to synthesize. An alternative way to manipulate the singlet/triplet ratio is to control the spin orientations of electrons and holes and form singlets or triplets preferentially, which is also the foundation for spintronics[65,66]. In spintronic devices, ferromagnetic electrodes are utilized to inject spin polarized electrons and holes into the organic layer. Electrons and holes can be paired with either parallel or anti-parallel orientations to form triplets or singlets by adjusting an external magnetic field (direction and strength). Therefore, spin injection and transport are the critical factors in determination of singlet/triplet ratio in spintronic devices. Currently, the mismatch of conductivity of metal electrodes and organic semiconductors is the major problem in the realization of spin injections[67,68,69]. Later on, it was discovered that without ferromagnetic electrodes, external magnetic field still can vary

EL intensity and conductivity in non-magnetic OLEDs through tuning intersystem crossing, which will be further discussed in the following sections.

1.4 Magnetic field effect on excitonic processes

As discussed above, the spin-dependent processes such as singlet-triplet intersystem crossing, spin-dependent exciton dissociation and exction-charge reaction, are extremely important in determining maximum efficiency of an OLED. However, critical understanding of those spin-dependent electronic and optical processes is still lacking.

The magnetic field is believed to be an effective tool to elucidate those spin dependent excitonic processes. It has been found that an external magnetic field can affect electroluminescence (EL) and resistance and photoconductivity in organic semiconductor based optoelectronics, namely magnetic filed effect on EL (MFE), resistance (magnetoresistance, MR), and photoconductivity (MFP), respectively. MFE, MR, and MFP are defined as equations 1.8, 1.9, 1.10, respectively.

$$MFE = \frac{EL_H - EL_0}{EL_0} \qquad \text{Equation 1.8}$$

$$MR = \frac{R_H - R_0}{R_0} = \frac{\frac{U}{I_H} - \frac{U}{I_0}}{\frac{U}{I_0}} = \frac{I_0 - I_H}{I_H}, \qquad \text{Equation 1.9}$$

$$MFP = \frac{PC_H - PC_0}{PC_0} \qquad \text{Equation 1.10}$$

where EL, R, I, PC are electroluminescence intensity, resistance, current, photocurrent, respectively. H and 0 represent with or without an external magnetic field.

Magnetic field effect was first studied in the anthracene in 1960s by Merryfield and Johnson[70,71]. It was found that the delayed fluorescence is enhanced by a low magnetic field, but it decreases at a higher field to a value even lower than its original value. Frankevich observed an external magnetic field can enhance photocurrent to several percentages in polymer photovoltaics[72]. Recently, with the development of OLEDs, the study of magnetic field effects was rejuvenated[73-80], but mainly on electroluminescence and device resistance. It was observed that an external magnetic field can increase EL intensity and reduce resistance in a non-ferromagnetic OLED. Although the mechanism for this magnetic field dependence is still not clear, some excitonic processes such as triplet-triplet annihilation, intersystem crossing, exciton dissociation, triplet-charge reaction may be involved in those magnetic phenomena. Those processes will be fully discussed in this dissertation.

1.4.1 Magnetic filed effect on triplet-triplet annihilation (TTA)

Two triple excitons T can fuse into one singlet exciton S and a molecule in ground state S_0 through triplet-triplet annihilation.

$$T + T \underset{k_{-1}}{\overset{k_1}{\rightleftarrows}} (TT) \underset{k_{-2}}{\overset{k_2}{\rightleftarrows}} S + S_0 + h\gamma \qquad \text{Equation 1-11}^{81}$$

where k_1 is the formation rate of a pair state and k_2 is the TTA rate causing delayed fluorescence. Accordingly, k_{-1} and k_{-2} are their dissociation rates. In TTA two interacting triplets would have nine partially degenerated pair states since each triplet has three different components. The annihilation rate to generate singlets can be calculated by

$$\gamma_{TTA} = \frac{1}{9} k_1 \sum_i^9 \frac{k_2 S_i^2}{k_{-1} + k_2 S_i^2} \qquad \text{Equation 1-12}^{70,71}$$

where i means ith pair state. Since the delayed fluorescence comes from generated singlet exciton, its intensity is proportional to the TTA constant γ_{TTA}. γ_{TTA} is greater when the more uniformly the singlet characters spread over the triplet pairs[70]. At zero field only three out of nine triplet pairs have singlet characters. The presence of an external magnetic field can cause the mixing of the zero-field states, resulting in singlet characters spreading over more triplet pairs, leading to an enhanced TTA rates. Consequently, the delayed fluorescence intensity increases with increasing magnetic field strength. However, at a high magnetic field, where the external-field-caused Zeeman splitting is larger than zero-splitting, the number of triplet pairs having singlet components decreases to two out of nine triplet pairs. As a result, the fluorescence intensity decreases to value even lower than the zero-field value. Recently, Davis[73] and Belaid[74] also applied this theory to explain the observed magnetic field effect on electroluminescence in Alq_3- and Anthracene-based OLEDs, respectively.

1.4.2 Magnetic field effect on intersystem crossing

After electrons and holes are injected into the organic layer from cathode and anode in an organic semiconductor, they further relax into singlet and triplet polaron pairs: (^{1}PP) and (^{3}PP) which can be considered as precursors of singlet excitons and triplet excitons. The main difference among free charge carriers, polaron pairs and excitons is the distance between positive and negative polarons. If the distance is larger than the Coulomb capture radius, the positive and negative polarons will not interact with each other and they can be considered as free charges. Once the distance is smaller than the Coulomb radius, they form polaron pairs, in which both charge and spin become important. The

polaron pairs further decay into singlet or triplet excitons where the distance is so small that the wave-functions of negative and positive polarons can overlap.

The singlet and triplet polaron pairs can convert to each other though intersystem crossing. It was found that an external magnetic field can affect the conversion between singlet and triplet polaron pairs as follows. At zero-field, since singlets and triplet polaron pairs are degenerate, they are mutually convertible and the conversion rate is mainly determined by hyperfine effects. In the presence of external magnetic filed greater than hyperfine strength, triplet states are split into three non-degenerate states ($^3PP_+$, $^3PP_0$, $^3PP_-$) due to the external magnetic field caused Zeeman effect, in which only ^1PP and $^3PP_0$ are still mutually convertible while the conversion between ^1PP and $^3PP_+$, or $^3PP_-$ are blocked. As we know, EL comes from singlet excitons in fluorescent materials and its intensity is proportional to the population of singlet excitons. Hence magnetic field enhances singlet polaron pairs and final singlet excitons by partially blocking the conversion from singlet to triplet polaron pairs[75].

1.4.3 Magnetic field effect on exciton dissociation

Excitons can be also formed in organic semiconductors by photo-excitation as shown in Figure 1.12. After absorbing higher energy photons, electrons in the molecules jumped directly from ground state into the singlet excited states, forming singlet excitons. Some of them convert to triplet excitons through intersystem crossing. Others can either decay radiatively with light emission (photoluminescence) or further convert to polaron pairs[82]. The polaron pairs can further dissociate into free positive polarons or negative polarons similar to the reverse processes of exciton formation in electroluminescence.

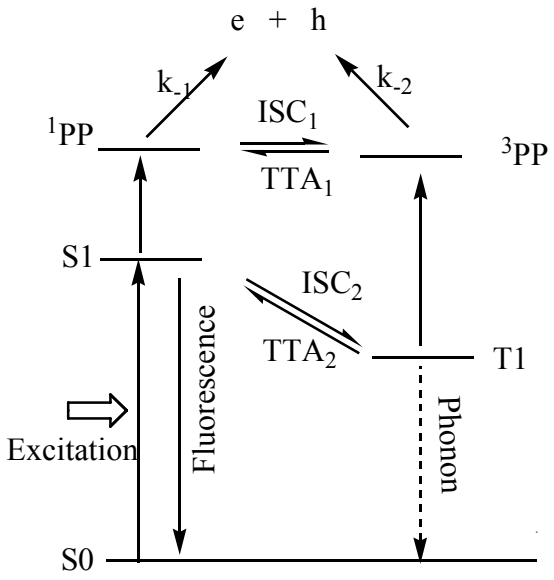


Figure 1.12 The scheme for generation of photoluminescence and photocurrent. S1, T1 are singlet and triplet excitons, respectively; S0 is ground state; ISC and TTA represent intersystem crossing and triplet-triplet annihilation, respectively.

If the organic film is put between two electrodes, the polarons can generate electricity (photocurrent) which is the basic principle of photovoltaic.

It was found that a low external magnetic field can enhance the photocurrent to a few percentages. As discussed in above section, magnetic field can enhance the formation of singlet polaron pairs. Since the singlet polaron pairs have larger dissociation rate compared with that of triplet polaron pairs[83], the enhanced singlet polaron pairs lead to enhancement in the total photocurrent. Thus investigation of magnetic field effect on photocurrent also gives information of the transition between singlet and triplet excited states.

1.4.4 Magnetic field effect on triplet-charge reaction

In the presence of magnetic field, especially high magnetic field, the degenerate triplet excitons or polaron pairs can be split into three different states: T_+, T_0, T_-, according to Zeeman Effect. These three triplet states are unevenly populated due to different decay rates. At same time, there always exist free charges trapped in the semiconductor layer which can further react with excitons. In principle, both triplets and singlets can react with those charges; however, triplets live much longer than singlets so that triplets are more likely to react with charge carriers[84]. Consequently, spin-polarized charge carriers including both electrons and holes can be generated through triplet-charge reaction. At high field, the spin-polarized charge carriers will be aligned with the same orientation, facilitating further formation of triplet excitons instead of singlet excitons, leading to a decrease in electroluminescence. Meanwhile, the triplet-charge reaction reduces the average lifetime of triplets by increasing non-radiative transition, resulting in a decrease of MR (enhanced conductance). This mechanism is plausible to explain magnetic field-reduced electroluminescence; however, it is difficult to explain the enhanced EL at low field as frequently observed by other groups[31-38].

1.4.5 Magnetic field effect on light emitting efficiency.

Lupton[85]studied magnetic field effect on both fluorescence and phosphorescence in a ladder-type poly(p-phenylene) (PhLPPP), and found positive magnetic effects on both fluorescence and phosphorescence at same time. Therefore, it was concluded that the magnetic field effects are basically due to the enhanced radiative decay efficiency of both singlet and triplet while their spin polarizations are conserved[86]. It was claimed that no

magnetic field dependent mutual-conversion between singlet and triplet occurs under electrical field for their devices. This completely new conclusion challenges the popular concepts about conversion of singlet and triplet concepts.

We also noticed that Cölle[81] proposed that the magnetic field can influence the charge balance factor by facilitating the minority charge injection through the study of instantaneous electroluminescence, delayed electroluminescence and phosphorescence in Alq_3- based devices. The EL efficiency enhancement is basically due to the optimized exciton formation fraction γ in equation 1.7. According to this mechanism, the numbers both singlet and triplet exciton would increase due to the enhanced γ, thus both fluorescence of singlet excitons and phosphorescent from triplet excitons should increase. However, in the same measurement, no change from phosphorescent was detected with variation of an external magnetic field. Therefore this mechanism still has problems to fully explain the magnetic field effect on electroluminescence without further modification.

Wohlgenannt groups[79,80, 87] extensively investigated magnetoresistance of a series organic light emitting diodes including both conjugated polymers and small molecules. Their results basically invalidated all the existing theories but unfortunately they have not reported a possible mechanism so far.

1.5 Research objective

Based on the observations in the literature, an external magnetic field does change electroluminescence intensity and conductivity and it is possible that a magnetic field can modify the singlet and triplet formation ratio through intersystem crossing, TTA, triplet-

charge reaction or even enhanced decay rate without any change of the singlet/triplet ratio. Apparently, as briefly discussed in above, these existing mechanisms are still speculative and even self-contradictory in explaining the newly-observed magnetic field effects although they might be valid in certain systems at certain conditions. Therefore, it is fairly reasonable to conclude that no existing mechanism so far is available to fully understand the magnetic field effect on the electroluminescence and magnetoresistance.

In this dissertation, we will further investigate the critical factors that control the magnetic field effect on electroluminescence and magnetoresistance and develop a reasonable model to explain how a magnetic field can affect the electroluminescence and conductivity in non-magnetic OLEDs. The understanding of the magnetic phenomena will also shed more light on the excitonic processes, charge injection and transport in an OLEDs. Consequently it will benefit the better design and optimization of organic semiconductor based optoelectronics not only OLEDs but also photovoltaic cells, organic memories, organic lasers, and organic transistors. Furthermore, based on the understanding of the magnetic field phenomena, we will be able to tune both the magnitude and sign of the magnetoresistance and magnetic field dependent electroluminescence, leading to the formation a new branch of organic optoelectronics: Organic Magneto-Optoelectronics.

1.6 Outline of thesis

The outline of these is as the following. The basically properties of organic semiconductors and operation of OLEDs were reviewed in chapter 1. Our own results about magnetic field phenomena, especially magnetoresistance and magnetic field effect

on electroluminescence, will be presented in chapter 2. Meanwhile, a possible model will be proposed to explain the observed magnetoresistance and magnetic field dependent electroluminescence. In that model, we consider that the magnetoresistance and magnetic field dependent electroluminescence arise from the consequence of magnetic field influenced excitonic processes in an OLED, e.g. intersystem crossing, spin-orbital coupling, and exciton-charge reaction. By proper manipulation of these factors, both magnitude and sign of magnetoresistance and magnetic field effect on electroluminescence are possible to be tuned. The spin-orbital coupling effects including both internal and external spin-orbital coupling effects will be further discussed in chapter 3. In chapter 4, a tunable magnetic field effects will be presented by fabrication of fluorescent polymer/phosphorescent dye composites based- OLEDs. The transport properties, interfacial spin-orbital coupling and energy transfer processes will be investigated to understand how those processes affect the magnetic field effects in an OLED. In chapter 5, a thin insulating layer will be inserted between an electrode and emitting layer to manipulate either electron or hole injection. Thus the balance of bipolar injection can be tuned by controlling the thickness of the insulating layer. Subsequently the bipolar injection effect on magnetoresistance will be investigated to test the validity of the proposed model. In chapter 6, the morphology effects on magnetoresistance and magnetic field dependent electroluminescence will be elucidated in the PFO based-OLEDs. Chapter 7 will summarize the whole dissertation.

2 MAGNETIC FIELD EFFECT ON ELECTROLUMINESCENCE AND MAGNETORESISTANCE IN ORGANIC LIGHT EMITTING DIODES

2.1 Introduction

Magnetic field effect on electroluminescence and current in an Alq_3 based OLED was first reported by Kalinowski[78]. Davis studied the same type OLED with a variety of different electrodes and found similar phenomena[76]. These phenomena were also confirmed by Frankevich[88] in the a poly(phenylene-vinylene) (PPV) type polymer based OLED. Wohlgenannt group[79,80] thoroughly studied a wide range of OLEDs based on different organic semiconductors and introduced the concept of magnetoresistance (MR) in this organic optoelectronics field. However, the exact mechanism for this magnetoresistance and magnetic field effect on electroluminescence (MFE) is still not clear.

In this thesis, we designed a series of experiments to study the same phenomena by prudently select different types of organic semiconductor with different spin-orbital coupling, energy gaps, different charge mobility and morphologies. Our goals were to understand the mechanisms behind these magnetic phenomena and develop effective techniques to tune the magnitude of these effects for future magnetic applications.

2.2 Experimental

All the chemicals in our studies were purchased from Aldrich or American dye sources. The devices were fabricated and characterized in our lab. The general procedure of experiments comprises of organic thin film formation, deposition of electrodes, and characterization of OLEDs, as shown in Figure 2.1.

2.2.1 Organic semiconductor materials

Two types of organic semiconductors used in this work include conjugated high molecular-weight polymer and low molecular-weight molecules. Conjugated polymers are basically a series of polymers with different energy gaps. The emission colors cover the whole visible light spectrum, e.g. blue polymer poly (9-vinylcarbazole) (PVK), blue polymer poly(9,9-dioctylfluorenyl-2,7-diyl) (PFO), green polymer poly(m-phenylenevinylene)-co-(2,5-dioctoxy-p-phenylenevinylene)] (PmPV), and red polymer-

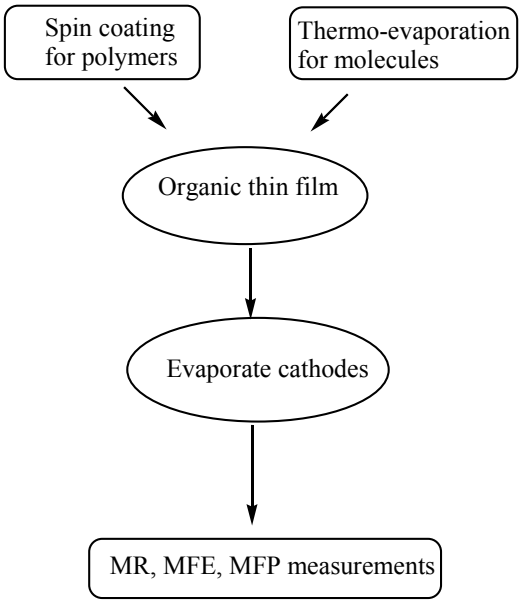


Figure 2.1 Procedure for device fabrication and characterization

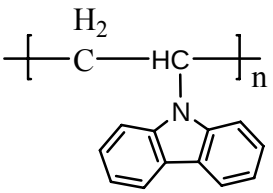
poly[2-methoxy-5-(2'-ethylhexyloxy)-1,4-phenylenevinylene] (MEH-PPV). Small molecules include both fluorescent materials and phosphorescent, tris-(8-hydroxylquinoline) aluminum (Alq_3), tris(2-phenylpyridine) iridium(III) ($Ir(ppy)_3$). The chemical structures are list in Figure 2.2. PVK, MEH-PPV, PmPV, Alq_3 were purchased from Aldrich company, while PFO and $Ir(ppy)_3$ were purchased from American Dye Sources company.

2.2.2 Device fabrication

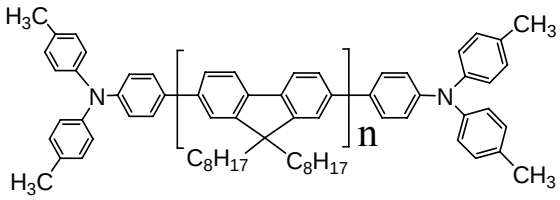
The device fabrication mainly includes three major steps: substrate cleaning; organic layer formation and metal electrode deposition. The basic structure of OLED used in this work is single layer architecture as shown in Figure 2.3. A metal electrode typically aluminum (Al) thin layer serves as electron injector while a transparent indium tin dioxide (ITO) layer works as a hole injection layer. The emitted light comes out form ITO side. For some cases, additional layers will be added between emitting layer and electrodes to manipulate charge injection. The fabrication method for such multilayer device will be presented specifically where it is discussed.

2.2.2.1 Substrate cleaning

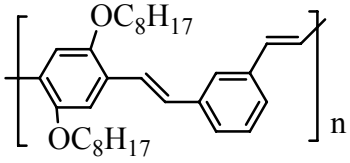
The ITO surfaces are easily contaminated by grease and dust during transporting and handling processes. Since the ITO is the hole injector, the cleaning of the surface is critical for the performance and longevity of the device. In our experiments, the ITO glasses were ultrasonic in acetone for 30mins. Then the ITO glasses were cleaned by detergent for another 30mins ultrasonic, followed by de-ionized water cleanse.



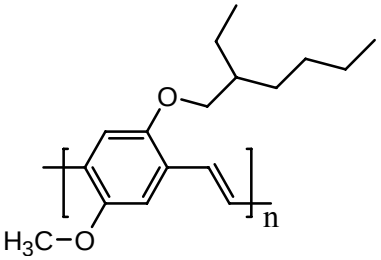
PVK



PFO

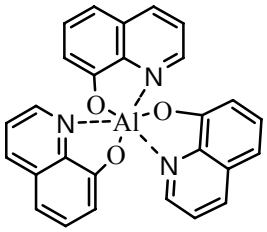


PmPV

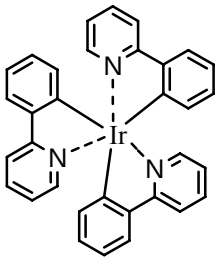


MEH-PPV

High-molecular-weight polymers



Alq_3



$Ir(ppy)_3$

Low-molecular-weight molecules

Figure 2.2 Chemical structures of some organic semiconductors used in experiments

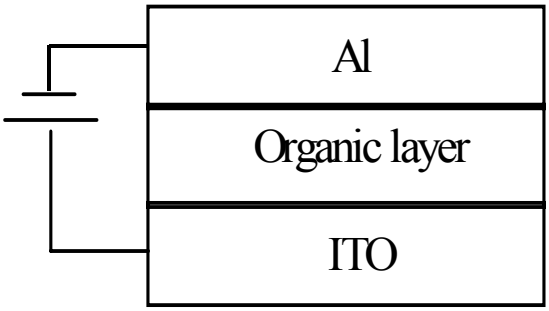


Figure 2.3 Basic single-layer OLED

2.2.2.2 Deposition of organic layer

Polymeric thin films and molecule thin films are formed by spin coating and vacuum deposition, respectively. Figure 2.4 shows the principle of spin-coating. First, polymer powders were first dissolved in chloroform ($CHCl_3$) to make a polymer solution. The concentrations were usually 5-15mg/ml. Then several drops of the polymer solution were put on the top of the pre-cleaned ITO glass substrates. With the presence of a vacuum, the ITO glass was sucked against the head of spinner. During the fast rotation of the spinner, excess solution was spun off the substrate and the solvent in the remaining solution evaporated quickly, leaving a thin polymer film on top of the ITO substrate. Generally, the thickness of the polymer film was controlled by controlling the solution concentrations, spin speeds, spin time and the type of solvent. Lower concentration, higher spin speed, and longer spin time lead to a thinner film, while high boiling point solvent evaporates slower and gives thinner film. The thicknesses of the films were measured by a Dektak thickness profiler. A typical thickness of the polymer thin layer was controlled to be about 100nm in our experiments.

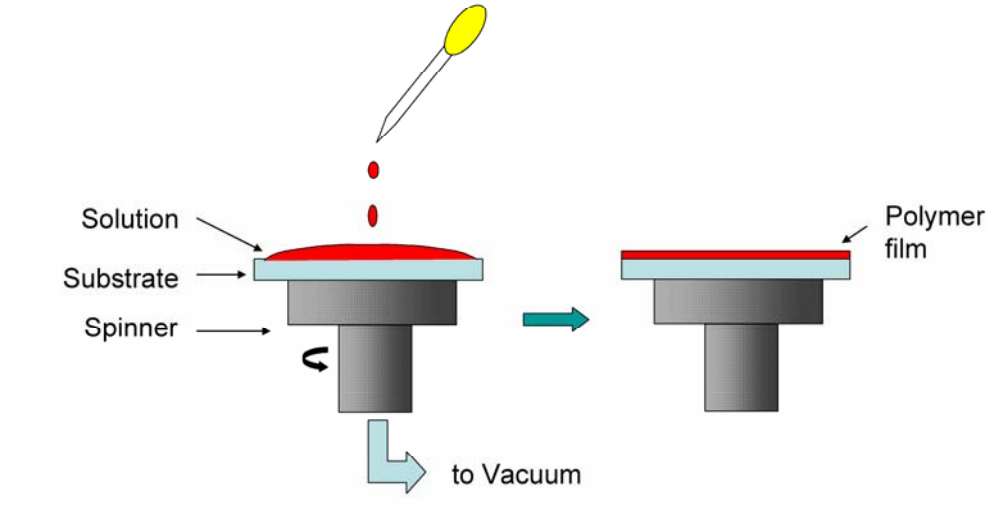


Figure 2.4 Formation of polymer thin film by spin coating

Small molecules films can not be made by spin coating due to low viscosity of their solutions. In stead, they can be formed by vacuum deposition as shown Figure 2.5. First the molecule powders were put into the heating boat in the vacuum chamber, while the ITO glass substrates were located on the bottom of the substrate holder. Then at a vacuum of 2×10^{-6} torr, the boat was heated up until the molecules started evaporation. The molecules deposited on top of the ITO glass forming an organic layer. The evaporation speed was controlled at 2Å/s. The thickness of the layer was monitored by the thickness detector located beside the substrate as shown in Figure 2.5. The thicknesses of the molecule films were also characterized by the same Dektak thickness profiler as used for polymer films.

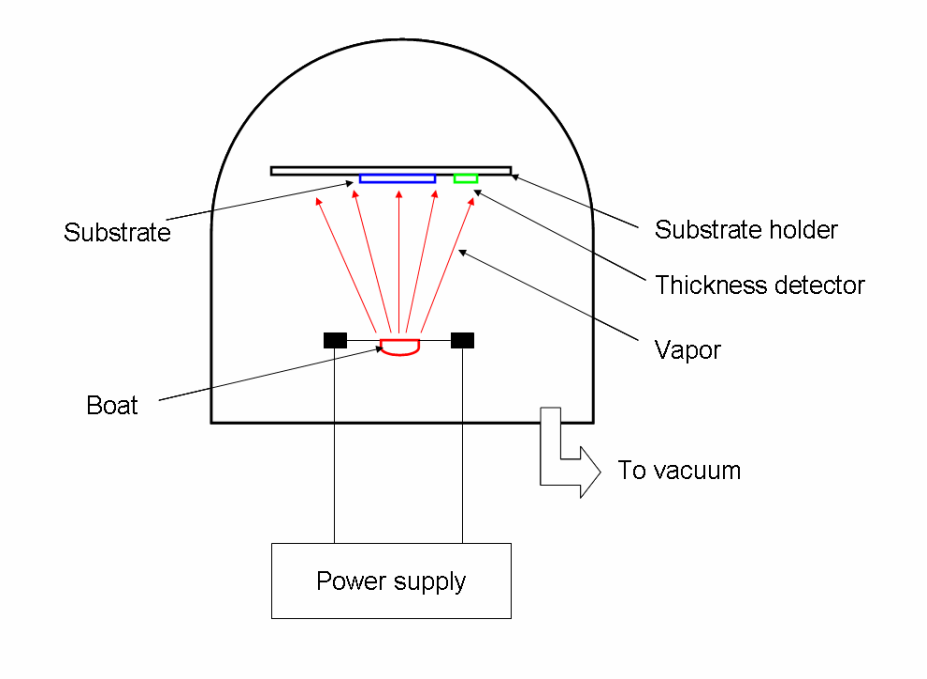


Figure 2.5 Thermal evaporation of molecule based thin films

2.2.2.3 Deposition of electrodes

The ITO glasses with deposited polymer films or molecule films were transferred into a glove-box which was filled with nitrogen gas. Then they were assembled into pre-patterned masks. After that, the masks were put beneath the substrate holder and aluminum (Al) wire was put into the boat in the thermal evaporator for thermal evaporation. The thermal evaporation for metal electrode was similar to that for the evaporation of molecules. A typical 20nm thick of Al electrode was deposited on top of the organic layer with pre-patterned shape, which finished the fabrication of an ITO, metal electrode sandwiched single layer OLED.

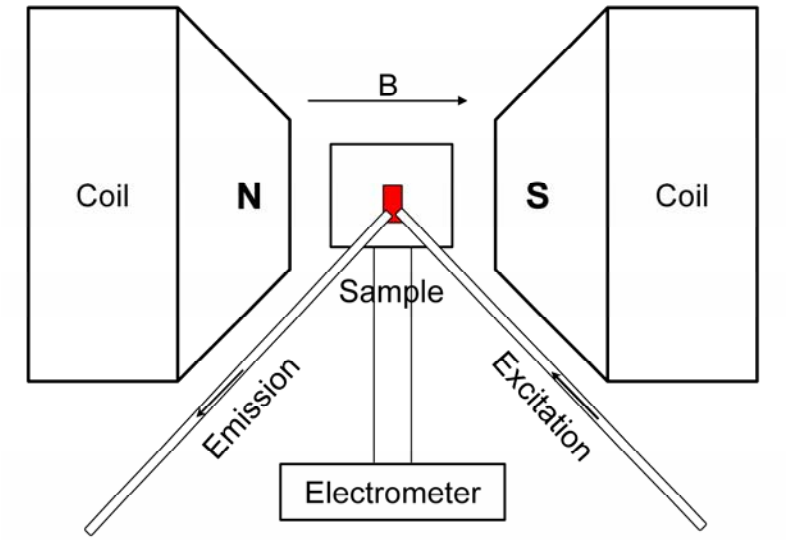


Figure 2.6 Setup for the magnetic field dependent electroluminescence, photocurrent and magnetoresistance measurements

2.2.3 Devices characterization

The fabricated devices were put between the poles of an electrical magnet for magnetic measurements as shown in Figure 2.6. The magnetic field direction was parallel to the device plane. The magnetic field strength was adjusted by the current supplied by a power supply which was controlled a Labview program. The magnetic field strength is proportional to the supplied current and the exact value of magnetic field was calibrated by a gauss meter.

For the magnetic field effect on electroluminescence measurement, there were two modes to supply current to operate the OLED, namely constant voltage mode and constant current mode. In constant voltage mode, a constant voltage was applied on the OLED by Keithley 2400 electrometer (Figure 2.6) and the electroluminescence was

conducted through an optical fiber to a Fluorog fluorescence detector where both the intensities and spectra were recorded. In constant voltage mode, the applied voltage was kept constant and the electroluminescence intensity change and current change were recorded to calculate the MFE and MR (equations 1.8, 1.9). Generally the magnitudes of MFE are different at constant current mode and voltage mode, which will be further discussed in the next section.

For the photoluminescence measurement, the photo-excitation was supplied by the same Fluorog spectrometer through the other optical fiber to illuminate the sample (Figure 2.6). The photoluminescence intensity and spectrum were recorded by the same way as the electroluminescence measurements. Under photo-excitation, the photocurrent were also measured by the same Keithley 2400 electrometer. The photocurrent change at zero bias with the external magnetic field was recorded to calculate the magnetic field effect on photocurrent, MFP (equation 1-10). This dissertation mainly focuses on the magnetic field effect on electroluminescence and magnetoresistance. The photocurrent measurements are used to support our arguments in certain cases.

2.3 Universality of MR and MFE

In this dissertation, magnetic field effects have been investigated in a wide range of polymers and molecules based OLEDs. Figures 2.7 and 2.8 list the results from some selected devices. It can be seen that an external magnetic field can either increase or reduce the electrical resistance, leading to a positive or negative MR (Figure 2.7) while the magnetic field usually enhances electroluminescence, namely positive MFE, whatever the sign of the MR (Figure 2.8). The general trend of both MR and MFE is that

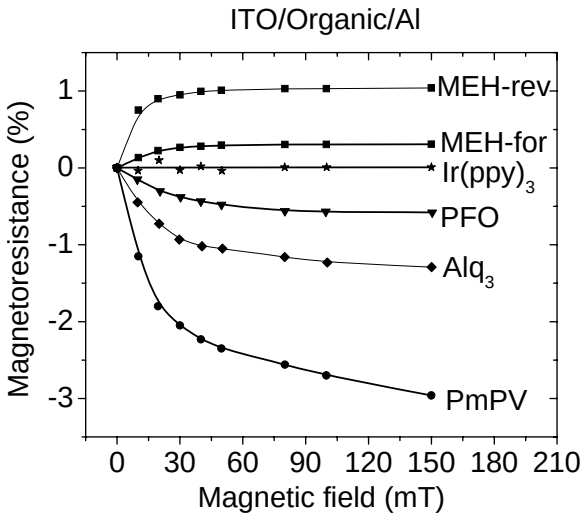


Figure 2.7 Magnetoresistances in typical single-layer OLEDs

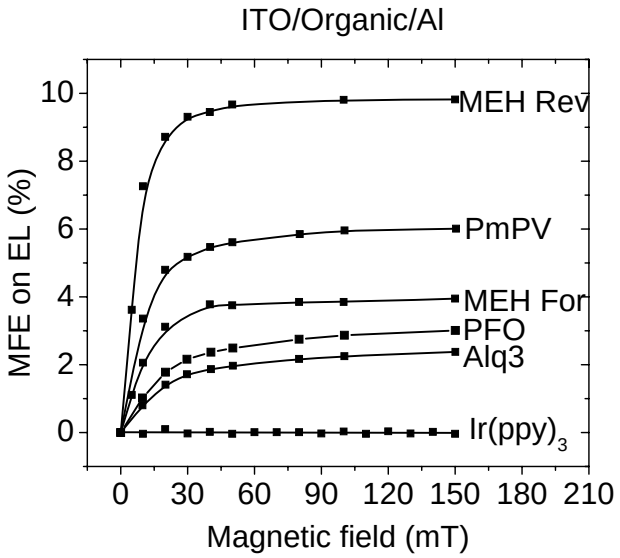


Figure 2.8 Magnetic field effect on electroluminescence in typical single-layer OLEDs

they change quickly with a low magnetic field until around 30-50mT, then they gradually saturate with the higher magnetic field. MR and MFE do show universality in almost all the measured florescent materials as claimed by Wohlgenannt[79]. However, there are some critical issues need to be pointed out. Unlike fluorescent materials, some phosphorescent materials e.g. $Ir(ppy)_3$ show very negligible magnetic field on both electroluminescence and magnetoresistance.

Furthermore, a positive MFE accompanied with a negative MR is frequently reported in the literature; however, the positive MFE unusually accompanied with a positive MR has never been reported so far.

Based on these results, there are several questions need to be answered. Why can an external magnetic affect the electroluminescence and conductivity in these non-magnetic materials? What is the relationship between MFE and MR? Why can an external magnetic field enhance electroluminescence while the driving current is actually decreasing? Why does a phosphorescent material show almost zero magnetic field dependence? And what is the reason causing different magnitude in different materials? Now we try to answer theses questions through selecting two systems as representatives for negative MR and positive MR systems.

2.4 Similar magnetic field effects between electroluminescence and resistance

Figure 2.9 shows the magnetic field effect on electroluminescence (MFE) and magnetoresistance (MR) in an ITO/PmPV (100nm)/Al OLED at liquid nitrogen temperature. MFE were measured at both constant current density of $20mA/cm^2$ and

constant 22V targeted to the same current density of 20mA/cm^2. The MR was measured at the same voltage mode. It can be seen that electroluminescence intensity increases rapidly with magnetic field in the low field range and then slowly saturates in the range from 50mT to 150mT. Meanwhile, the MR decreases with magnetic field following a similar trend. Since the decrease of magnetoresistance corresponds to the increases of driving current at same voltage, it is very natural to conclude that MFE actually comes from MR. However, the enhancement of constant current mode EL is about 6% at 150mT while the voltage mode magnetic field effect EL is about 8.5%. The difference of 2.5% is roughly same to the magnitude of the magnetoresistance (-2.6%).

It is also worthy to mention that the magnetic field can not change the electroluminescence spectrum and the both photoluminescence intensity and spectrum are not sensitive to external magnetic field.

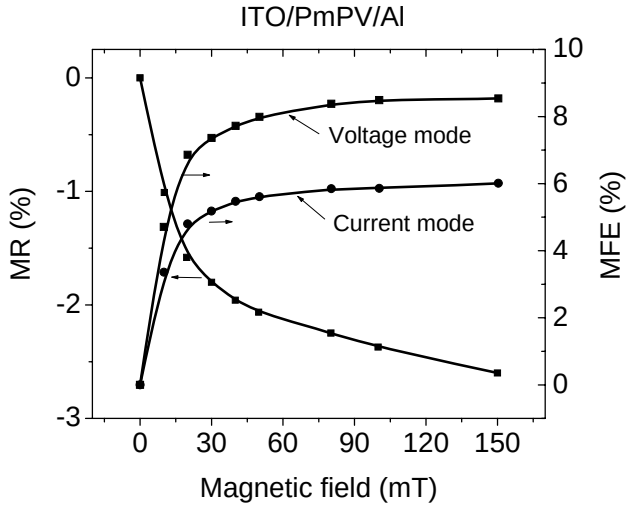


Figure 2.9 Magnetic field effect on electroluminescence and magnetoresistance in an ITO/PmPV/Al device

2.5 Opposite magnetic field effect on electroluminescence and resistance

In an ITO/MEH-PPV/Al device, the MR and MFE at both constant voltage and current at current density of 20mA/cm^2 were also measured as shown in Figure 2.10. The MFEs at both forward and reverse bias increase with the magnetic field, however, the MR also show a positive value, which means the electroluminescence increase with magnetic field while the current actually decreases with the same magnetic field at constant voltage mode. Therefore, MFE should not be determined by MR.

Detailed study shows the magnitude of MFE at constant current density of 20mA/cm^2 is 3.9 % at 150mT while the MFE at constant voltage mode is about 3.4%, smaller than that in current mode. The value of MR at same voltage mode is +0.4%, equilibrium to a 0.4% decrease of current density. The value is also similar to the difference of voltage mode and current mode MFE (3.9%-3.4%=0.5%).

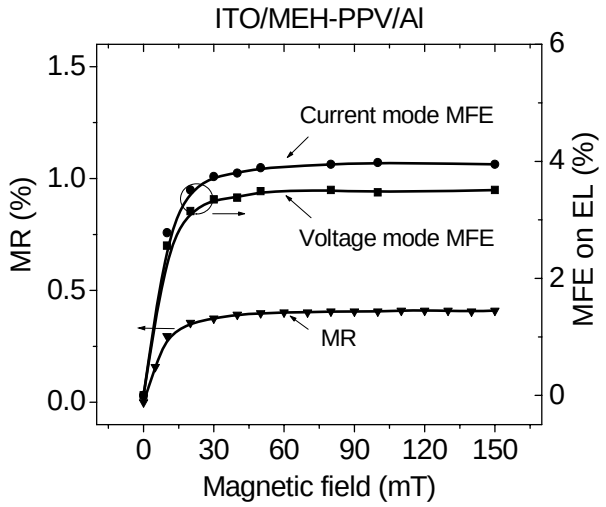


Figure 2.10 Magnetic field effect on electroluminescence and magnetoresistance in an ITO/MEH-PPV/Al device

2.6 The relationship between magnetic field effect on electroluminescence and resistance

From above discussion, it is obvious that the MFE is not due to MR since in MEH-PPV system electroluminescence actually increases with the external magnetic field with the resistance increases (current decreases) with the same field. Actually the electroluminescence can be expressed as

$$EL \propto \eta(B) I(B) \qquad \text{Equation 2-1}$$

where η is the quantum efficiency and I is the current flowing through the devices. Accordingly, the electroluminescence enhancement comes from two parts: efficiency and current change. Indeed, in the constant current mode, electroluminescence intensity increases with magnetic field indicating the enhancement of electroluminescence efficiency η. However, the current changes are different in PmPV and MEH-PPV systems. In PmPV system, resistance decreases with magnetic field and accordingly current increases with the field. Therefore, the voltage mode MFE is larger than that in constant mode. In MEH-PPV system, at constant voltage mode, the MFE comprises of efficiency enhancement and current decease. The voltage mode MFE is smaller than that of constant current mode. Hence, it is clear that magnetic field effect on EL and current are two independent processes, which might be caused by similar mechanism since the magnetic field dependence is very similar.

2.7 Mechanisms for MR and MFE

It has been shown that the MFE is not due to MR. Then what is the exact reason causing both MFE and MR? Now let us start from the existing possible models in the literature to explore the mechanism for MFE and MR.

2.7.1 Failure of triplet-triplet annihilation (TTA) mechanism

TTA rate has been proven to be sensitive to external magnetic field[70]. It is true that a low field enhances the formation of singlets, leading to enhancement of electroluminescence. However, TTA only contributes to the delayed fluorescence which accounts less than 0.1% in total emission[81]. In case of PmPV, about 6% EL enhancement was detected under a magnetic field of 150mT at current density of 20mA/cm^2. If it were due to TTA, the TTA rate should increase more than 6000% which is unreasonable. Therefore, the increase of singlet is unlikely due to TTA.

2.7.2 Magnetic field enhanced singlet polaron pairs

Kalinowski[75] attributed the enhanced electroluminescence to the magnetic field enhanced singlet number. It was assumed that the singlet and triplet polaron pairs are degenerated and they can mutually convert to each other at zero magnetic field. With the presence of an external magnetic filed, the three components of the triplet polaron pairs split and the conversion of singlet polaron pairs to triplet polaron pairs is partially blocked. As a result, the singlet polaron pairs actually increases with magnetic field. Consequently the singlet exciton and electroluminescence increases with a magnetic field. However, there are at least two issues this model is hard to explain.

Firstly, since the singlet and triplet polaron pairs are degenerated, a magnetic field blocks the transition from singlet but at same time it also blocks the transition from the triplets to singlets. Because the singlet polaron pairs have a larger conversion rate to relax into excitons, dynamically the mutual conversion of singlet and triplet benefits the formation of singlet excitons. Therefore the magnetic field effect should lead to a decrease of electroluminescence after the magnetic field blocked the transition between singlet and triplet polaron pairs.

Secondly, even it is true that singlet exciton increases with a magnetic field, it is still hard to explain the enhanced electroluminescence with enhanced resistance in MEH-PPV system and enhanced electroluminescence with reduced resistance in PmPV system at the same time. Therefore, this model only partially explains the MFE and MR and obviously it is not a universal model to explain the observed magnetic phenomena.

2.7.3 Magnetic field enhanced reaction yield

Lupton[85] investigated the magnetic field effect on both fluorescence and phosphorescence in PhLPPP based- devices. It was concluded that magnetic filed can not change the intersystem crossing and the enhanced electroluminescence is basically due to the magnetic field enhanced reaction yield if considering the light emission process as chemical reactions.

$$S_1 \rightarrow S_0 + h\gamma(fluorescence) \qquad \text{Equation 2.2}$$

$$T_1 \rightarrow S_0 + h\gamma(phosphorescence) \qquad \text{Equation 2.3}$$

It is true that the magnetic field does increase the efficiency of the electroluminescence. As shown in Figure 2.9 and 2.10, at constant current mode, the

electroluminescence intensities in both PmPV and MEH-PPV systems increase with magnetic field, supporting this argument. However, the enhancement can either come from the enhanced number of singlet exciton or enhanced radiative decay of singlet exciton with its population unchanged. Lupton model actually claims the second possibility. To investigate the second possibility, magnetic field dependent photoluminescence was also measured for PmPV and MEH-PPV. No detectable magnetic field effect on photoluminescence can be observed, consistent with the findings of other groups[89]. In the photoluminescence, the intersystem crossing is negligible since both PmPV and MEH-PPV are basically hydrocarbon materials with very small spin-orbital coupling. Thus the number of the singlet exciton would not change in this measurement. According to the enhanced reaction yield model, the photoluminescence efficiency should increase since the radiative decay of singlet exciton would increase, which is contradictory to the experimental observation.

Furthermore, it is also hard to interpret why the enhanced reaction yield can lead to either reduced or enhanced current flowing through the device at constant voltage mode without any change in the number of singlet and triplet excitons. Therefore it is also unlikely to be reason for MFE and MR.

According to the magnetic field enhanced minority injection model proposed by Cölle[81], the electroluminescence would increase with more balanced electron-hole injection with magnetic field. However, in MEH-PPV based devices, the current clearly decreases with an external magnetic field while the electroluminescence intensity increases. Therefore, there is no existing model can fully account for the magnetic field dependent electroluminescence and magnetoresistance.

2.8 Possible mechanism

In this section, we will try to develop a possible mechanism based on the results obtained in this dissertation and theories developed in the literature.

2.8.1 Determination of magnetic field effects on polaron pair or exciton states

It was observed that the PL intensity shows a negligible dependence on magnetic field strength (Figure 2.11). As we know in photoluminescence process, singlet exciton forms directly with illumination of excitation, which can weakly convert to triplet exciton by intersystem crossing. If the intersystem crossing in this stage were sensitive to external magnetic field, PL intensity would be changed by the field, which is contradictory to our experimental results. One may argue that the intersystem in PmPV or MEH-PPV is week; the photoluminescence change may be too smaller to be detected. To further inspect this possibility, magnetic field effect on photoluminescence of 5,10,15,20-Tetraphenyl-21H,23H-Porphine (TPP) was also measured since TPP has a much larger intersystem crossing rate from singlet to triplet[90]. Still, no clear MFE on photoluminescence can be detected. Therefore, the intersystem crossing between singlet and triplet excitons should not be sensitive to an external magnetic field.

Based on the same device, the MFE on photocurrent was observed at zero bias with the illumination of 350nm light, corresponding to the maximum absorption of PmPV. The photocurrent increases with magnetic field to about 1.5% at 150mT. Similar effects were also reported in other systems[78,82]. As we know the photocurrent comes from the polaron pair states while the photoluminescence from exciton states. It has been reported that magnetic field can enhance the formation of singlet polaron pairs and reduce triplet-

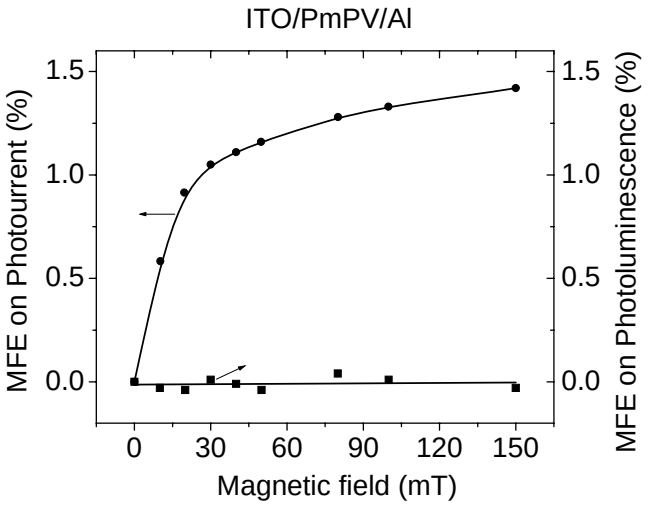


Figure 2.11 Magnetic field effect on photoluminescence and photocurrent in ITO/PmPV/Al device

polaron pair states though intersystem crossing. Since the singlet polaron pair has larger dissociation rate into free charges than that of triplet polaron pairs. Thus the net result of the magnetic field effect on intersystem crossing causes the enhancement of photocurrent. Therefore, it can be concluded that magnetic field does have significant effects on the intersystem crossing between singlets and triplets in polaron pair states, but not in exciton states.

2.8.2 Excited states related magnetic field effect on electroluminescence and magnetoresistance

Photocurrent results provide a possibility that the observed MFE and MR may be also related to intersystem crossing between polaron pair states. Obviously, there exist

similar polaron pair states in electroluminescence process. To clarify the MR is also related to the excited states, the voltage dependent MR was studied in ITO/PmPV/Al device, as shown in Figure 2.12.

In Figure 2.12, below the threshold voltage no electroluminescence can be detected since the electroluminescence requires bipolar injection (both hole and electron injection). Below threshold voltage, only week hole current flow through the device since the barrier for hole injection is lower and the hole mobility is larger than that of an electron. Beyond threshold, both hole and electron injection occur and electroluminescence can be detected. From Figure 2.12, it can be seen that the magnetoresistance is negligible below the threshold and increases rapidly with applied voltage beyond the threshold. Cölle[81] also reported that no magnetoresistance can be observed in an Al/Alq_3/Al device, where only electron current can go through the device and polaron pairs cannot form. Therefore, from the voltage dependent magnetoresistance, it can be concluded that the magnetoresistance is also related to excited states.

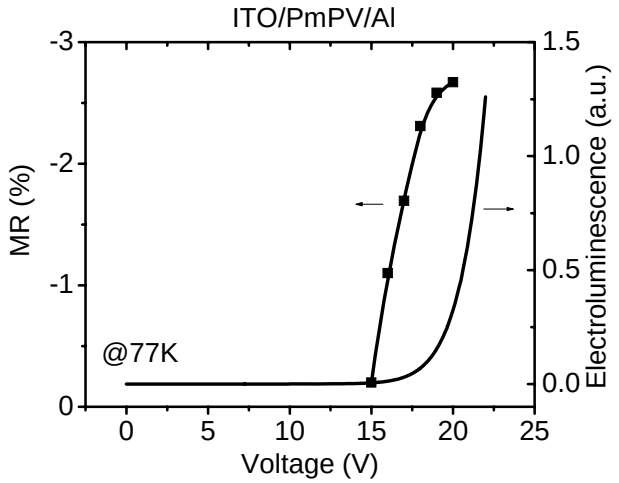


Figure 2.12 Voltage dependent magnetoresistance

2.8.3 Mechanism for magnetic field effect on electroluminescence

Based on the magnetic field effect on photocurrent, electroluminescence and magnetoresistance, we propose that the magnetic field can modify the intersystem crossing by considering the exchange energy between singlet and triplet, as shown in Figure 2.13. Once the polaron pairs have defined spin configurations and the electron and hole feel each others' spin, there exists an exchange energy. The exchange energy between singlet and triplet exciton has been determined to be around 0.7ev[14]. Since a polaron pair has a longer distance than its exciton, the exchange energy should be less than the exchange energy between singlet and triplet exciton. Thus a mediate magnetic field as used in our study can manipulate the transition between singlet and triplet polaron pairs through an external Zeeman Effect.

Without an external magnetic field, triplet polaron pairs have lower energy than the singlet polaron pairs. The transition between the singlet and triplet polaron pairs is due to hyperfine interaction[75]. With the presence of an external magnetic field, the Zeeman Effect causes the $^3PP_+$ tilt upward and at certain field, the singlet polaron pair ^1PP and $^3PP_+$ are degenerate. The transition between them is allowed at this condition. Since the singlet polaron pairs have larger decay and dissociate rate due to its ionic characteristic[60], dynamically, more triplet polaron pairs convert to the singlet polaron pairs. Accordingly both electroluminescence and photocurrent show positive magnetic field dependence, as commonly observed in our experiments[89].

The lack of MFE on photoluminescence might be due to a relatively large exchange energy between singlet and triplet exciton in which moderate magnetic field would not be able to modify the intersystem crossing rate; however, in the polaron pair stage the-

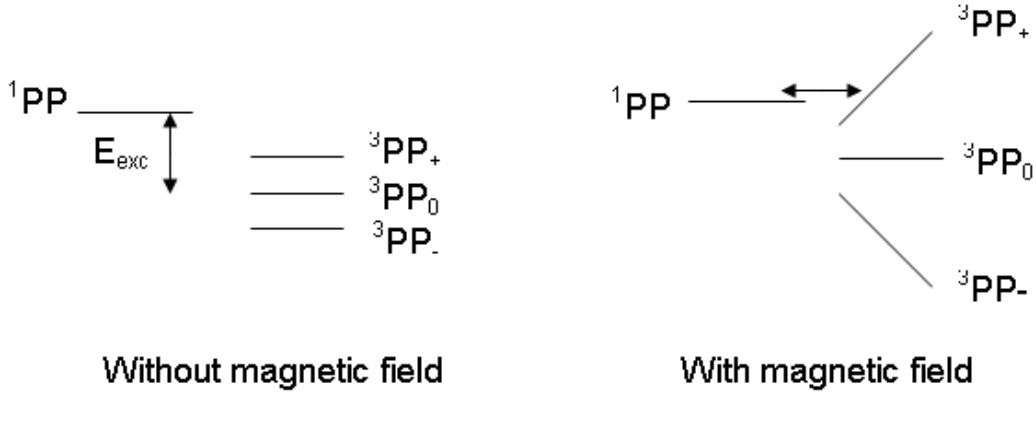


Figure 2.13 Proposed magnetic field effect on the intersystem crossing between singlet and triplet polaron pairs

exchange energy is much smaller and more sensitive to weak or moderate external magnetic field as used in our work. Thus, the magnetic field effect can be observed in electroluminescence but not in photoluminescence.

2.8.4 Mechanism for magnetoresistance

In electroluminescence process, the formed polaron pairs after charge injection can also dissociate to form free charges, which is similar to the case in the photocurrent process[91]. A low magnetic field can enhances the transition from triplet to singlet polaron pairs due to Zeeman splitting and leads to an increase of singlets and a decrease triplets. This magnetic field effect causes two consequences to the magnetoresistance. First, the increase of singlets not only leads to an increase of EL intensity but also dissociate into more free charges due to the fact that singlet polaron has a larger dissociation rate than that of the triplet polaron pair[91]. The dissociated electron and hole drift to anode and cathode interface, respectively, resulting in a reduced build-in field and enhanced charge

injection ($-MR_S$). On the other hand, the decrease of triplets reduces the triplet-charge reaction yield[92,93] and generates less free charges, giving a positive magnetoresistance ($+MR_T$). As a result, the observed magnetoresistance might reflect the sum of these two opposite components, as illustrated in Figure 2.14. The observed positive magnetoresistance suggests that the triplet-charge reaction dominates the magnetoresistance in the MEH-PPV OLEDs, while for the negative MR, e.g. in PmPV system, the dissociation mechanism might be the dominating process.

2.9 Summary

In this Chapter, a wide range of organic semiconductors were investigated. Almost all the fluorescent materials show magnetic field effect dependent electroluminescence and magnetoresistance. Magnetic field universally enhances electroluminescence; however, the MR can be a positive or negative value, for examples positive MR in MEH-PPV and negative MR in PmPV system.

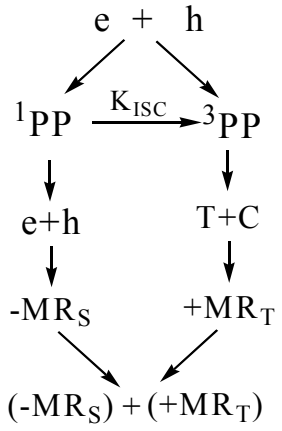


Figure 2.14 The principle for the formation of negative and positive magnetoresistance

We proposed a magnetic field modified intersystem crossing mechanism to explain the MFE and MR. An external magnetic field can enhance the formation of singlet polaron pairs and reduce the formation triplet polaron pair states. The enhanced singlet polaron pair states directly leads to the positive MFE. While the MR is determined by two factors: polaron pair dissociation and triplet-charge reaction. Magnetic field enhanced formation of singlet leads to more free charges which drift to opposite electrodes under electrical field and reduce the built-in field. As a result the charge injection increases with magnetic field (negative magnetoresistance). The reduction of triplet polaron pairs generates less free charges and leads to a positive MR accordingly. The final magnetoresistance is determined by the sum of the two processes.

3 SPIN-ORBITAL COUPLING EEFECT ON MAGNETORESISTANCE AND MAGNETIC FIELD DEPENDENT ELECTROLUMINESCENCE

3.1 Introduction

In chapter 2, a magnetic field modified intersystem crossing mechanism has been developed to interpret the magnetoresistance and magnetic field effect on electroluminescence by considering both exciton dissociation and triplet-charge reaction processes. For organic semiconductors, singlet-triplet intersystem conversion rate is determined by hyperfine interaction and spin-orbital coupling[46]. Because the proton dipole moment in the hyperfine interaction is much weaker than the electron orbital dipole involved in the spin-orbital coupling, spin-orbital coupling is essentially the determining factor for intersystem crossing.

There are two ways to tune the spin-orbital coupling: dispersing heavy metal atoms into organic materials, namely external heavy-atom effect[94]; or attaching heavy metal atoms to organic molecules, namely internal heavy-atom effect[95]. The external heavy-atom effect can be readily obtained by dispersing heavy metal atoms into organic materials. However, the insolubility of metal particles together with the large discontinuity of dielectric constant at the material interface creates a significant difficulty in obtaining a uniform dispersion and an effective interfacial interaction in metallic/organic material composites.

To avoid the dispersion problem in the external heavy-atom effects, we studied a polarity dependent magnetoresistance (MR) and magnetic field effect on electroluminescence (MFE). The principle is to push the recombination zone close to metal electrode at one bias and far away at the other bias. Subsequently, the organic semiconductor will experience stronger spin-orbital coupling in the region close to the metal electrode and weaker spin-orbital coupling away from the metal electrode. To investigate the internal heavy-atom effect, two low-molecular-weight dyes, Alq_3 and $Ir(ppy)_3$ were selected to study the magnetic field dependent electroluminescence and magnetoresistance since the two dyes have almost same electronic energy levels[96] and the major difference is the type of metal (Al and Ir) incorporated in the chemical structures.

3.2 Experimental

For the external heavy-atom effects, MEH-PPV was selected since it has a smaller energy gap. As a result, it is relatively easy to achieve electroluminescence at both forward and reverse bias. The basic procedure for device fabrication has been shown in chapter 2. 100nm thick MEH-PPV films were first spun cast on top of pre-cleaned ITO glasses, followed by thermal evaporation of 20nm thick aluminum electrode at 2×10^{-6} torr to finish the fabrication of ITO/MEH-PPV/Al single layer devices. 80nm Alq_3 and $Ir(ppy)_3$ films were thermal evaporated on top of pre-cleaned ITO glasses, followed by deposition of aluminum electrode same as the MEH-PPV devices. The devices were measured at liquid nitrogen temperature for better signal/noise ratio and stability. The magnetic field varied in the range from 0-150mT.

3.3 Realization of working OLED at both forward and reverse biases

Figure 3.1 shows MEH-PPV device works at both forward and reverse bias due to its small energy gap[97]. The forward and reverse bias configurations are shown in Figure 3.1 (b). The HOMO and LUMO of MEH-PPV are 5.0ev, 2.8ev, respectively. The work-function of Al and ITO are 4.2ev and 4.8ev, respectively[28]. Therefore, there is almost no injection barrier for hole injection at forward bias. The injection barrier for electron injection is roughly 1.4ev at forward bias. When the device is reverse biased, the barrier for hole injection and electron injection are 0.8ev and 2.0ev, respectively. From Figure 3.1 (a), it can be seen the device turns on at 5V at forward bias and 11V at reverse bias since the barrier at reverse bias the charge injection for both electron and hole are larger than that in forward bias.

3.4 Identification of the recombination zones

The emitting zones at forward and reverse bias can be identified by comparing the electroluminescence spectra at forward or reverse bias and photoluminescence spectrum. Figure 3.2 shows that the reverse EL spectrum has a blue shift of 15 nm relative to the forward EL spectrum that is similar to the PL spectrum with typical bulk emission characteristics. Because the bandgap energy at the surface is larger than that of bulk in a polymer thin film[98], this blue spectral shift suggests that the reverse injection yields a narrow electron-hole capture zone close to the ITO/MEHPPV interface whereas the forward injection corresponds to a broad capture zone containing the surface nearby the MEHPPV/Al interface and the MEHPPV bulk. [Figure 3.2(a)]. The PL spectrum is shown to represent the emission from bulk MEH-PPV.

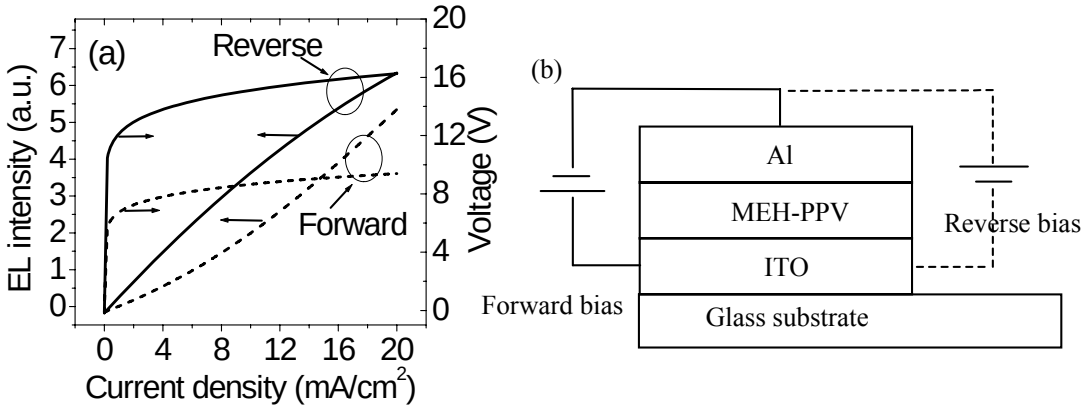


Figure 3.1 (a)EL-current-voltage characteristics of ITO/MEHPPV/Al OLED at forward and reverse biases. (b) Device structure and definition of forward and reverse bias.

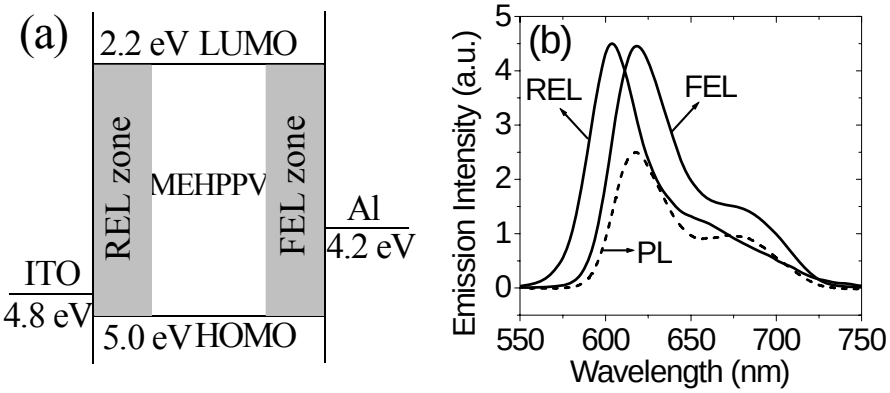


Figure 3.2 (a) Schematic electron-hole recombination zones in ITO/MEHPPV/Al at forward and reverse biases. (b)Forward and reverse EL spectra from ITO/MEHPPV/Al OLED.

3.5 Bias dependent magnetoresistance

Figure 3.3 shows that magnetic field increases resistance or decreases current (positive MR) at both reverse and forward bias. The positive magnetoresistance contains an increase with the field from 0 to 50 mT and then a saturation from 50 mT up to 150 mT. The reverse- and forward-saturated magnetoresistances are 1.0 % and 0.3 %, respectively.

According to the proposed model, an external magnetic field can enhance the polaron pair dissociation and reduce triplet-charge reaction leading to negative MR and positive MR. As shown in Figure 3.2, the charge injection barriers are very different, much lower for hole injection at both forward and reverse bias. There exist a large fraction of excess free charges which can interact with polaron pairs, especially triplet polaron pairs since they have much longer lifetime. Therefore the magnetic field on triplet-charge reaction would be dominating in ITO/MEH-PPV/Al device at both forward and reverse bias. Accordingly, the final MR would be positive as observed in the experiment.

3.5.1 Balancing degree of charge injection

There are two possibilities which can account for the difference in magnetoresistance when the applied voltage is changed from forward to reverse polarities: balancing degree of bipolar injection or spin-orbital coupling in different electron-hole (e-h) recombination zone. It is known that changing the applied bias from forward to reverse polarities can largely affect the balancing degree of the bipolar injection due to the different potential barriers for electron and hole injection in OLEDs with anode and-

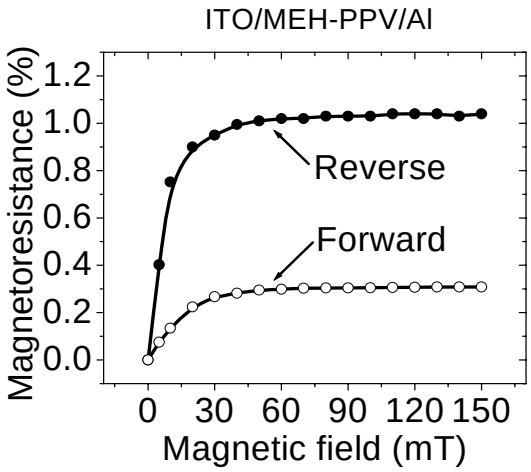


Figure 3.3 Magnetoresistances from MEH-PPV OLEDs with Al cathode at forward and reverse biases

cathode of dissimilar work-functions. We can expect from the band diagram [Figure 2.2 (a)] that the reverse bias results in a more unbalanced electron and hole injection and thus a reduced ratio between the excited states and charge carriers relative to the forward bias in the ITO/MEHPPV/Al OLED. The reduced ratio of excited states can lead to lower magnetoresistance. As a result, the reverse bias would yield a decreased magnetoresistance with respect to the forward bias, which is contradictory with the experimental results shown in Figure 3.3. Therefore, the bipolar injection may not be the main reason in this system.

3.5.2 Spin –orbital coupling effect

During the thermal vacuum deposition of the metal electrode, metal atoms inevitably penetrate into the semiconductor layer. The delocalized π electrons of the

MEH-PPV will penetrate into the orbital field of metal atoms when MEH-PPV segments are close to metal atoms. As a consequence, the π electron spin dipoles μ can interact with the orbital dipoles B of metal atoms, enhancing the polymer spin-orbital coupling at the MEH-PPV/metal interface in organic semiconductor devices. The interaction energy can be calculated by

$$E = \vec{\mu} \bullet \vec{B} \qquad \text{Equation 3-1}$$

where magnetic dipole moment μ due to electron spin motion, and B is the magnetic field from orbital motion. B can be calculated by

$$B = \frac{\mu_0 Zev}{4\pi r^2} \propto Z \qquad \text{Equation 3-2}$$

where Z is the atomic number of the metal atom in this case. Thus heavier atoms give larger spin-orbital coupling. Obviously, the bulk of the polymer experiences less metal-atoms-enhanced spin-orbital coupling effect. In the ITO/polymer side, no indium or tin atoms can penetrate into polymer film. Thus the enhancement of spin-orbital coupling is also very limited at the ITO/polymer side.

With the presence of an external magnetic field, the recombination zone is pushed to the MEH-PPV and aluminum electrode at forward bias and the interfacial spin-orbital dipole interaction competes with the external Zeeman Effect and consequently weakens the dependence of singlet/triplet ratio on magnetic field. Therefore, the dominant triplet-charge reaction experiences a less influence of magnetic field, giving a reduced $+MR_T$ compared with that in reverse bias where no enhancement of spin-orbital coupling. To confirm the effect of metal electrode on spin-orbital coupling, the magnetic field-

dependent electroluminescence (MFE) at constant current was also studied in Figure 2.4. In general, a positive MFE can be due to magnetic field-increased singlets through external Zeeman Effect at low field[76,99]. Therefore, increasing spin-orbital coupling can lead to a decrease in the MFE by weakening the external Zeeman Effect. Figure 2.4 shows the positive MFEs from the MEH-PPV OLEDs with ITO anode and Al cathode at both forward and reverse injection current of 20 mA/cm^2. The magnetic field dependent electroluminescence includes an increase with the field from 0 to 50 mT and then saturate in the field range from 50 mT up to 150 mT. Moreover, the reverse injection yields a largely increased electroluminescence dependence of magnetic field as compared with the forward injection at the constant current. The maximal MFEs are 9.8 % and 3.5 % for reverse and forward biases, respectively, in the ITO/MEHPPV/Al OLED. This bias polarity-dependent MFE supports that the excited states experience a stronger spin-orbital coupling at forward bias with the e-h capture zone nearby the MEHPPV/metal interface and a weaker spin-orbital coupling at reverse bias with the e-h capture zone away from the metal electrode, respectively

3.6 Enhancement of spin-orbital coupling by using a heavier metal electrode

To further confirm the metal effect, the Al electrode was replaced by a gold (Au) electrode. The selection of gold has two advantages: firstly, gold has a similar work-function (5.0ev) as that of ITO (4.8ev). In the ITO/MEH-PPV/Au OLED, only small difference exists between forward bias and reverse bias for bipolar injection as shown in-

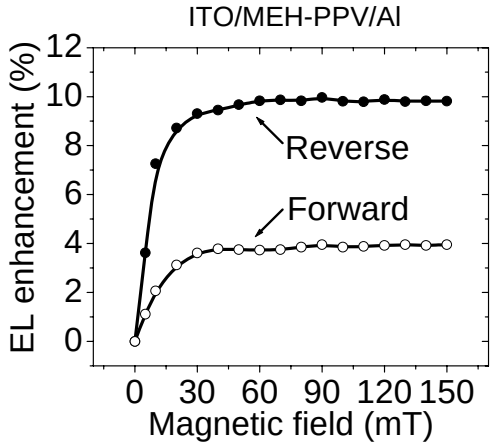


Figure 3.4 Magnetoresistances from MEH-PPV OLEDs with Al cathode at forward and reverse biases

Figure 3.5. At reverse bias, the voltage just slightly higher than that of forward bias, consistent with the estimation based the energy diagram

Secondly, gold has much larger atomic number compared with aluminum. According to equation 3.2, the gold can further enhance the spin-orbital coupling of MEH-PPV when the π electrons of MEH-PPV penetrate into the vicinity of the gold orbital.

Similar to the ITO/MEH-PPV/Al, the recombination zones at reverse bias and forward bias are close to ITO/MEH-PPV interface, MEH-PPV/Au interface, respectively, as shown in the Figure 3.6. Electroluminescence is much weaker in ITO/MEH-PPV/Au diodes because of more unbalanced charge injection, the electroluminescence signal is noisy; however, it is clear that electroluminescence spectrum is 10nm blue shifted compared with the forward electroluminescence spectrum which is similar to the photoluminescence spectrum.

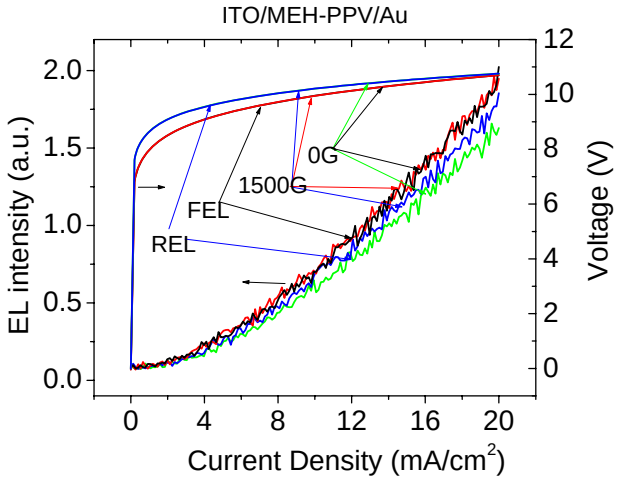


Figure 3.5 Electroluminescence-voltage-current characteristics for ITO/MEH-PPV/Au OLED at both forward and reverse bias. REL, FEL represents the electroluminescence at reverse bias and forward bias, respectively. 0G, 1500G is the magnetic field strength

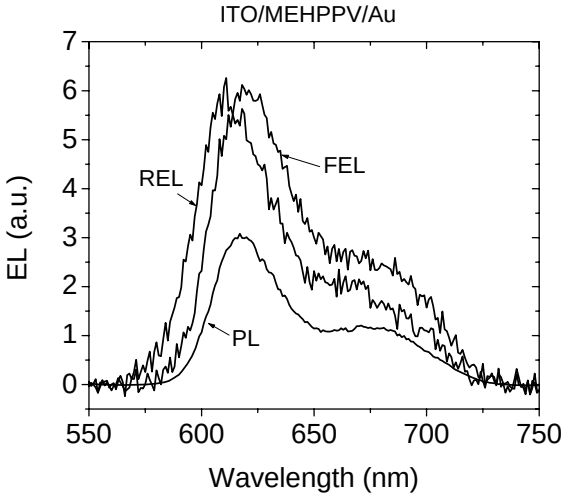


Figure 3.6 Forward and reverse electroluminescence and photoluminescene spectra from ITO/MEHPPV/Al OLED

The magnetic field effect on electroluminescence at forward and reverse bias was shown in Figure 3.7 (a). At reverse bias it shows almost same magnetic field effect, compared with ITO/MEH-PPV/Al, however the magnetic field effect at forward is further reduced to a negligible value. At reverse bias, the magnetic field effect was not affected by metal type since the recombination zone is far away from metal electrode, while at forward bias, gold atoms enhances the spin-orbital coupling strength of MEH-PPV and further reduce the magnetic field effect as predicted based on the model. Similarly, the forward magnetoresistance shows much smaller value than that at reverse bias, as shown in Figure 3.7(b). The bias dependent MFE and MR in ITO/MEH-PPV/Au OLEDs further supports the observed bias dependence is not mainly due to the bipolar injection effects, since the bipolar injection at both forward and reverse biases are similar (Figure 3.5).

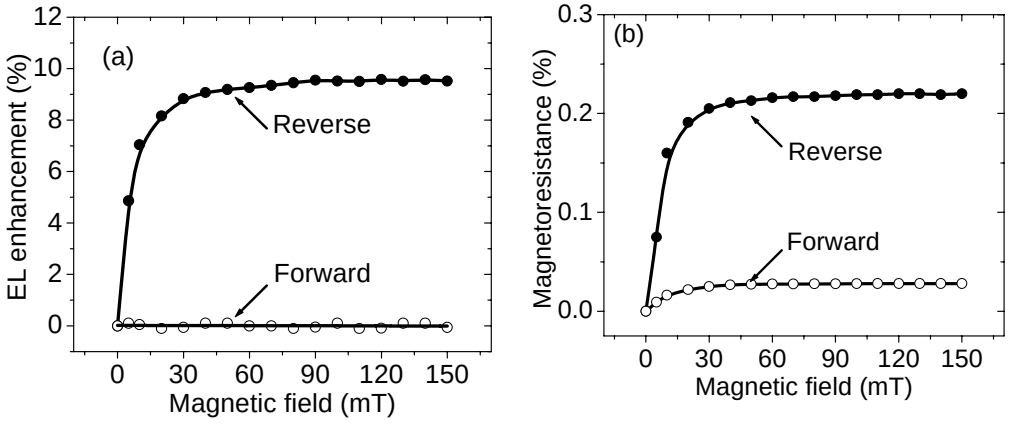


Figure 3.7 Magnetic field effect on EL and magnetoresistance from the MEHPPV OLED with gold electrode at forward and reverse biases

3.7 Reduction of spin-orbital coupling by separating MEH-PPV from the Metal electrode

After an inert buffer layer was inserted between the MEH-PPV and the metal electrode in the MEH-PPV OLED, the emtting zone at forward bias is close to the MEH-PPV/PMMA interface due to the small potential barrier at the ITO/MEH-PPV for hole injection and the large potential barrier at the PMMA/Au for electron injection. Thus, the use of PMMA buffer layer can minimize the effect of metal electrode on polymer spin-orbital coupling by eliminating the metal atomic diffusion into the MEH-PPV and avoiding the penetration of π electrons into the orbital field of metal atoms. It is found the forward magnetoresistance is significantly increased when the 15 nm thick buffer layer of poly(methyl methacrylate) (PMMA) is used between the MEH-PPV and the gold electrode (Figure 3.8). In addition, the double-layer MEH-PPV/PMMA OLED also shows a largely increased forward magnetic field effect as compared to the single-layer MEH-PPV OLED at the injection current of 20 mA/cm^2 (inset in Figure 3.8). This result confirms the different MFE and MR is truly due to metal atoms enhanced spin orbital coupling in MEH-PPV/metal electrode interface.

3.8 Internal spin-orbital coupling effect

To investigate the internal spin-orbital coupling effect, magnetic field dependent electroluminescence and magnetoresistance were investigated in OLEDs based on a fluorescent Alq_3 and a phosphorescent $Ir(ppy)_3$. The OLEDs based on Alq_3 and $Ir(ppy)_3$ were fabricated by same procedures as mentioned in the experimental section. The-

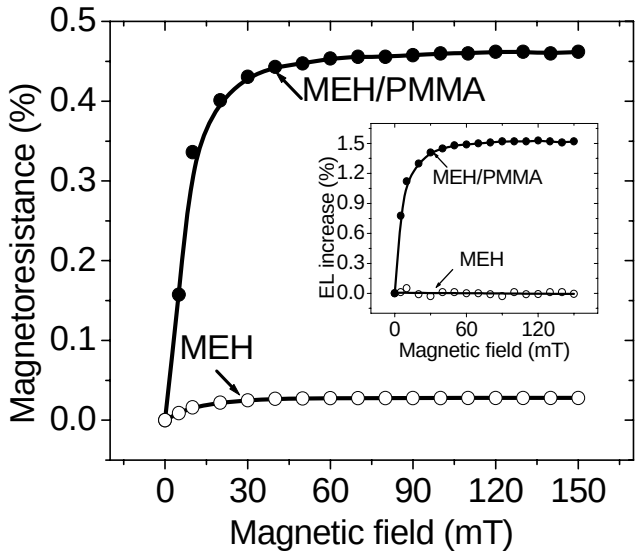


Figure 3.8 Magnetoresistances from double-layer MEHPPV/PMMA (dots) and single-layer MEHPPV (circles) OLEDs with ITO and Au electrodes. Inset shows the MFEs with/out the PMMA layer

magneticfield effect on electroluminescence and magnetoresistance was shown in Figure 3.9. It can be seen that the electroluminescence increases rapidly with magnetic field and gradually saturates at higher field at a value of 2.5%. Magnetoresistance decreases with magnetic field, showing a negative MR, indicating the magnetic field effect on polaron pair dissociation is the dominating process. However, both electroluminescence and resistance have no magnetic field dependence in the ITO/$Ir(ppy)_3$/Al device.

It has been reported that the LUMO and HOMO are 3.2ev and 5.7ev for Alq_3 and 3.0ev and 5.4ev for $Ir(ppy)_3$, respectively[109]. The mutually similar HOMO and LUMO minimize the influence of charge injection on the MFE and MR. Thus the different magnetic behavior should be related to their chemical structures.

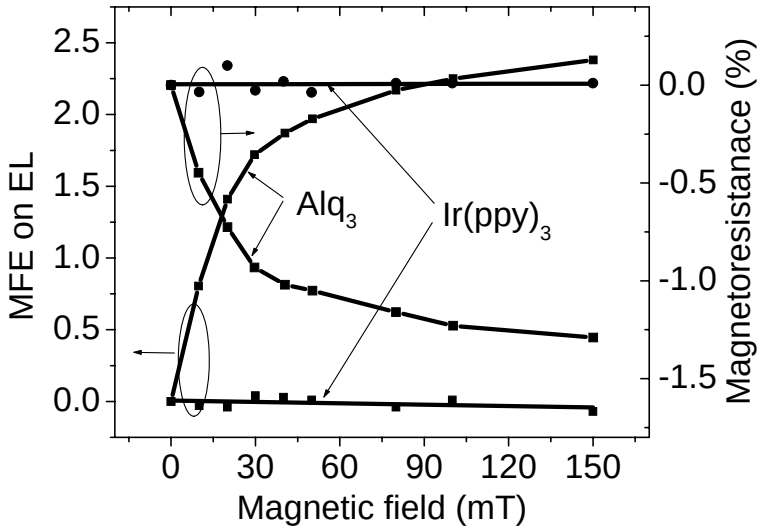


Figure 3.9 Magnetic field effect on electroluminescence and magnetoresistance for Alq3 and Ir(ppy)3 based OLEDs

The major difference for these two molecules is the type of the metal atoms in the center of the chemical structure. The structure was shown in chapter 2. It is known that the phosphorescent $Ir(ppy)_3$ has almost 100% conversion from singlet to triplet exciton through intersystem crossing due to its strong spin orbital coupling. The light emission comes from the triplet excitons.

The spin-orbital coupling has two effects: spin flip, defined as intersystem crossing; and splitting of degenerate triplet levels, named as intrinsic Zeeman Effect. This intrinsic Zeeman Effect is given by the Zeeman parameter D. It is also known that an external magnetic field can split the triplet levels and yield an external Zeeman Effect. The competition between the intrinsic Zeeman Effect and the external Zeeman Effect determines the singlet-triplet intersystem crossing in an external magnetic field. For most

organic materials with aromatic molecular structures, the Zeeman parameter D (intrinsic Zeeman Effect) is about 1~10 μeV[100], showing a weak ~ moderate spin-orbital coupling strength. This small Zeeman parameter suggests that an external magnetic field ranging from 10 mT to 100 mT can cause a significant MFE. For phosphorescent materials such as $Ir(ppy)_3$, the D is usually greater than 100 μeV[11,12]. This large Zeeman parameter implies that a low magnetic field (< 1 Tesla) can not induce an appreciable MFE, as observed in $Ir(ppy)_3$ system.

3.9 Summary

In this Chapter, it is proven that the magnetic field effect on electroluminescence and magnetoresistance are sensitive to spin-orbital coupling of an organic semiconductor due to either internal or external heavy atom effects. These findings further confirm that the MFE and MR are results of magnetic field modified excitonic processes, essentially intersystem crossing in polaron pair states. The lack of magnetic field effects in ITO/$Ir(ppy)_3$/Al further excludes the magnetic field enhanced bipolar injection, reaction yield, and transport mechanisms in this system.

4 TUNABLE MAGNETIC FIELD DEPENDENT ELECTROLUMINESCENCE AND MAGNETORESISTANCE IN FLUORESCENT POLYMER/PHOSPHORESCENT DYE COMPOSITES

4.1 Introduction

It is already known that due to the coexistence of singlet and triplet polaron pairs, fluorescent organic semiconductors can show magnetic field dependent electroluminescence (MFE) and magnetoresistance (MR), caused by a magnetic field modified intersystem crossing. For organic semiconductors, spin-orbital coupling is essentially the determining factor for intersystem crossing. In principle, the magnetic field effect on electroluminescence and magnetoresistance can be gradually tunable if the spin-orbital coupling of the material can be controlled.

As discussed in the former chapters, the spin-orbital coupling can be tuned by at least by the following ways:

1) Incorporating different heavy atoms with a series of atomic numbers into a molecules or polymers.
2) Using different metals with a series of atomic numbers as electrodes
3) Disperse heavy metal particles into the polymer matrix.

Obviously the first method effect requires delicate organometallic reactions to systematically change the spin-orbital coupling strength. It requires tedious synthesis work. For the second method, the low work-function metals used as cathodes usually

have low atomic numbers. Heavy metals, like gold, are seldom used as a cathode since they usually have much higher work-function. Also it does not work for double layer devices, e.g. with an electron transport layer, as frequently used to enhance the OLED performance. For the third method, the insolubility of metal particles together with the large discontinuity of dielectric constant at the material interface creates a significant difficulty in obtaining a uniform dispersion and an effective interfacial interaction in metallic/organic material composites.

In this chapter, a phosphorescent dye $Ir(ppy)_3$ with larger intrinsic spin-orbital coupling was used to dope a polymer PVK with moderate intrinsic spin-orbital coupling strength. The phosphorescent dye $Ir(ppy)_3$ can be easily dissolved in common solvents e.g. chloroform, toluene. Thus an uniform dispersion of $Ir(ppy)_3$ in PVK can be expected. After contact, π electrons in PVK can penetrate into the vicinity of the heavy atom to mix the spin-orbital coupling of the two materials.

4.2 Experimental

The $Ir(ppy)_3$ molecules were mixed with the PVK and PMPV by different weight ratios up to 5wt% in chloroform, respectively, forming $Ir(ppy)_3$ doped polymer composite solutions. The 100 nm thick films of the polymer/$Ir(ppy)_3$ composite or pristine polymers were spin cast on pre-cleaned ITO glass substrates from the respective chloroform solutions. The spin-cast films were then dried under vacuum at 70°C for twelve hours, ensuring the removal of solvent molecules. The uniform dispersion of $Ir(ppy)_3$ molecules in the PVK matrix was monitored by the morphological and electron-dispersion-spectral analyses based on the TEM (transmission electron microscopy) measurements[101]. The

single- and double-layer OLEDs were fabricated with the architectures of ITO/$Ir(ppy)_3$+PVK/Al and ITO/PVK/$Ir(ppy)_3$/Al, respectively, by thermally evaporating aluminum (Al) electrode under vacuum of $2x10^{-6}$ Torr. The magnetoresistance was measured at a constant voltage targeted to the injection current of 20 mA/cm^2 for the OLEDs. The MFE was characterized at both constant voltage and current modes. The magnetic field effect on photocurrent (MFP) is also measured at zero bias with illumination of 330nm light which corresponds to the maximal absorption of PVK.

4.3 Tunable magnetoresistance in $Ir(ppy)_3$ doped polymer composite

It can be seen in Figure 4.1 that the $Ir(ppy)_3$+PVK composite shows an $Ir(ppy)_3$ concentration-dependent negative magnetoresistance at constant voltage, based on the single-layer OLEDs with ITO and Al electrodes. Here, the PVK and $Ir(ppy)_3$ are defined as high and low magnetoresistant materials, respectively. The magnetoresistance includes a rapid increase with the magnetic field from 0 to about 50 mT and then becomes saturated. The maximal magnetoresistance are -4.0 % for the neat PVK, -2.0 % for the PVK doped with 1 wt% $Ir(ppy)_3$, and -1.2 % for the PVK doped with 5 wt% $Ir(ppy)_3$, and negligible value for the neat $Ir(ppy)_3$.

Figure 4.2 shows the electroluminescence enhancement with magnetic field at both constant voltage mode and constant current mode. The maximum of magnetic field effect on electroluminescence for neat PVK is 10%, 6% for voltage mode and current mode, respectively, while the MFE for $Ir(ppy)_3$ is almost zero at either voltage or current mode. The difference between the two modes reflects the values of the magnetoresistance.

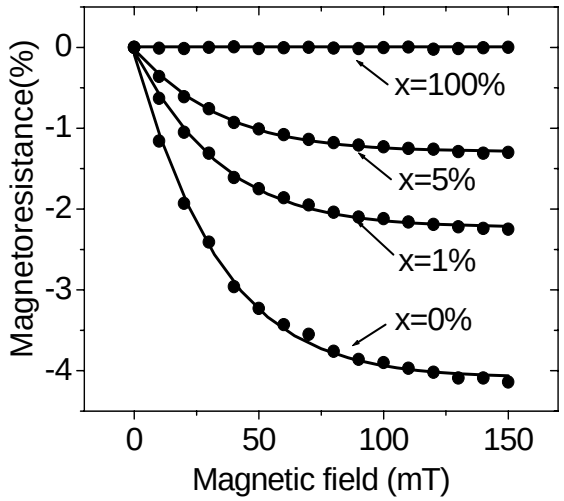


Figure 4.1 Magentoresistance as a function of magnetic field. x is the weight concentration of $Ir(ppy)_3$ dopant in the composite LED of ITO/$Ir(ppy)_3$(xwt%)+PVK/Al.

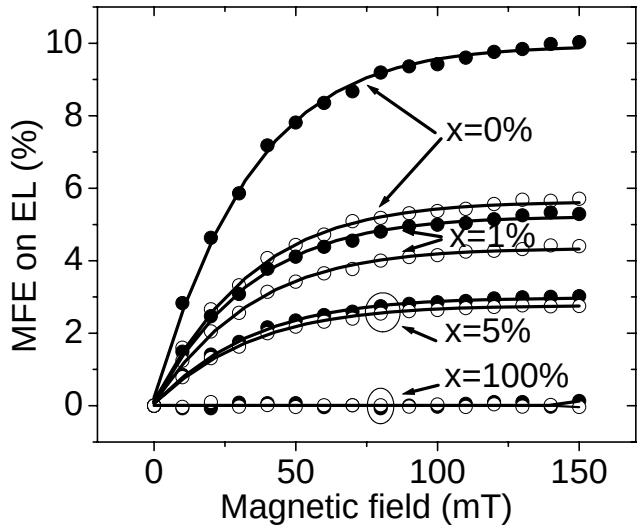


Figure 4.2 MFE from composite at constant voltage (dots) and current (circles). x is the weight concentration of $Ir(ppy)_3$ dopant in the composite LED of ITO/$Ir(ppy)_3$(xwt%)+PVK/Al.

However, in polymer/dyes composites, there are three possible mechanisms, leading to the observed tunable MFE and MR, such as charge transport, energy transfer, and intermolecular spin-orbital interaction, which will be discussed in the following sections.

4.4 Charge transport channel effects on magnetoresistance

The charge transport may be proximately divided into two components through PVK matrix and $Ir(ppy)_3$ dopant in the PVK + $Ir(ppy)_3$ composite OLEDs. These two transport components lead to high and low magnetoresistance channels in a parallel connection [Figure 4.3 (a)]. As a consequence, varying the $Ir(ppy)_3$/PVK ratio could change the relative transport distribution between the high and low magnetoresistance channels and thus yield an $Ir(ppy)_3$ concentration-dependent magnetoresistance in the composites.

When the condition of two parallel PVK and $Ir(ppy)_3$ transport channels is removed by using the double-layer OLED with the architecture of ITO/PVK/$Ir(ppy)_3$/Al [Figure 4.3 (b)], it was observed that the use of the PVK hole-transport layer results in a negative magnetoresistance (Figure 4.4 (a)). The -0.4 % magnetoresistance is obtained when the 50 nm thick PVK hole-transport layer is used. This magnetoresistance decreases with the decrease of the PVK thickness and becomes negligible when the PVK thickness is reduced to 4 nm. Again, the PVK thickness-dependent magnetoresistance can be further suggested by the difference between the MFEs measured at constant voltage and current [Figure 4.4 (b)]. It is evident that the charge transport through two parallel-

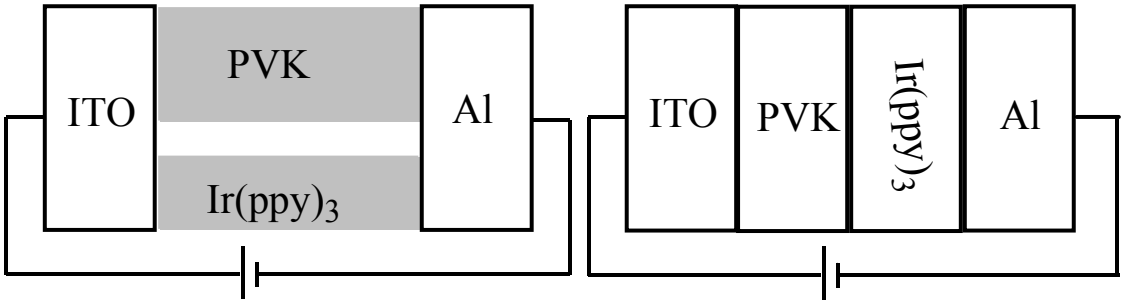


Figure 4.3 Schematic transport channels for the PVK $Ir(ppy)_3$ composite (a)parallel connection and (b) series connection

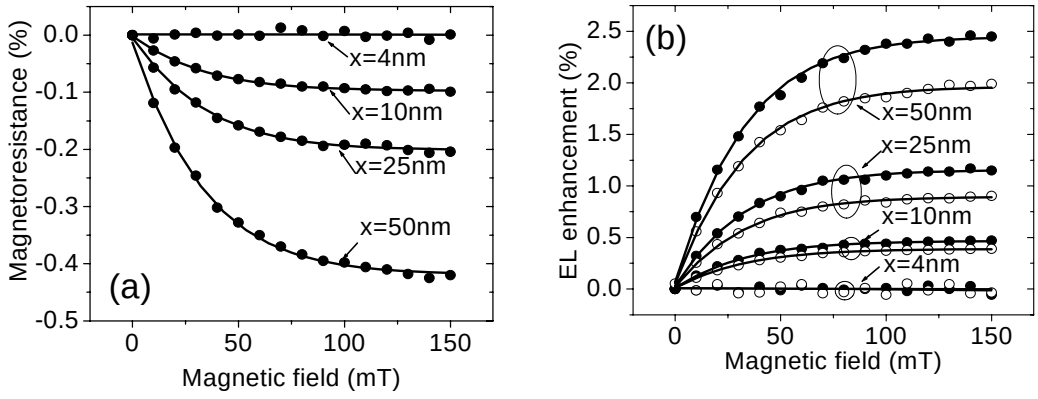


Figure 4.4 (a) Magnetoresistance and (b) magnetic field effect on EL at constant voltage (dots) and current (circles), respectively, in double-layer OLEDs of ITO/PVK(xnm)/$Ir(ppy)_3$(80nm)/Al. x is the thickness of PVK layer

magnetoresistance channels is not accountable for the $Ir(ppy)_3$ concentration-tunable magnetoresistance. In addition, the result from the magnetoresistance of the double-layer OLED implies that the intermolecular interaction is formed at the PVK/$Ir(ppy)_3$ layer interface and consequently affects the magnetoresistance

4.5 Energy transfer effects on magnetoresistance

In fluorescent polymer/phosphorescent dye composites, there two possible energy transfer channels from the polymer matrix to dye molecules: Förster energy transfer and Dexter energy transfer. Förster energy transfer is a dipole-dipole mechanism and its transfer rate can be expressed as

$$k_{D\to A} = \frac{K^2 J 8.8\times 10^{-28}}{n^4 \tau_0 r^6} \qquad \text{Equation 4.1}$$

where K is an orientation factor, n is the refractive index of the medium, τ0 is the radiative lifetime of the donor, r is the distance between donor (D) and and acceptor (A), and J the spectral overlap between the absorption spectrum of the acceptor and the fluorescence spectrum of the donor[102]. Dexter energy transfer occurs through an electron exchange mechanism and its rate can be expressed by

$$k_{ET} \propto [h/(2\pi)]P^2 J \exp[-2r/L] \qquad \text{Equation 4.2}$$

where r is the distance between donor (D) and acceptor (A), L and P are constants, J is the spectral overlap integral. It can be seen both Förster and Dexter energy transfer require spectral overlap J between the absorption spectrum of the acceptor and fluorescence spectrum of the donor. However, Förster energy transfer is a long range interaction while the Dexter energy transfer only occurs at short range.

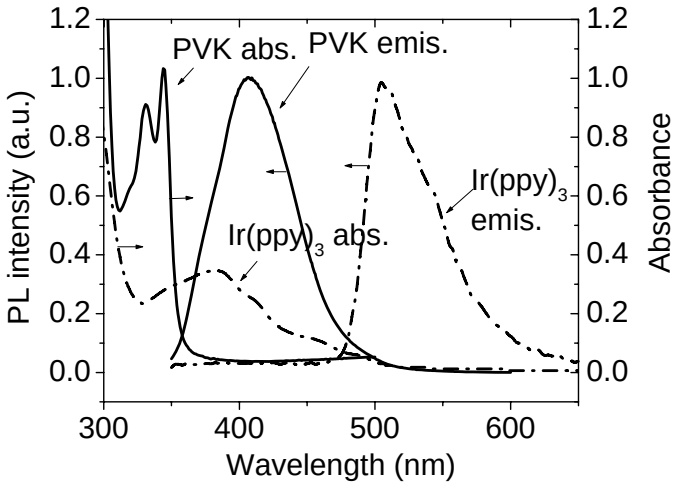


Figure 4.5 Normalized emission spectra and absorption spectra for PVK and $Ir(ppy)_3$

4.5.1 Energy transfer-dependent magnetic field effect on electroluminescence

Figure 4.5 shows the normalized emission spectra and absorption spectra for PVK and $Ir(ppy)_3$. It can be seen that there are a larger overlap between the emission spectrum of PVK and absorption spectrum of $Ir(ppy)_3$. Thus In PVK/$Ir(ppy)_3$ system, energy transfer occurs from the PVK to $Ir(ppy)_3$ through Förster and Dexter processes[103,104,105] (Figure 4.6) when PVK chains and $Ir(ppy)_3$ molecules are placed within a close proximity in either composite or double-layer structure. Energy transfer can shift magnetic field effects between different components in a polymer composite. It can be seen in Figure 4.2 that the electro-phosphorescence from $Ir(ppy)_3$ dopant shows a significant magnetic field dependence in the PVK/$Ir(ppy)_3$ composite while the neat $Ir(ppy)_3$ does not exhibit an appreciable MFE, due to large spin-orbital coupling. When the weak-spin-orbital-

coupling PVK and strong-spin-orbital-coupling $Ir(ppy)_3$ are mixed, the magnetic field-increased singlets in the PVK matrix can be reflected as an magnetic field-increased triplets in the $Ir(ppy)_3$ dopant due to Förster and Dexter transfer, especially in the case where the Förster transfer becomes dominant at distance of greater than 1 nm between an excited PVK and an unexcited $Ir(ppy)_3$ (Figure 4.6). This energy transfer-dependent MFE can occur in composite or double-layer structure when the PVK chains and $Ir(ppy)_3$ molecules are in close contact (Figure 4.2 and Figure 4.4 (b)). As a result, the long-distance Förster and short-distance Dexter energy transfer essentially form a mechanism to induce magnetic field-dependent singlet/triplet ratio in a strong-spin-orbital-coupling phosphorescent dopant through a weak-spin-orbital-coupling polymer matrix based on polymer phosphorescent dye composite.

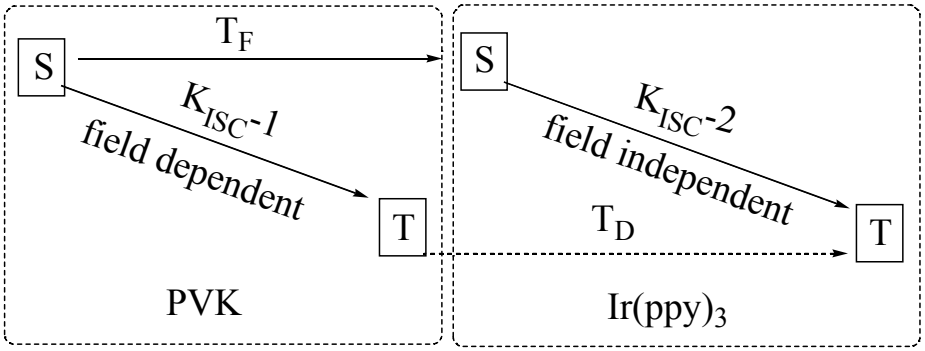


Figure 4.6 Intersystem crossing and (Förster T_F and Dexter T_D) energy transfer in the PVK + $Ir(ppy)_3$ composite. K_{ISC}-1 and K_{ISC}-2 are magnetic field independent and independent intersystem crossing in PVK matrix and $Ir(ppy)_3$ dopant, respectively

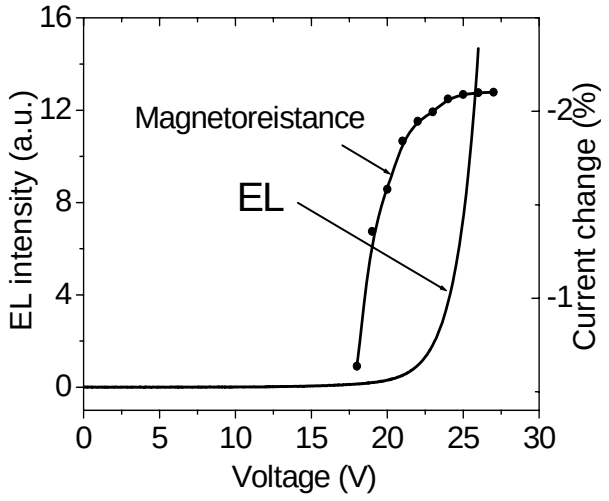


Figure 4.7 Voltage-dependent magnetocurrent and EL intensity in PVK/ (1wt%)Ir(ppy)$_3$ composite LED. The magnetoresistance was measured at the field of 150 mT.

4.5.2 Energy transfer-dependent magnetoresistance

We further note that the redistribution of singlet/triplet ratio in excited states between the weak-spin-orbital-coupling polymer matrix and the strong-spin-orbital-coupling Ir(ppy)$_3$ dopant can lead to a substantial tuning of magnetoresistance when the excited states contribute to the magnetic field effects. Figure 4.7 shows that the magnetoresistance dramatically decreases when the applied bias is lower than the threshold voltage for generating electroluminescence in PVK + Ir(ppy)$_3$ composite. This voltage-dependent magnetoresistance can be observed in other organic semiconducting materials as shown in chapter 2 [106]. Nevertheless, it can be supported from the

experimental results in Figure 4.7 that the excited states significantly contribute to the magnetoresistance.

4.6 Intermolecular spin-orbital interaction

We now consider the intermolecular spin-orbital interaction in $Ir(ppy)_3$ doped polymer composite by comparing magnetoresistance and MFE observed in an energy-transfer and non-energy-transfer polymer/$Ir(ppy)_3$ composites. In general, the delocalized π electrons in polymer matrix can penetrate into the large field of molecular orbit of heavy-metal complex when the polymer chains and $Ir(ppy)_3$ molecules are brought into contact[94,95]. This penetration leads to an intermolecular spin-orbital interaction between the spin dipoles of polymer matrix and the orbital dipoles of $Ir(ppy)_3$ dopant, modifying the effective spin-orbital coupling of polymer matrix in the composite. Therefore, mixing a strong-spin-orbital-coupling molecule and a weak-spin-orbital-coupling polymer forms a mechanism to adjust polymer spin-orbital coupling strength.

4.6.1 Energy transfer system

When both fluorescence from the PVK matrix and the phosphorescence from the $Ir(ppy)_3$ dopant are observed in the dilute PVK + (0.3wt%)$Ir(ppy)_3$ composite (Figure 4.8 (a)), it can be seen in Figure 4.8 (b) that the $Ir(ppy)_3$ dispersion slightly decreases the fluorescence-based MFE amplitude of the PVK matrix as compared to the value of neat PVK. The MFE amplitudes are 5.6% and 5.1% for the neat and 0.3wt% $Ir(ppy)_3$ doped PVK OLEDs, respectively (Figure 4.8 (b)). This experimental result suggests that the $Ir(ppy)_3$ dopant enhances the spin-orbital coupling of PVK matrix. The enhanced spin-

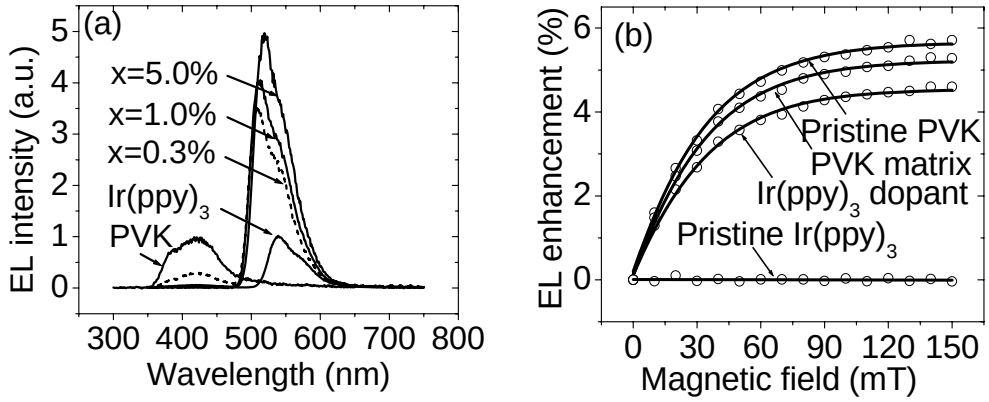


Figure 4.8 Electroluminescence spectra of pristine PVK, pristine $Ir(ppy)_3$, and PVK + (x%)$Ir(ppy)_3$ composite LEDs. (b) Fluorescence- and phosphorescence-based MFEs from PVK matrix and $Ir(ppy)_3$ dopant in the dilute PVK + (0.3wt%)$Ir(ppy)_3$ composite. The MFEs from pristine PVK and $Ir(ppy)_3$ are also shown as reference.

orbital coupling further competes with the magnetic field in intersystem crossing and thus results in a reduction of fluorescence-based MFE from the PVK matrix. The reduction of fluorescence-based MFE in the PVK matrix can be then reflected as a decrease of phosphorescence-based MFE in the $Ir(ppy)_3$ dopant through dominant Förster energy transfer from the PVK matrix to the $Ir(ppy)_3$ dopant in their composite.

4.6.2 Non-energy transfer system

Furthermore, when the PVK is replaced by poly(m-phenylenevinylene-co-2,5-dioctyloxy-p-phenylenevinylene) (PMPV), the negligible spectral overlap between the emission of PMPV and the absorption of $Ir(ppy)_3$ (Figure 4.9) indicates that the dominant Förster transfer is significantly reduced in the PMPV + $Ir(ppy)_3$ composite.

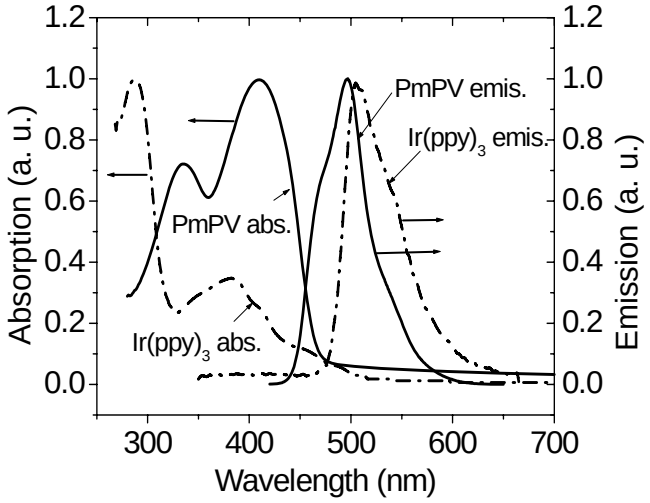


Figure 4.9 Normalized emission spectra and absorption spectra for PmPV and $Ir(ppy)_3$

Figure 4.10 shows that the MFE slightly decreases with the $Ir(ppy)_3$ concentration. The MFE amplitude changes from 6.0% for neat PMPV to 5.6% for 5wt% $Ir(ppy)_3$ doped PMPV. The emission spectra in Figure 4.9 indicates that the PMPV and $Ir(ppy)_3$ emit in a similar spectral range. Hence, the MFE observed from the composite should be associated with both fluorescence from PMPV matrix and phosphorescence from $Ir(ppy)_3$ dopant. We know that the relative ratio between the fluorescence- and phosphorescence-based MFE amplitudes is determined by the energy transfer in the $Ir(ppy)_3$ doped polymer composite. Since the energy transfer is minimized in the PMPV/$Ir(ppy)_3$ composite, the observed MFE should be mainly due to the dependence of magnetic field on intersystem crossing in the PMPV matrix. Therefore, the experimental data of $Ir(ppy)_3$ concentration-dependent MFE in Figure 4.10 provides an additional experimental-

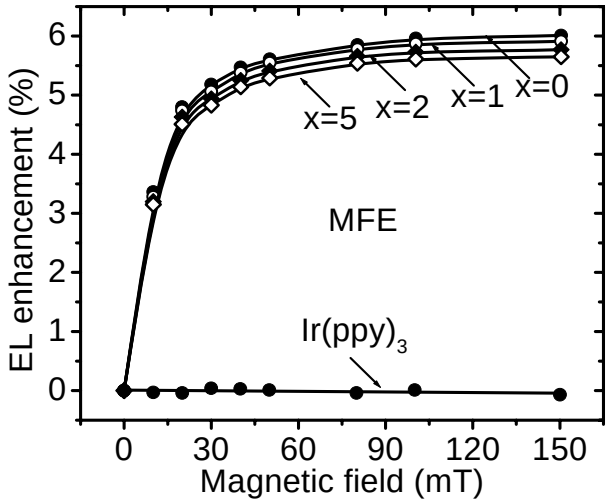


Figure 4.10 Magnetic field effect on electroluminescence in ITO/PmPV/Al based on the PmPV/$Ir(ppy)_3$ composites. x% represents the concentration of $Ir(ppy)_3$ in PmPV

evidence that the spin-orbital coupling of polymer matrix can be enhanced due to the intermolecular magnetic interaction upon the $Ir(ppy)_3$ dispersion. It is interesting to note that the dispersed $Ir(ppy)_3$ only slightly decreases the magnetoresistance in this non energy-transfer composite (Figure 4.10). The magnetoresistance decreases from 2.3 % for neat PMPV to 2.0 % for 5wt% $Ir(ppy)_3$ doped PMPV. This result further indicates that the so called high and low magnetoresistance channels do not play an important role in tuning magnetoresistance when strong-spin-orbital-coupling molecules are uniformly dispersed in a weak-spin-orbital-coupling polymer matrix.

Clearly, the relative distribution of excited states through energy transfer can lead to a substantial tuning of magnetic field effects in $Ir(ppy)_3$ doped polymer composite. As a result, the comparison between the magnetic field effects measured from the non energy transfer PMPV + $Ir(ppy)_3$ and energy-transfer PVK + $Ir(ppy)_3$ composites (Figures. 4.1-

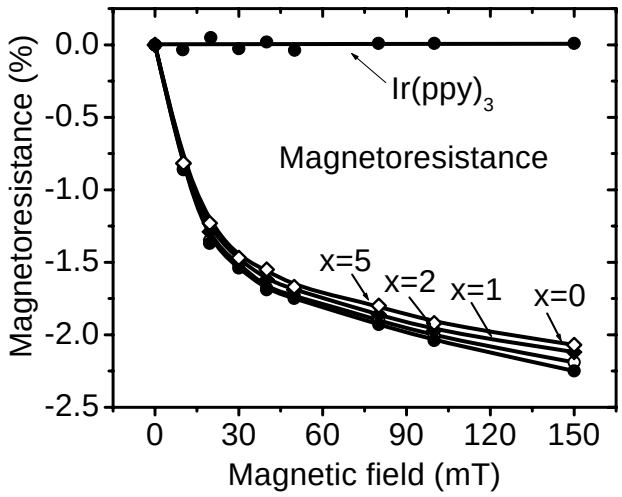


Figure 4.11 Magnetoresistances from PMPV + (x%)$Ir(ppy)_3$ composite OLEDs

and 4.4) shows that the energy transfer and intermolecular spin-orbital interaction[106,107] play rough and fine tuning for the MR and MFE when a strong-spin-orbital-coupling $Ir(ppy)_3$ and a weak-spin-orbital-coupling polymer are mixed.

4.7 Magnetic field effect on photocurrent

We now discuss how excited states and spin-orbital coupling can affect the magnetoresistance in organic semiconducting materials. It can be seen in Figure 4.12 that an external magnetic field increases the photocurrent, generating a magneto-photocurrent in the $Ir(ppy)_3$+PVK composite. The photocurrent quickly increases with the magnetic field from 0 to about 50 mT and is then saturated. This photocurrent enhancement can be attributed to the magnetic field-increased singlet electron-hole pairs in the PVK matrix due to the external Zeeman effect [108,109], based on the fact which the dissociation of -

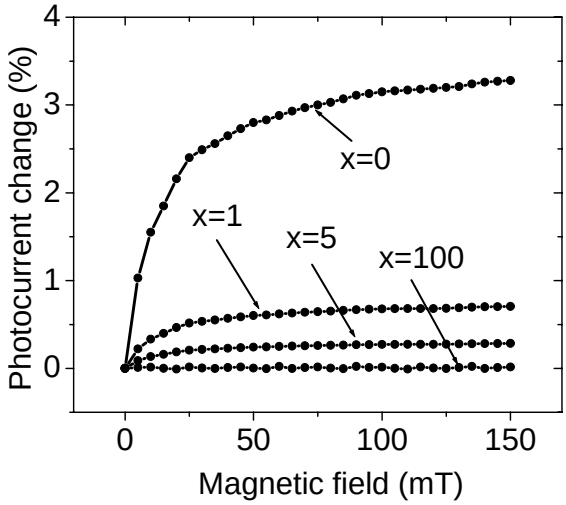


Figure 4.12 Photocurrent as a function of magnetic field in the composite OLEDs of ITO/Ir(ppy)3(xwt%)+PVK/Al under the light illumination of 0.1 mW/cm2 at 330 nm

singlet electron-hole pairs is largely greater than that of the triplet electron-hole pairs in bulk materials[83,108]. In particular, we should note that the magnetic field-induced photocurrent enhancement decreases with increasing the $Ir(ppy)_3$ concentration, showing a concentration-tunable magneto-photocurrent in the $Ir(ppy)_3$+PVK composite. The magnetic field-induced photocurrent enhancements are 3.6 % for the neat PVK, 0.8 % for 1 wt% $Ir(ppy)_3$ doped PVK, 0.3 % for 5 wt% $Ir(ppy)_3$ doped PVK, and 0 % for the neat $Ir(ppy)_3$

4.8 Possible mechanism for the dye-doping-tunable magnetic field effect on EL and magnetorsistance

When the magnetoresistance is taken into account, the dissociated charge carriers can be drifted to the interfaces between the $Ir(ppy)_3$ and PVK components in the-

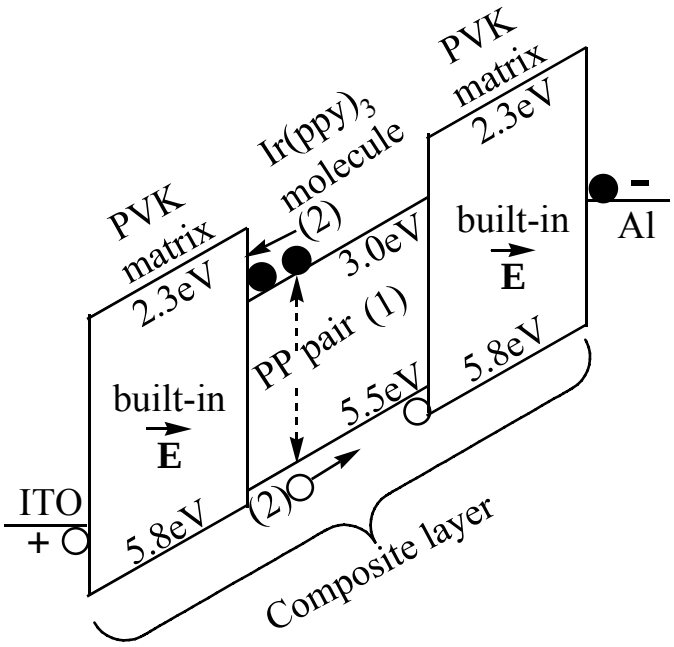


Figure 4.13 Formation of built-in electric field due to the dissociation of electron-hole pairs in $Ir(ppy)_3$+PVK composite OLED

PVK/$Ir(ppy)_3$ composite OLED under the influence of applied bias, forming a built-in electric field applied on the PVK, as shown in Figure 4.13. This built-in electric field can further tilt the energy bands of the PVK and consequently enhances the electron and hole injection into the PVK matrix, leading to a negative magnetoresistance in the $Ir(ppy)_3$+PVK composite. On the other hand, the $Ir(ppy)_3$ reduced enhancement of magneto-photocurrent suggests that an external magnetic field has less effects on the density of singlet states upon dispersing $Ir(ppy)_3$ in the composite. This can be attributed to the increase of spin-orbital coupling of PVK matrix caused by $Ir(ppy)_3$ dopant. The increase of spin-orbital coupling can reduce the effects of magnetic field on the singlet/triplet ratio. As a consequence, the modification of spin-orbital coupling can

affect the density of dissociated charge carriers and the resultant magnetoresistance in organic materials.

4.9 Summary

In summary, mixing a strong-spin-orbital-coupling molecule and a weak-spin-orbital-coupling polymer can lead to a substantial tuning of magnetoresistance and MFE. The underlying mechanism of tuning magnetoresistance and MFE relies on the energy transfer of excited states between the two components and the modification of spin-orbital coupling in $Ir(ppy)_3$ doped polymer composite. The magneto-photocurrent implies that the dissociation of excited states contribute to the magnetoresistance in organic semiconducting materials. The energy transfer and modification of spin-orbital coupling can change the overall singlet/triplet ratio and consequently affect the yield of dissociated charge carriers. Furthermore, the dissociated charge carriers form built-in electric field and contribute to the magnetoresistance in organic semi-conductive materials. As a result, mixing a strong-spin-orbital-coupling molecule and a weak-spin-orbital-coupling polymer presents a new pathway to tune magnetic field effects (magnetoresistance and MFE) through energy transfer and intermolecular spin-orbital interaction.

5 BIPOLAR INJECTION EFFECTS ON MFE AND MR

5.1 Introduction

Magnetic field effect on electroluminescence (MFE) and magnetoresistance (MR) are essentially related to the magnetic field modified intersystem crossing in polaron pair states. It has been shown that MFE and MR depends on the competition of enhanced polaron pair dissociation and reduced triplet-charge reaction processes. In the system showing negative MR, the polaron pair dissociation process is dominating, while the positive MR system, the triplet-charge reaction is the dominating processes. In previous chapters we focused on the manipulation of intersystem crossing to tune the magnetoresistance and magnetic field effect on electroluminescence. In principle, without change the intersystem crossing, magnetoresistance still can be also manipulated by enhancing or reducing the contribution from triplet-charge reaction process. As we know, triplet-charge reaction can be effectively controlled by varying the ratio of injected electrons and holes. In the ideal case, the ratio of electron and hole is 1 (completely balanced) and the triplet-charge reaction would be the minimum. On the contrary, if the charge injection is unbalanced, the triplets will have more chance to collide with free charges, either electrons or holes. The triplet-charge reaction should be more significant.

Based on this concept, a PMMA insulating layer was used to be inserted between semiconductor layer and an electrode to increase the charge injection barriers for one type charge and leave the other unchanged. Therefore, the balancing degree of injected

electrons and holes can be effectively controlled by simply increasing or decreasing the thickness of the insulating layer in the double-layer organic light emitting diodes.

In this chapter, three different semiconductors, MEH-PPV, PVK, and Alq_3 were selected to prove the feasibility of this concept. MEH-PPV based devices work at both forward and bias. Thus it enables us to study bipolar injection effects at both electron dominating and hole-dominating cases for the same device by simply changing polarity. PVK and alq_3 were selected because they are good representatives for hole transport[110] and electron transporting materials[111], respectively.

5.2 Experimental

The MEH-PPV or PVK layer was deposited onto pre-cleaned glass by spin coating from its chloroform solution. The PMMA layer was spun cast on top of deposited MEH-PPV or PVK layer from its nitromethane solution. Nitromethane cannot dissolve the MEH-PPV and PVK, ensuring the first layer undestroyed. The film thicknesses were characterized by DekTek-II surface profiler. The gold (Au) or aluminum (Al) electrode was prepared by thermal evaporation at a vacuum of $2x10^{-6}$ Torr. To fabricate the ITO/PMMA/Alq_3 or $Ir(ppy)_3$/Al devices, the PMMA layer was first deposited on ITO glass followed by formation of Alq_3 or $Ir(ppy)_3$ thin film through thermal evaporation. Thermal evaporation of 20nm Al electrode finishes the fabrication of the device. The MR was measured at constant voltage adjusted to the injection current of 20 mA/cm^2 and the MFE was measured at either constant voltage or current mode (constant 20 mA/cm^2) for the related OLEDs in liquid nitrogen temperature.

5.3 Modification of bipolar injection by changing bias polarity

The device structure and energy diagram was shown in Figure 5.1. Au was selected as the electrode because it has a work function of 5.1ev[112] close to that of ITO and in the ITO and Au sandwiched single layer MEH-PPV device, the bipolar injections at forward and reverse bias are similar. Then a thin insulating (PMMA) layer was inserted between MEH-PPV layer and Au electrode to reduce electron injection at forward bias and hole injection at reverse bias to tune the electron/hole ratio and triplet-charge reaction accordingly.

Figure 5.2 shows the MR of ITO-Au sandwiched MEH-PPV/PMMA double layer OLED under a current density of 20mA/cm^2 at liquid nitrogen temperature. As shown in Figure 5.2, the MR at forward bias has a small positive value. After insertion of PMMA, the magnitude of MR at forward bias increases with the thickness of PMMA from 0.03%-

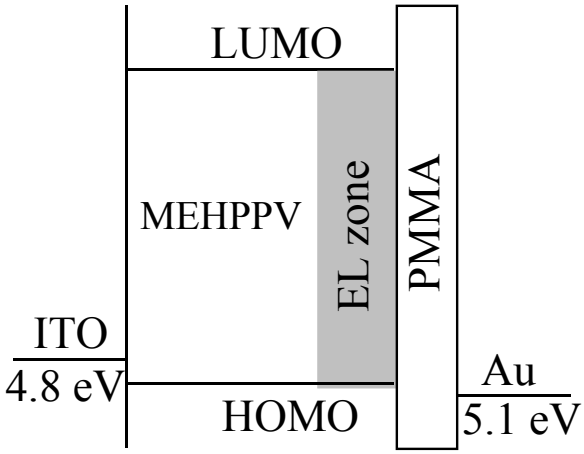


Figure 5.1 Structure of ITO/MEH-PPV/PMMA/Au OLED. Varying the thickness of PMMA layer changes the bipolar injection, hence, the ratio of electrons and holes

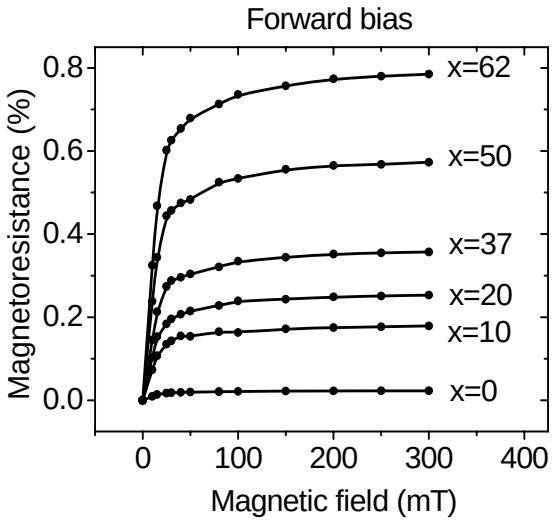


Figure 5.2 Forward magnetoresistance as a function of magnetic field for the double-layer ITO/MEHPPV/PMMA(xnm)/Au OLEDs

at 0nm PMMA to 0.78% at 62nm PMMA. At reverse bias, after insertion of 10nm PMMA, MR changes sign from positive to negative. The value of the negative MR increases with PMMA thickness to -1.09% at 37nm and then decreases with PMMA thickness to -0.43% at 62nm (Figure 5.3). The devices break down with further increasing PMMA film thickness.

The PMMA layer between MEH-PPV layer and Au electrode could cause two consequences: enhanced interfacial resistance and modified bipolar injection

5.3.1 Enhanced interfacial resistance

It is possible that the insertion of PMMA accentually enhanced interface resistance since PMMA is insulating. In the literature, MR was proposed to be a bulk effect[80] and it can be expressed as

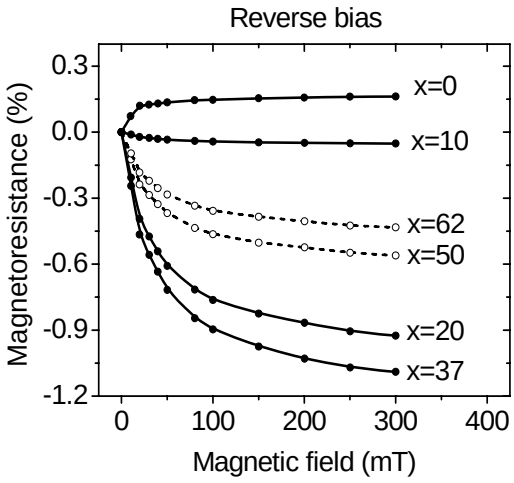


Figure 5.3 Reverse magnetoresistance as a function of magnetic field for the double-layer ITO/MEHPPV/PMMA(xnm)/Au OLEDs

.

$$MR = \frac{\Delta R_b}{R_b + R_i} \times 100\% \qquad \text{Equation 5-1}$$

where ΔR_b is magnetic field caused resistance change in bulk, R_b is bulk resistance, and R_i is interfacial resistance. Therefore, insertion of PMMA layer actually increase R_i, as a result the magnitude of MR should decrease. However, the MR actually increases with the thickness of PMMA at forward bias which suggests that enhanced interface resistance is unlikely the reason causing the observed MR change.

5.3.2 Modified bipolar injection

As we know, PMMA is a electronically insulating material[113], it increases electron injection and hole injection barriers at forward and reverse bias, respectively (Figure 5.4). Therefore, insertion of PMMA reduces the electron/hole ratio further in ITO/MEH-

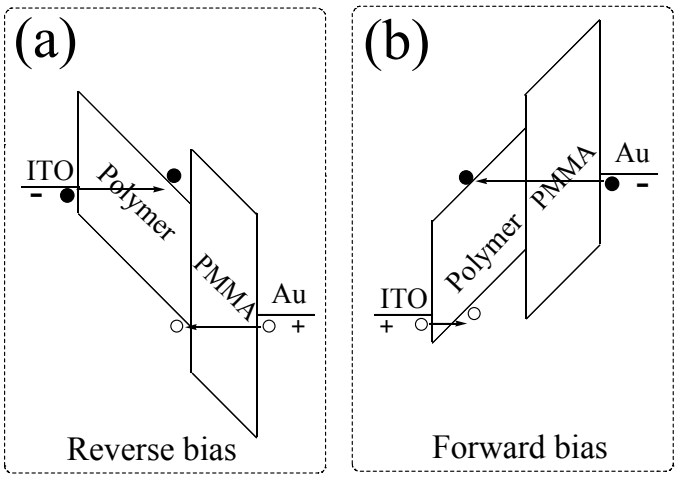


Figure 5.4 Band diagrams for reverse (a) and forward (b) charge injection in the double-layer ITO/MEH-PPV/PMMA/Au OLED. Dots and circles are electrons and holes

PPV/PMMA/Au devices at forward bias. Hence, the triplet charge-triplet reaction process becomes even more dominating, leading to a larger positive MR as observed in the experiment. At reverse bias, a thin PMMA layer reduces hole injection and charge injection is more balanced although both charge injection are difficult. Consequently, magnetic field effect on charge-triplet reaction process become less important and the magnetic field dependent polaron pair dissociation process becomes more dominating, causing more negative MR. However, further increasing PMMA thickness causes a transition from hole-dominating current to electron-dominating current, leading to unbalanced charge injection again. As a result, the MR becomes less negative, which is also observed in our experiments.

Organic semiconductors can be divided into two types: hole transport materials and electron transport materials. In hole transport materials, hole has much larger mobility than electron while in electron transport materials, electron has larger mobility[110,111]. To

further test the validity of this model, the electron injection and hole injection were manipulated in the hole transport materials PVK and electron transport materials Alq_3 based OLEDs, respectively.

5.4 Modification of bipolar injection by reducing electron injection

The structure and energy diagram of ITO/PVK/PMMA/Al is shown in Figure 5.5. The MRs in different PMMA thickness OLEDs were shown in Figure 5.6. It can be seen that with insertion of PMMA layer, the negative MR is gradually changed from -1.17% without PMMA layer to +1.49% with 25nm PMMA layer at 300mT. The devices failed to work with further thicker PMMA layer. The sign of MR changes from negative to positive when the PMMA thickness is 15nm. The HOMO and LUMO for PVK are 5.8eV and 2.3 eV[114], respectively. The injection barriers for hole injection is 1.0ev, similar to that for electron injections 0.9ev. The charge injection is relatively balanced even though electron and hole have different mobility. Therefore, in ITO/PVK/Al single-layer device, the magnetic field effect on polaron pair dissociation process still outweighs the triplet-charge reaction process, showing a negative MR. After insertion of PMMA, electron injection becomes even more difficult and triplet-hole reaction gradually becomes the dominating process and the MR gets more positive as observed in our experiment.

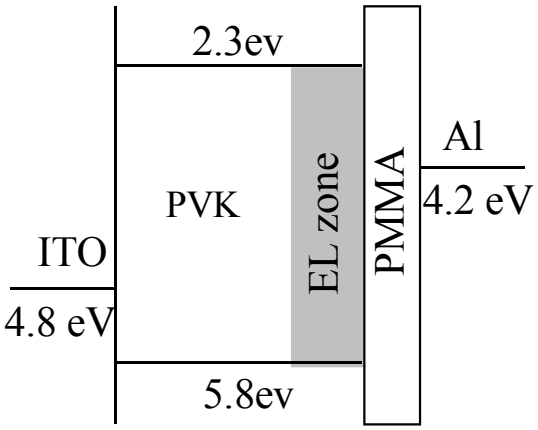


Figure 5.5 Band diagram for the ITO/PVK/PMMA/Al OLED

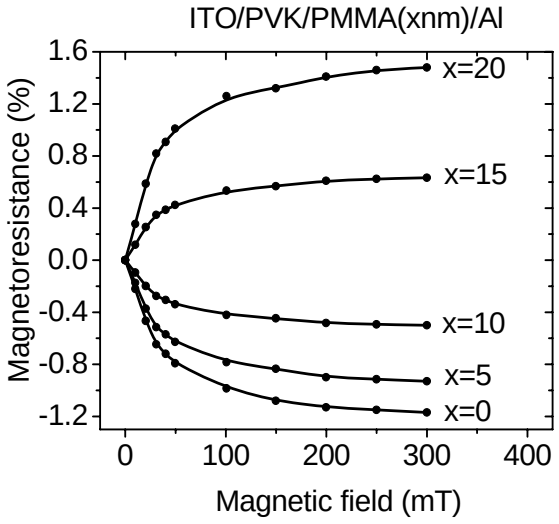


Figure 5.6 Magnetoresistance as a function of magnetic field for the ITO/PVK/PMMA(xnm)/Al double-layer OLEDs

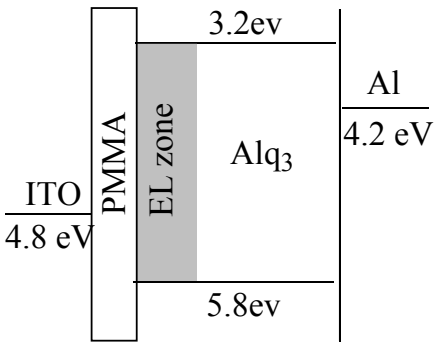


Figure 5.7 Band diagram for the OLED of ITO/ PMMA / Alq_3/Al

5.5 Modification of bipolar injection effect by reducing hole injection

For the Alq_3 based OLED, The PMMA layer was inserted between anode and Alq_3 layer to tune the hole injection barrier (Figure 5.7). Without PMMA, the MR shows a small negative value at liquid nitrogen temperature, consistent with other groups[81]. Insertion of PMMA layer reduces hole injection and the current becomes more electron dominating. This transition from negative MR to positive MR occurs in the device with a 5-10 nm thick PMMA layer. Further increasing the thickness of PMMA layer, the contribution of triplet-electron reaction outweighs that from the dissociation process, leading to a positive MR as shown in Figure 5.8.

Combined study of MEH-PPV, PVK, and Alq_3 based devices confirms that there are two processes determining the sign and magnitude of magnetoresistance. It requires very balanced charge injection to minimizing the positive contribution from the triplet-charge reaction. For positive MR, it requires unbalanced charge injection to enhance triplet charge reaction. Practically it is relatively difficult to obtain balanced charge injection especially for single layer devices. Therefore the utilization of positive MR may have more practical advantages, e.g. easy fabrication, low cost, larger magnitudes.

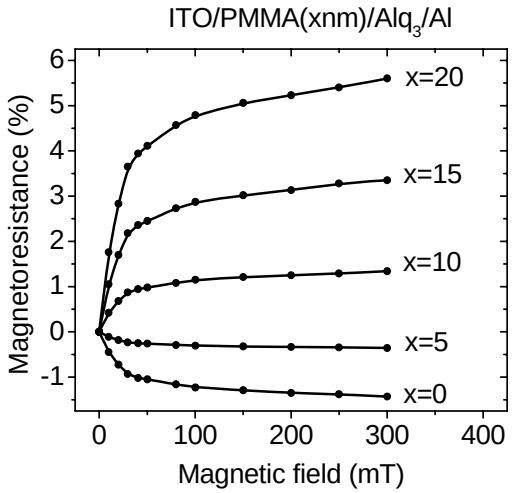


Figure 5.8 Magnetoresistance as a function of magnetic field for the ITO/ PMMA(xnm)/Alq_3/Al double-layer OLEDs

5.6 Investigation of possible change of the triplet-charge reaction constant

Triplet-charge reaction can be expressed as

$$r_{T-C} = k_{T-C}[T][C] \qquad \text{Equation 5.2}$$

where k_{T-C} is the triplet-charge reaction rate constant, [T] is the triplet polaron pair population and [C] is free charge population including either electron or hole[92]. Accordingly, there are two possibilities for an external magnetic field to change the triplet-charge reaction: the change of reaction constant k_{T-C} and the change of triplet polaron pair population [T].

It is known that magnetic field has a negligible effect on the singlet-triplet intersystem crossing in phosphorescent materials (Figure 3.10). Therefore, the phosphorescent dye $Ir(ppy)_3$ was used as a control experiment to investigated the issue: whether or not the reaction constant k_{T-C} can change at different levels of [C] in the presence of an external magnetic field. In this system, the only possible varying parameter would be k_{T-C} since [T] is a constant. Any change in MR with different thickness of PMMA would directly lead to the change of k_{T-C}.

For simplicity, Figure 5.9 only shows the MR for the devices with 0nm and 20nm PMMA layers. It is clearly that MR does not change with the thickness of PMMA. It supports that the bipolar injection has a negligible effect on MR if the triplet polaron pair population keeps constant. Therefore, it can be concluded that the magnetic field caused triplet population [T] change is the main reason for the change of triplet-charge reaction, while the reaction constant k_{T-C} does not change with the magnetic field.

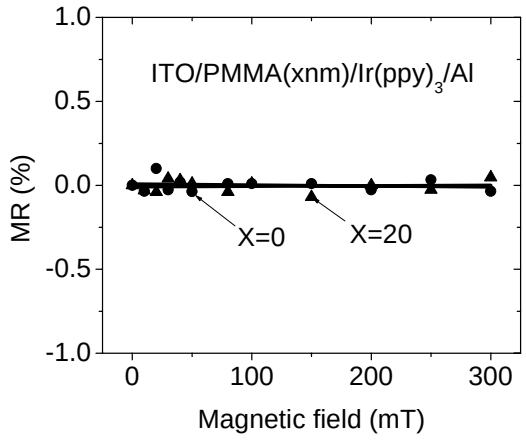


Figure 5.9 Magnetoresistance as a function of magnetic field for the ITO/ PMMA(xnm)/$Ir(ppy)_3$/Al double-layer OLEDs

5.7 bipolar injection effects on MFE

It has been shown that bipolar injection has strong influence on both sign and magnitude of magnetoresistance due to modified triplet-charge reaction. It seems that the bipolar injection would not have any effect on the population of singlets and the electroluminescence would only change with magnetic field through the intersystem crossing. The magnitude of MFE, would keep constant when the triplet-charge reaction varies. However, in an OLED, the generated secondary electrons and holes through triplet-charge reaction still have chance to recombine and give off light emission. The fraction of this secondary electroluminescence in the total electroluminescence depends on how severe of the triplet-charge reaction is.

It is known that triplets are split in to three components by a magnetic field and the three components are unevenly populated because of their different decay rates. As a result, in the presence of magnetic field the secondary electrons and holes are essentially spin polarized after they react with one component of the triplets preferentially. The spin polarized electrons and holes facilitate the formation triplet polaron pairs and triplet excitons in the expense of singlets. Thus, it can be expected that triplet-charge reaction reduces the electroluminescence, leading to a negative MFE.

In principle, the MFE is also determined by two processes with opposite contributions: magnetic field enhanced singlets and triplet-charge reaction caused reduction of singlets. In this section, the bipolar injection effects this electroluminescence were investigated in both hole transport material, PVK and electron transport material, Alq_3 to prove this concept.

5.7.1 Bipolar injection effects on MFE in a hole transport material

ITO/PVK/PMMA/Al devices were fabricated and test by same methods as in section 5.2. Figure 5.10 shows electroluminescence intensity increases rapidly at low magnetic field and gradually saturates at around 100mT at constant current density of 20mA/cm^2 for the devices with 0, 5, 10nm PMMA layer. The magnitude of MFE changes with the PMMA thickness from 7.8% for the device without PMMA to -4% for 20nm PMMA device. The MFE changes sign at a PMMA layer thickness between 10 to 15nm. Figure 5.11 shows magnetic field effects on EL intensities of 5nm, 20nm PMMA devices at constant voltage or current mode, as representatives of positive and negative MFE, respectively. At constant voltage mode, the voltage is targeted to a current density of 20mA/cm^2 at zero field which is same as that at constant current mode. For 5nm PMMA devices the shapes of MFE on EL at current and voltage modes are similar, but the magnitude at voltage mode is 1.0% larger than that of current mode at 3000Oe, however, the value is 1.4% smaller for the 20nm PMMA device than that of corresponding current mode. The values are roughly same as the value of magnetoresistance (Figure 5.6), supporting the equation 2-1.

5.7.2 Bipolar injection effects on MFE in an electron transport material

MFEs for ITO/PMMA/Alq_3/Al OLEDs were shown in Figure 5.12. The electroluminescence for single layer alq_3 device increases quickly with magnetic field at low field range (<30mT) and gradually saturates at higher field. The magnitude of MFE on EL is 2.63% at constant current density of 20mA/cm^2, consistent with the results-

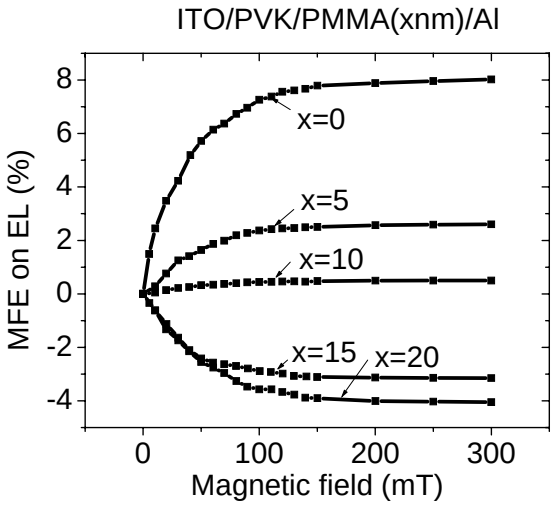


Figure 5.10 Magnetic field dependent electroluminescence for the ITO/PVK/PMMA(xnm)/Al OLEDs

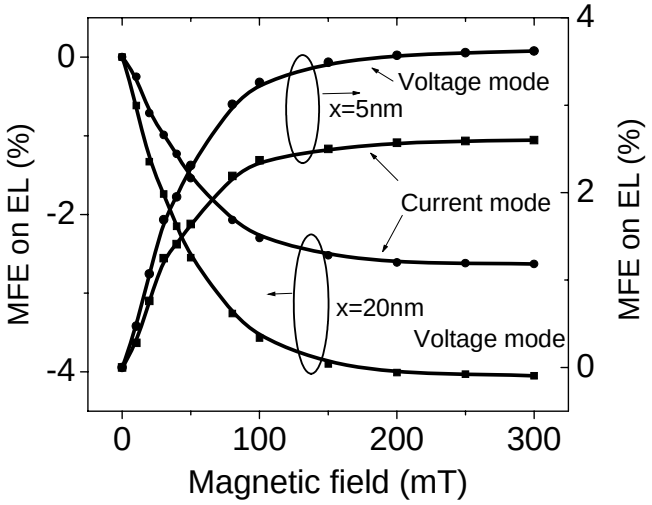


Figure 5.11 Magnetic field effects on electroluminescence at voltage mode and current mode for ITO/PVK/PMMA(xnm)/Al OLEDs

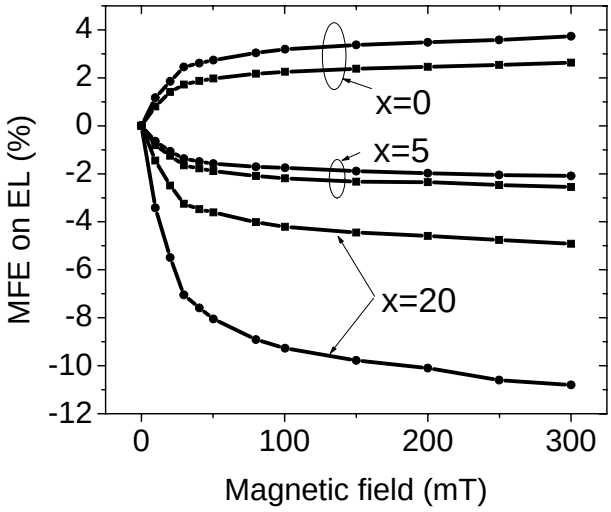


Figure 5.12 Magnetic field effects on electroluminescence at voltage mode and current mode for ITO/PMMA(xnm)/Alq_3/Al OLEDs

in the literature. After a PMMA layer with different thicknesses (5, 10, 15, 20nm) was inserted between anode and alq_3 layer, the positive MFE gradually decreases -4.9% for 20nm PMMA device. We also noticed that the magnetoresistance also changes from negative to positive. Interestingly, for the 5nm PMMA device, the magnetoresistance is negative (current increases with magnetic field at constant voltage), however, the MFE shows a negative value which further confirms the MFE at constant current mode is not due to magnetoresistance. The gaps of constant current and voltage mode are +1.1%, +0.46%, and -5.9% for single layer alq_3, 5nm PMMA, and 20nm PMMA devices, respectively which are also close to corresponding magnetoresistance -1.43%, -0.36%, +5.6% (the sign of current change is opposite to that of MR), considering experimental

error. Combined results in either the hole transport or electron transport material based devices, triplet-charge reaction does largely reduce the magnitude of MFE.

5.8 Summary

Magnetic field can enhance the formation of singlet polaron pair states and reduce the triplet polaron pair states. As a result, total polaron pair dissociation is enhanced and triplet-charge reaction is reduced by the magnetic field, leading to a negative magnetoresistance and a positive magnetoresistance, respectively. Intentional enhancement of the triplet charge reaction can increase the positive magnetoresistance. Based on this concept, the original positive magnetoresistance in ITO/MEH/Au was tuned to be a negative MR by reducing the hole injection through insertion of an insulating PMMA layer at reverse bias, while the positive magnetoresistance was enhanced by reducing electron injection at forward bias. This concept was also successfully applied in PVK, a typical hole transport material and Alq_3, a typial electron injection material based OLEDs. The original negative magnetoresistances in PVK and Alq_3 systems were tuned by reducing electron injection and hole injection, respectively. It can be concluded that larger negative magnetoresistance is expected when charge injection is balanced, while larger positive magnetoresistance can be obtained in case of severe unbalanced charge injection.

Magnetic field effect on electroluminescence can also be tuned by changing the bipolar injection, due to triplet-charge injection induced spin polarization of injected electrons and holes. The result of spin polarization of electrons and holes leads to preferential formation of triplet excitons in the expense of singlet excitons, leading to a

decrease of MFE. Combined with the magnetic field enhanced singlets process, the magnetic field effect on electroluminescence actually also depends on two competing processes: magnetic field effect on triplet/singlet transition and triplet-charge reaction. This concept was proven by the observation of a tunable of magnetic filed effect on electroluminescence from both PVK and Alq_3 based devices by tuning electron injection and hole injection, respectively.

6 MORPHOLOGY EFFECTS ON MAGNETIC FIELD DEPENDENT ELECTROLUMINESCENCE AND MAGNTORESISTANCE

6.1 Introduction

In chapter 5, it has been shown that triplet charge reaction enhances the positive MR. In this chapter, we still focus on manipulating triplet-charge reaction by controlling the morphology of the organic semi-conducting layer. As we know if there are low energy domains in the amorphous polymer matrix, excited states can be either formed in or transferred to low energy domains from amorphous matrix under photo-excitation or electrical excitation. Meanwhile the low energy domains can also trap free charge carriers in electroluminescence process. Therefore, the exciton, especially triplet excitons would have more chance to react with the trapped charges. Based on this concept, the magnetic field effects were investigated in a poly(9,9-dioctylfluorenyl-2,7-diyl) (PFO) based devices to elucidate the morphology effects.

We note that crystalline phases can be formed in addition to the amorphous phase in fluorene conjugated polymer thin films. The crystalline structures can act as "quantum wells" to confine both excitons and free charges. Chen[115,116] and Misaki[117] have recently shown the morphological evidence of the crystalline phase formed in the PFO films prepared by polymer melt and frication transfer. However, it is especially difficult to control the formation of such crystalline phase in spin-cast films due to rapid solvent evaporation, creating an obstacle for controlling morphology. We developed a new

method of using a mixture of two dissimilar organic solvents for spin-cast to adjust the crystalline/amorphous phase densities. It is also found that similar crystalline structure can also form through annealing at a temperature higher than its glass transition temperature.

6.2 Experimental

The chemical structure of the PFO was shown in chapter 1. Two types of solvents: single $CHCl_3$ and mixed ODCB/$CHCl_3$ were used to spin-cast the PFO thin films, yielding $CHCl_3$-based and ODCB/$CHCl_3$-based thin films for the studies of the morphology-dependent MFE and magnetoresistance. The boiling-points of the $CHCl_3$ and ODCB are 62°C and 180°C, respectively. The 80 nm thin films were spin-cast on ITO glass at the spinning-speed of 1000 RPM. Thermal evaporation of 20nm aluminum electrode finishes the fabrication of the devices. For photoluminescence and absorbance measurements, 80nm thin PFO films were deposited on regular glass slides.

The absorption and photoluminescence (PL) were measured with Perkin-Elmer Lambda 35 UV/VIS and SPEX Fluorolog 3 Spectrometers, respectively, in nitrogen atmosphere. The excitation wavelength for the PL measurements was 380 nm selected from an UV lamp based on the maximum absorption of the PFO. Morphological studies were carried out using a Hitachi field emission TEM at 200 kV. Particularly, the thin films spun-cast on a 1"x1" glass slides were floated off on the surface of water at room temperature and then transferred onto a 400-mesh copper grid for the TEM microscopic imaging measurements. Micro-electron diffraction was conducted on the spin-cast thin films under parallel beam condition with a 50-μm or a 10-μm condenser aperture.

Magnetic field effect on electroluminescence and magnetoresistance were measured at same conditions as in the previous chapters.

6.3 Spectroscopic evidence for the formation of crystalline structure in solvent treated PFO films

During spin coating, the low boiling point $CHCl_3$ evaporates very fast and the ODCB evaporates slowly. The use of a high boiling-point organic solvent may allow polymer chains to have sufficient time to interact with each other during spin-cast due to the relatively slow solvent-evaporation[118]. In general, this interchain interaction favors phase separation in the immiscible polymer blends or crystallization in the polymers with certain regularities. Therefore, for the $CHCl_3$/ODCB based films, the PFO chains have relatively longer time to pack and form ordered structure.

In case of pure $CHCl_3$ based thin films, the polymer chains maintain the amorphous structure in the solutions due to the fast evaporation of $CHCl_3$. As shown in Figure 6.1, the photoluminescence spectrum for a $CHCl_3$ based film has three peaks located at around 420nm, 445nm, and 465nm. This spectrum has been proven to be related to the amorphous structure of PFO. When the mixed ODCB/$CHCl_3$ solvents were used, the PFO spin-cast film experiences a significantly spectral change as the volume concentration of the ODCB increases. In particular, the addition of the ODCB gradually decreases the intensity of high-energy PL peak at 420 nm but largely increase the intensities of the peaks at 440nm, 465nm, and 500nm. The new spectra are related to crystalline PFO. This spectral change has been suggested as an indication of the formation of the crystalline structure[119].

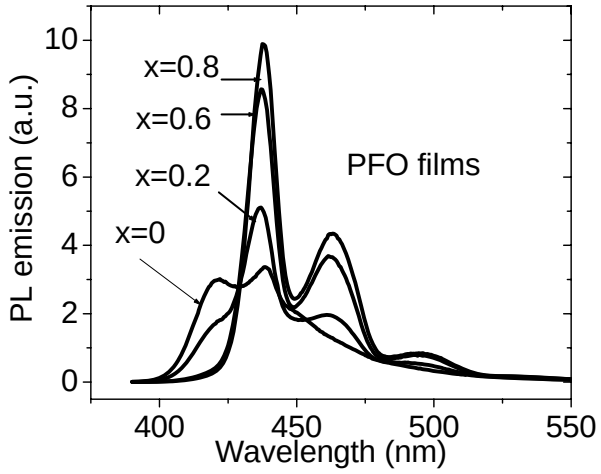


Figure 6.1 Photoluminescence spectra of PFO films spin-cast from combined ODCB(x%)/chloroform solvent. The emission gradually changes from amorphous PFO to crystalline PFO

In addition, a new peak at 435 nm is also shown in the UV-Vis absorption spectra of the PFO spin-cast films when the mixed ODCB/$CHCl_3$ solvents were used (Figure 6.2). This new absorption peak has been also assigned to the PFO crystalline structure.[120- 123] . In absorbance spectra of $CHCl_3$/ODCB based films, majority absorptions come from the amorphous PFO and the crystalline structures only account for a small fraction, suggesting the morphology of crystalline dispersed in amorphous matrix. It also can be seen that the absorbance edge of the crystalline is located at 448nm while that for amorphous structure is 429nm, indicating the crystalline structure has a lower energy level than that of amorphous structure.

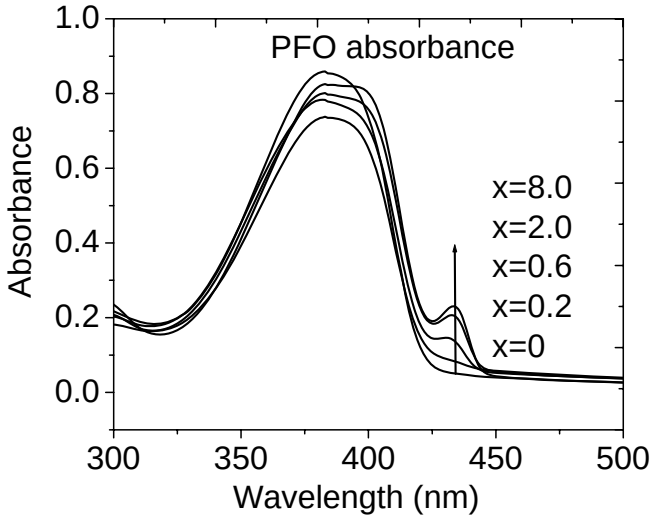


Figure 6.2 Absorption spectra of $Ir(ppy)_3$(0.1%)/PFO films spin-cast from combined ODCB(x%)/chloroform solvent

Therefore, the crystalline structures actually act like "quantum wells". Excitons formed in amorphous matrix can be transferred to and confined in those "quantum wells", enhancing the photoluminescence efficiency as shown in Figure 6.3. The photoluminescence efficiency of the PFO spin-cast film increases at the concentration (<1%) and then saturates at higher ODCB concentration. The maximum photoluminescence efficiency enhancement can be 1.6 times higher for the $CHCl_3$+2%ODCB film compared with the one made from pure $CHCl_3$ solution.

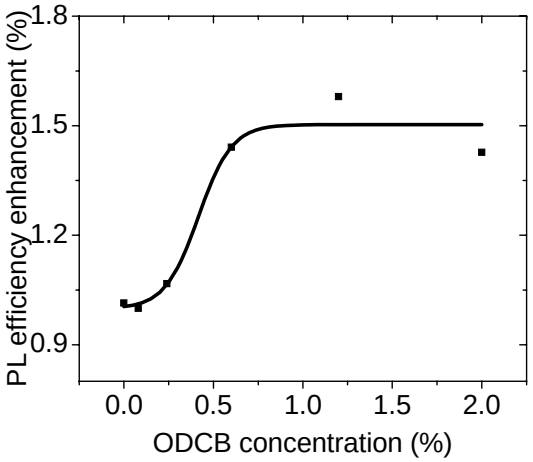


Figure 6.3 Fluorescent efficiency for the PFO films spin-cast from mixed ODCB/$CHCl_3$ solvents

6.4 Microscopic evidence for the formation of crystalline structure in solvent treated PFO films

Although the formation of solvent-induced crystalline phase has been suggested by photoluminescence and absorption spectra, direct morphological evidence has not been demonstrated for the PFO spin-cast thin films. We carefully examined the morphologies of the PFO spin-cast from $CHCl_3$ and mixed ODCB/$CHCl_3$ by using TEM and electron diffraction. When the single $CHCl_3$ solvent was used, the PFO forms a uniform morphology in the TEM microscopic image in Figure 6.4 (a). The typical diffusive electron diffraction pattern suggests an amorphous structure formed in the $CHCl_3$-based PFO film. However, when the mixed ODCB/$CHCl_3$ solvents were used, a faint diffraction ring is appeared around the diffusive pattern from the PFO film, although the bright-field TEM image still shows a homogenous morphology, as shown in Figure 6.4 -

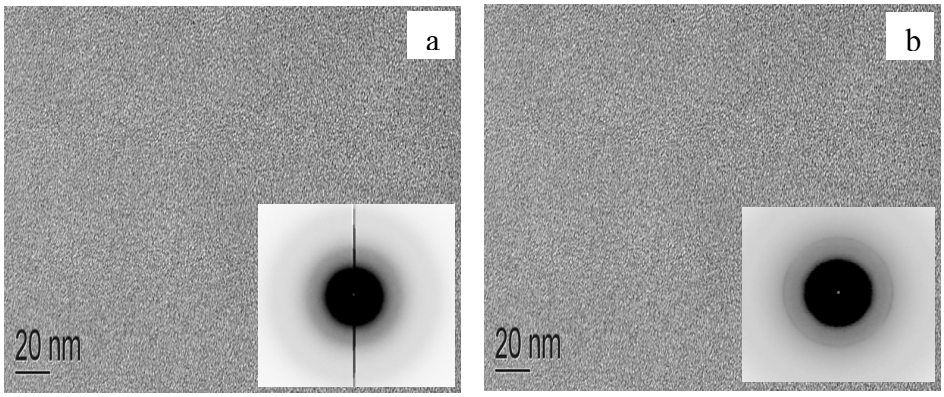


Figure 6.4 TEM microscopic images and inverted electron diffraction patterns. a $CHCl_3$-based PFO film. b ODCB(2%)/$CHCl_3$-based PFO film

(b). This faint ring is a direct morphological evidence of the low-density crystalline phase induced by the ODCB in the PFO spin-cast film. From the electron diffraction ring, the crystalline interplanar spacing was calculated to be 3.61±0.03Å. It is evident that the crystalline domains are randomly distributed in the background of the continuous amorphous phase. We note that the amorphous and crystalline structures do not have an appreciable contrast in the bright-field mode. This should be the reason that the crystalline structure is not shown in the TEM microscopic image (Figure 6.4(b)).

6.5 Evidence for crystalline structures in annealed PFO films

The crystalline structure can also be formed by annealing. The chloroform-based PFO thin films were annealed for 100 minutes at the temperatures of 80°C and 100°C, higher than the glass transition temperature of the PFO of 70°C[124,125]. As compared with the ODCB-induced absorption, the broad absorption shoulder around 430 nm from the annealed films in Figure 6.5 can be considered as an indication of the crystalline structure formed in the chloroform-based PFO films due to the thermal treatment. The broad-

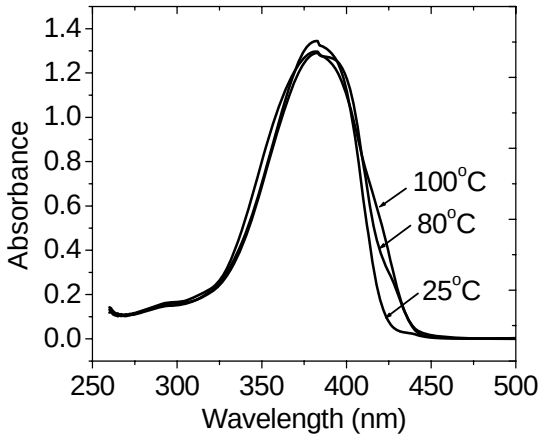


Figure 6.5 Absorption spectra of chloroform-based films before and after annealing at 80°C, 100°C for 100 minutes

spectral shoulder suggests that the thermal annealing induced crystalline structures are less regular and more random in domain-size than the ODCB induced crystalline structures. Furthermore, thermal annealing clearly increases the fluorescence intensity with the spectral feature of crystalline structure in the chloroform-based PFO films (Figure 6.6), which is similar to the fluorescence enhancement and spectral characteristics induced by the addition of the ODCB solvent. We also note that there is no change observed in the absorption and fluorescent spectra when the PFO films were annealed at a temperature (such as 50°C) lower than the Tg of the PFO, indicating an absence of the formation of the crystalline structure due to the lack of sufficient chain movement. Therefore, it is confirmed that the crystalline structures can be induced by either ODCB treatment or annealing.

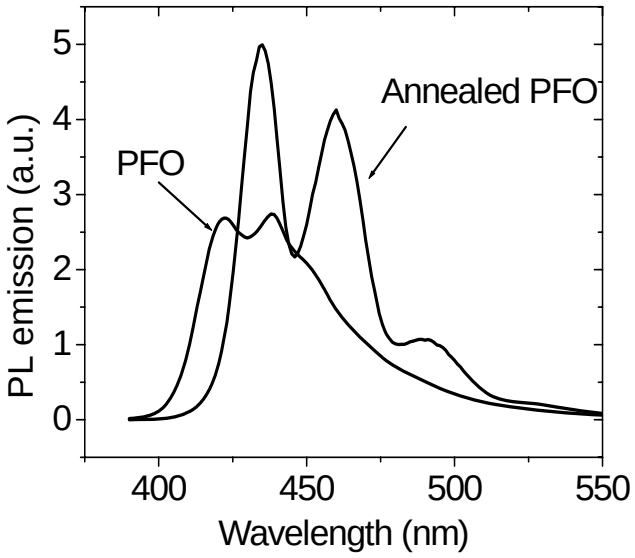


Figure 6.6 PL spectra of chloroform-based films before and after annealing at 100°C for 100 minutes

6.6 Application of a phosphorescent dye as a probe to clarify exciton-confinement characteristic of the crystalline domains

The formation of crystalline structures through solvent treatment or annealing has been proven by the absorbance and photoluminescence measurement. The enhancement of photoluminescence efficiency suggests the crystalline structures can act as "quantum wells" to spatially confine the excitons. To further confirm the confinement, a phosphorescent dye was used to monitor the energy transfer in PFO/$Ir(ppy)_3$ composite films. In the spin-cast film of the $Ir(ppy)_3$/PFO composite, the mixed $CHCl_3$/ODCB solvents should result in three phases: randomly distributed PFO crystalline structure, continuous PFO amorphous structure, and dispersed $Ir(ppy)_3$. The energy transfer occurs through three channels: from amorphous matrix to crystalline domains; from amorphous

matrix to dispersed dye molecules; and from crystalline domains to dye molecules. In pure $CHCl_3$ based PFO films, it only exists one energy transfer channel, from PFO amorphous matrix to dispersed dye molecules. Therefore comparison of the energy transfer in these two composite films enables us to clarify the confinement of the induced crystalline domains.

6.6.1 Energy transfer in PFO/Ir(ppy)$_3$ composites

In conjugated polymer/phosphorescent dye composites, there is an energy transfer from singlet excitons formed in polymer matrix to singlet excitons in phosphorescent dye through Förster transfer process. Because of strong spin-orbital coupling of the phosphorescent dye, the singlets excitons can convert to triplet excitons through intersystem crossing. To determine if there is a light emission from the triplet excitons in phosphorescent dyes depends on the energy levels of the triplet excitons and triplet excitons in the polymer matrix. If the triplet energy level is lower than that of the polymer matrix, phosphorescence occurs, e.g. the PVK/Ir(ppy)$_3$ system in chapter 4. Otherwise the Dexter energy transfer from the triplet excitons in dye molecules to triplet excitons in polymer matrix occurs as in this case PFO/Ir(ppy)$_3$ (Figure 6.7). As we know the triplet excitons cannot radiatively decay to generate light emitting in PFO. Incorporation of Ir(ppy)$_3$ in PFO matrix basically reduces the total light emission intensity.

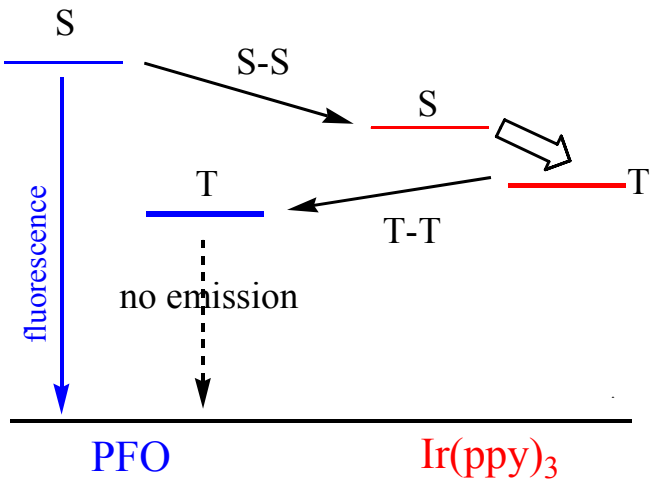


Figure 6.7 Possible energy transfer in PFO/$Ir(ppy)_3$ composites

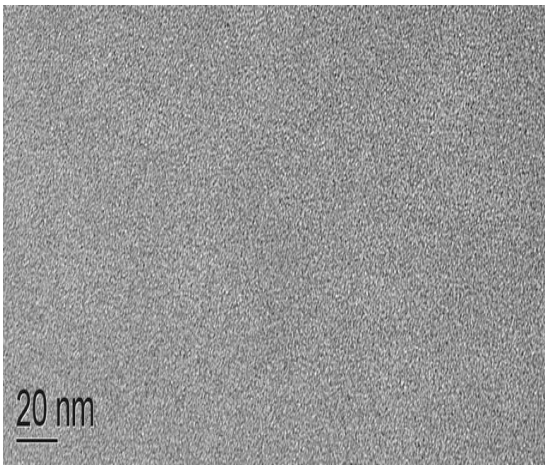


Figure 6.8 TEM image for PFO/0.1wt% $Ir(ppy)_3$ composite film

6.6.2 Quenching rate in PFO/Ir(ppy)$_3$ composite films

Now we utilize this property to study the quenching rate in $CHCl_3$/ODCB and pure $CHCl_3$-based PFO/Ir(ppy)$_3$ composite films. Up to 0.1wt% of Ir(ppy)$_3$ was used to dope the polymer ensuring the uniform dispersion, which has been confirmed by the TEM measurement. No aggregation of Ir(ppy)$_3$ molecules in PFO film can be observed in TEM image as shown in Figure 6.8.

The quenching rate in the $CHCl_3$/ODCB(2%) -based film and pure $CHCl_3$-based film was shown Figure 6.9. It can be seen that shows a relative slower fluorescence quenching rate as compared to the $CHCl_3$ based film. The slower quenching rate can be interpreted by the confinement of induced crystalline structures. In $CHCl_3$/ODCB-based PFO films, the coexisted solvent-induced crystalline/amorphous phases can be considered as random quantum-wells[126] based on the energy difference between the amorphous and the crystalline phases (Figure 6.2). Due to the very fast Förster energy transfer between these two phases,[127-129] the excited states mainly generated in the amorphous phase can be transferred to the crystalline phase. The quantum-well like coexisted crystalline/amorphous structures spatially confine the excited states and therefore decrease the possibilities of the excitons being in close proximity with the dispersed Ir(ppy)$_3$ molecules, thus reducing the singlet-singlet energy transfer, as illustrated in Figure 6.10. In contrast, the PFO amorphous phase can significantly facilitate the exciton migrations through intra- and inter-chain relaxations, consequently leading to a high possibility for the excited states to closely encounter with the dispersed Ir(ppy)$_3$ molecules and therefore enhancing the singlet-singlet energy transfer (larger quenching rate).

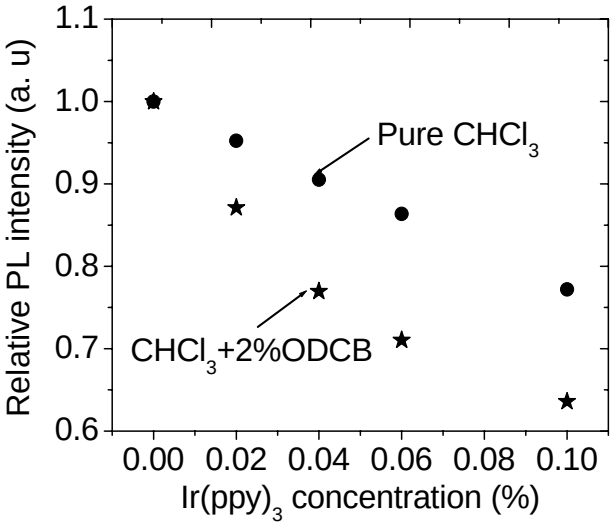


Figure 6.9 Relative fluorescence quenching as a function of $Ir(ppy)_3$ concentration for the $Ir(ppy)_3$(0.1%)/PFO films spin-cast from $CHCl_3$ (stars) and mixed ODCB(2%)/$CHCl_3$ (dots)

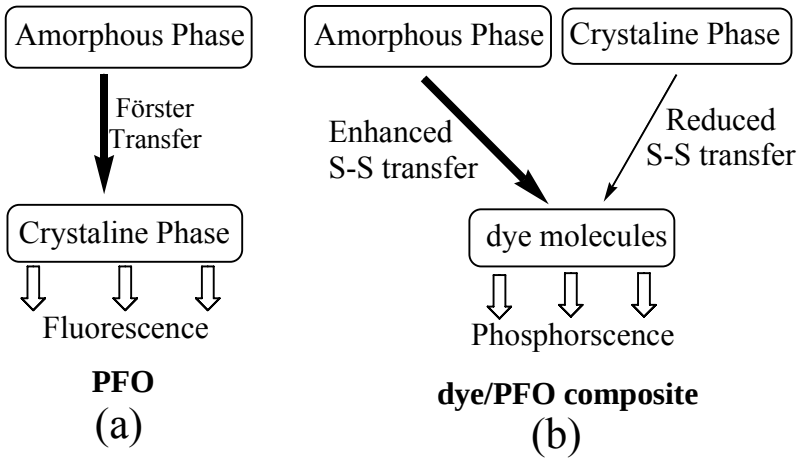


Figure 6.10 Schematic morphology-dependent exciton emission and energy transfer processes in (a) PFO and (b) dye/PFO composite films

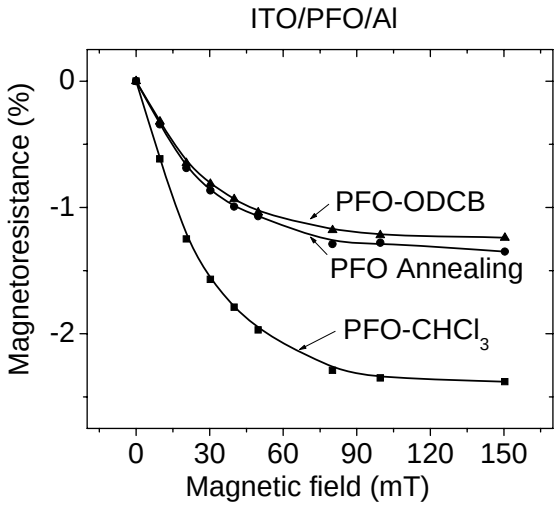


Figure 6.11 Magnetoresistance as a function of magnetic field in three types of PFO based single-layer ITO/PFO/Al OLEDs

Therefore, the enhanced photoluminescence efficiency and reduced energy transfer from PFO further confirm the existence of low-energy domains and their exciton–confinement characteristic.

6.7 Morphology dependent magnetoresistance and magnetic field effect on electroluminescence

Pure $CHCl_3$, $CHCl_3$-2%ODCB, and annealed PFO were utilized to fabricate OLEDs. The magnetoresistances for the three devices were measured at constant voltage targeted at same current 2mA/cm^2. The results were shown in the Figure 6.11. It can be seen that the magnetoresistance decreases with magnetic field and gradually saturated the range from 50mT to 150mT. The three curves show similar trend, however, the annealed and ODCB based devices show clear smaller value. As we know the magnetoresistance

comprises two contributions: polaron pair dissociation and triplet-charge reaction. The final magnetoresistance is determined by the sum of the two contributions. The detected negative magnetoresistance indicates the polaron pair dissociation is still the dominating process. However, after solvent treatment or annealing crystalline domains are induced in the PFO amorphous matrix, forming a "quantum well" structure. The quantum wells spatially confine excitons transferred from PFO amorphous matrix and at same time trap free charges, which can be visualized as Figure 6.12. Thus excitons, especially triplet excitons, have more chance to collide with charges and the exciton-charge reaction is enhanced, due to the confinement of the crystalline domains.

The low energy domains enhanced triplet-charge reaction also reflects in the magnetic field effect on electroluminescence. As shown in Figures 6.13, the magnetic field effect on electroluminescence increases with magnetic field. The magnitudes of MFE in the ODCB based and annealed ITO/PFO/Al OLEDs have smaller values than that in the pure $CHCl_3$ based device. As discussed in chapter 5, enhanced triplet charge-

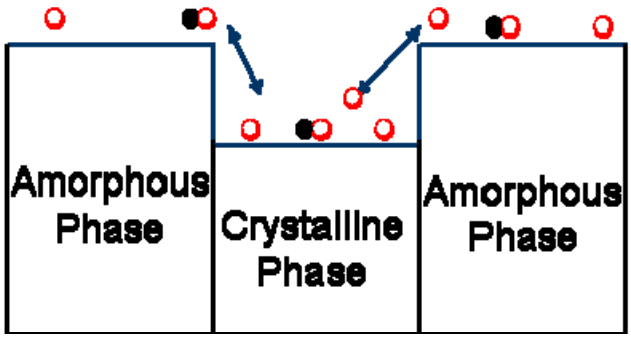


Figure 6.12 Visualization of the crystalline domains enhanced triplet-charge reaction

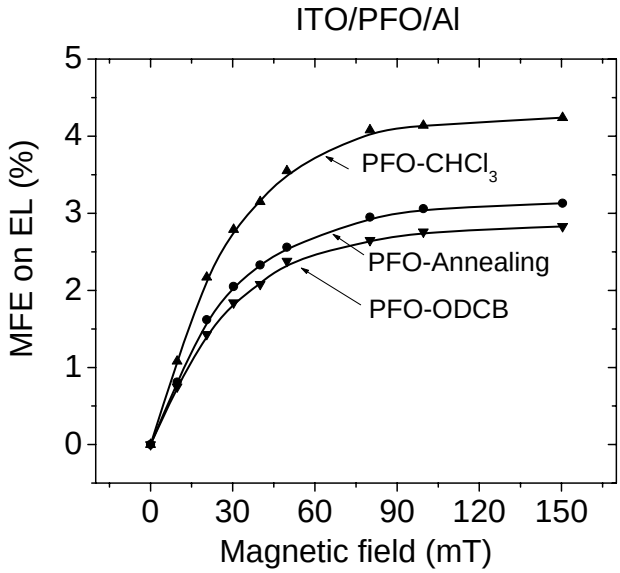


Figure 6.13 Magnetic field dependent electroluminescence in the three types of PFO based single-layer ITO/PFO/Al OLEDs

reaction generates spin-polarized electrons and holes, facilitating the formation of triplet excitons at the expense of singlet excitons. the magnitude of MFE decreases with the formation of low energy crystalline domains.

It is worthy to point out that bipolar injection might be different in the three devices, due to the formation of low energy crystalline domains in the ODCB and annealed devices. More balanced bipolar injection can lead to more negative magnetoresistance while unbalanced bipolar injection causes more positive magnetoresistance. To exclude this possibility, magnetic field effect on the photocurrent were also investigated, in which no bipolar injection effects involved.

6.8 Morphology dependent magnetic field effect on photocurrent

The PFO films were spin cast on the ITO glasses from PFO/$CHCl_3$ solutions with 0%, 0.5% and 2% ODCB. The thickness of the spin cast films were kept same, around 80nm. The ITO, Al electrodes sandwiched PFO ITO/PFO/Al devices have same structures as those for the electroluminescence measurement. The photocurrent was generated by the illumination of 380nm light according to its maximum absorption (Figure 6.2). Magnetic field effect on photocurrent (MFP, defined as equation 1-14) was measure at zero bias and the results were shown in Figure 6-14. Similar to MFE and MR, the photocurrent experiences rapid increase at low field and then gradually saturates at higher field (>50mT). However, the magnitudes of MFP are quite different, 0.91%, 0.63%, and 0.51% at 150mT for the 0%, 0.5%, and 2% OLED devices, respectively.

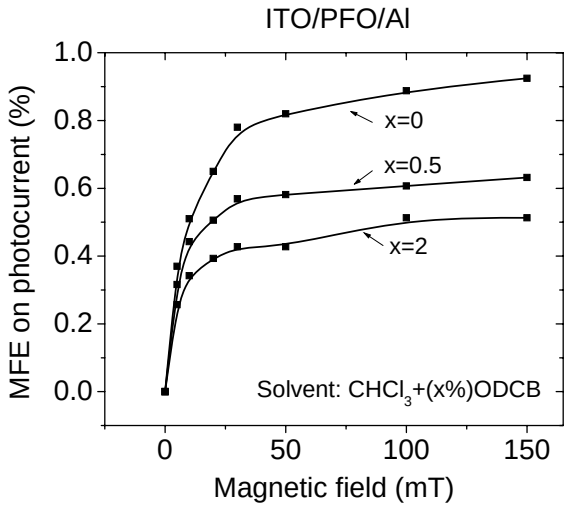


Figure 6.14 Magnetic field effect on photocurrent for ITO/PFO/Al photovoltaics

During light illumination, the formed excitons can dissociate into free charges through polaron pair states. Some charges are trapped in the polymer and they can further react with excitons, especially triplet excitons, to generate more free charges (Figure 6.15). Therefore, the detected photocurrent comprises of two contributions: dissociation and triplet-charge reaction. In pure $CHCl_3$ based device, exciton formed in amorphous matrix and dissociate into free charges with less triplet-charge reaction. When OLED is used, the crystalline domains form in the PFO films. Subsequently, they trap both exciton and free charges and enhance the triplet-charge reaction. As we know, magnetic field increases singlets and reduces triplets. As a result, magnetic field actually reduces triplet-charge reaction and corresponding photocurrent. That is exactly what we observed in the ODCB based devices. Furthermore, the density of the crystalline domains increases with the fraction of ODCB in $CHCl_3$ as suggested by Figure 6.3. It also explains the 0.5% ODCB device has a smaller reduction compared to the 2% ODCB device.

Combined study of magnetic field effect on electroluminescence, photocurrent, and magnetoresistance confirms the low energy crystalline domains do enhance the triplet-charge reaction leading to the reduction of negative magnetoresistance and reduced MFE and MFP.

This study further suggests it requires removal of traps in organic semiconductor films besides crystalline structures, such as chain defects, chains ends, and impurities, to achieve larger negative magnetoresistance and positive MFE by reducing triplet-charge reaction.

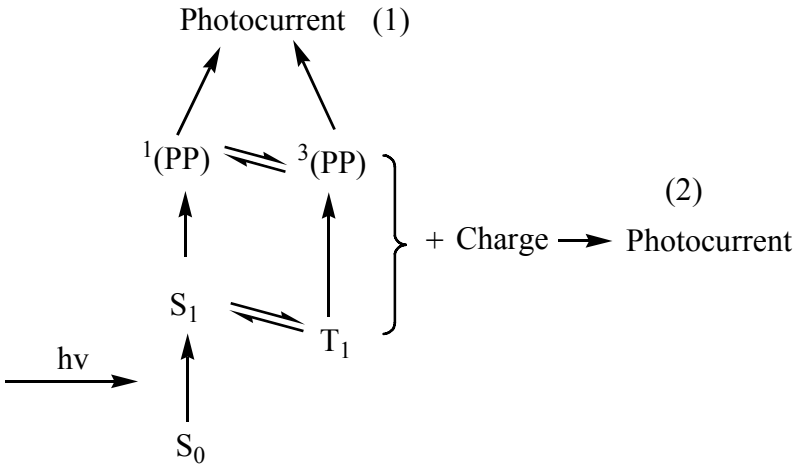


Figure 6.15 Formation of photocurrent in ITO/PFO/Al devices. Photocurrent has two contributions: polaron dissociation (1) and triplet-charge reaction (2)

6.9 Summary

The optical measurements confirms the formation of low energy crystalline domains formed in amorphous matrix in PFO films by using high boiling point solvent ODCB. The crystalline interplanar spacing is determined by electron diffraction to be 3.61±0.03Å. Photoluminescence efficiency measurement suggests the crystalline structure can form quantum well to spatially confine excitons. The exciton confinement was further verified by a dye probe to investigate the energy transfer from the PFO to the dispersed dye molecules. The confined excitons in the crystalline domains have more chances to react with trapped charges in the same domain, leading to reduced magnetic field effect on electroluminescence and magnetoresistance. The magnetic field effect on photocurrent study excludes the contribution from bipolar injection.

The study also suggests it is necessary to remove traps in the organic semiconductor films to achieve larger negative magnetoresistance and positive magnetic field effect on electroluminescence.

7 Conclusions

Recent research discovered that magnetic field effect can affect electroluminescence and charge injection in organic semiconductors. However, no existing mechanisms can fully explain the observed magnetic phenomena, although some of them may be partially correct for specific systems, which has been discussed in the introduction section.

We carefully investigated the magnetic phenomena in a wide range of organic semiconductors based OLEDs, and proposed that magnetic field effect on electroluminescence and magnetoresistance are related to magnetic field modified singlet-triplet intersystem crossing in polaron pair states and triplet charge reaction. Magnetic field enhances the formation of singlets and reduces the triplets, leading to two consequences: enhanced polaron pair dissociation and reduced triplet-charge reaction. the enhanced dissociation results in increases secondary free charges which can drift to opposite electrodes under electrical field and reduces the effective charge injection barriers, leading to enhanced current or reduced resistance (negative magnetoresistance).

The secondary electrons or holes can also be generated by triplet-charge reaction. Since magnetic field reduces triplet-charge reaction by decreasing the population of triplets, the number of secondary charges generated by triplet-charge reaction decreases with magnetic field, leading to enhanced charge injection barriers compared with the case at zero field. Subsequently, the current density at constant voltage is lower with the presence of magnetic field, resulting in a positive magnetoresistance. Therefore, the sign

and magnitude of final magnetoresistance in an OLED is determined by the two processes with opposite contributions.

In case of magnetic field effect on electroluminescence intensity, the electroluminescence increases with magnetic field due to the same magnetic field enhanced singlets polaron pairs and excitons accordingly. The triplet-charge reaction can cause a post-injection effect. The spin of injected electrons and holes can be polarized, pointing the same direction in the presence of an external magnetic field, facilitating the formation of triplet excitons in stead of singlet excitons. Therefore the triplet-charge reaction can cause a negative contribution to the magnetic field effect on electroluminescence. Similar to magnetoresistance, the magnetic field effect on electroluminescence also comprises of two opposite contributions. The final sign and magnitude is determined by the sum of the two contributions.

This model was also tested by manipulation of organic/metal electrode interfaces, dye doping, bipolar injection and morphology of the organic thin film. In chapter 2, it was found penetration of metal atoms enhances the spin-orbital coupling of the organic semiconductor. The internal Zeeman effects caused by the spin-orbital coupling compete with the external Zeeman effects caused by the external magnetic field. Thus enhanced spin-orbital coupling reduces the magnitudes of magnetic field effect on electroluminescence intensity and the magnetoresistance as exactly observed in the experiments.

In the fluorescent polymer/phosphorescent dye composites, we excluded the transport contribution and found the magnetoresistance and magnetic field effect on electroluminescence were determined by energy transfer process and intermolecular

interaction. Due to energy transfer process, the excited states were transferred from the polymer matrix to the dispersed dye molecules. The magnetoresistance and magnetic field effect on electroluminescence show part of dye's characteristics. Besides, the intermolecular interaction mixed the week spin-orbital coupling of the fluorescent polymer and the strong spin-orbital coupling of the phosphorescent dye, leading to the change of the magnetic field effects. Thus the magnitude of the magnetic field effects can also be tuned by controlling the concentration of the dye as observed in experiment and predicted by the proposed model.

On the other hand, according to the model, even magnetic field has same effect on the intersystem crossing; the triplet-charge reaction can also be tuned by intentionally controlling the bipolar injection. Unbalanced bipolar injection leads to severer triplet-charge reaction and more positive contribution to magnetoresistance and more negative contribution to the magnetic field effect on electroluminescence intensity. Experimentally, in the ITO/MEH-PPV/PMMA/Au devices, the positive magnetoresistance was changed to a negative magnetoresistance at the reverse bias where the bipolar injection becomes more balanced. At the forward bias the magnitude of magnetoresistance increases with the thickness of PMMA since the bipolar injection becomes more unbalanced. In the typical hole-transporting material, PVK and electron-transporting Alq_3, the electron injection and hole injection were controlled to realize the transition from a negative value to a positive value.

The triplet-charge reaction can also be morphologically controlled. As a representative, the morphology change and its effect on magnetoresistance were also investigated. The optical measurements and electron diffraction successfully confirmed

the existence of low energy crystalline domains dispersed in amorphous matrix. Photoluminescence efficiency and dye probed energy transfer measurements confirmed the exciton confinement in the crystalline domains. The low energy domains enhanced triplet-charge reaction by spatially confining the excitons and trapping charges. Combined study of magnetic field effect on electroluminescence, photocurrent, and magnetoresistance supports the triplet charge reaction reduces the negative magnetoresistance and the positive magnetic field effect on electroluminescence and photocurrent.

Therefore, we successfully built a bridge between internal excitonic processes and external magnetic characteristics in OLEDs. Scientifically, our model opens a new pathway to magnetically study the spin dependent excitonic processes, which is also the foundation for further development of spin-involved OLEDs, organic solar cells, organic lasers, and magnetic sensors. Technically, we developed severally ways to tune both sign and magnitude of the magnetic field effect on electroluminescence and magnetoresistance, leading to form a novel branch of electronics: organic magneto-optoelectronics. Actually these unique magnetic responses in non-magnetic materials are difficult to be fulfilled in their inorganic counterparts. Meanwhile, our work establishes a new way to inspect some very important issues in OLEDs such as balance of change injection, charge trapping, semiconductor/electrode interface, exciton dissociation and triplet-charge reaction, which are also critical in the other related organic optoelectronics e.g. photovoltaic cells, lasers.

LIST OF REFERENCES

1 Friend , R. H., R. W. Gymer, A. B. Holmes, J. H. Burroughes, R. N. Marks, C. Taliani, D. D. C. Bradley, D. A. Dos Santos, J. L. Brédas, M. Lögdlund, and W. R. Salaneck, *Electroluminescence in conjugated polymers*. Nature, 1999. **397**(14): p. 121-128.

2 Bradley, D. D. C., *Conjugated polymer electroluminescence*. Synthetic Metals, 1993. **54**(1-3): p. 401-415.

3 http://www.chemsoc.org/ExemplarChem/entries/2001/williamson/theory.html

4 Baigent, D. R., N. C. Greenham, J. Grtiner , R. N. Marks, R. H. Friend, S. C. Moratti, A. B. Holmes, *Light-emitting diodes fabricated with conjugated polymers — recent progress*. Synthetic. Metals, 1994. **67**(1-3): p. 3-10

5 Pope, M., H. Kallmann, and P. Magnante, *Electroluminescence in organic crystals*. Journal of Chemical Physics, 1963. **38**(8): p. 2042-2043.

6 Helfrich W. and W. G. Schneider, *Recombination Radiation in Anthracene Crystals*, Physics Review Letters, 1965. **14**(7): p. 229-231.

7 Vincett, P. S., W. A. Barlow and R. A. Hann, G. G. Roberts, *Electrical conduction and low voltage blue electroluminescence in vacuum-deposited organic films*, Thin Solid Films, 1982. **94**(2): p.171-183.

8 Tang, C. W. and S. A. Van Slyke, *Organic electroluminescent diodes,* Appllied physics letters. 1987. **51**(12): p. 913-915.

9 Burroughes, J. H., D. D. C. Bradley, A. R. Brown, R. N. Marks, K. Mackay, R. H. Friend, P. L. Burns and A. B. Holmes, *Light-emitting diodes based on conjugated polymers*, Nature, 1990. **347**(6293): p. 539-541.

10 Braun D. and A. J. Heeger, *Visible light emission from semiconducting polymer diodes*, Appllied Physics Letters, 1991. **58**(18): p. 1982-1984.

11 Baldo, M. A., D. F. O'Brien, Y. You, A. Shoustikov, S. Sibley, M. E. Thompson and S. R. Forrest, *Highly efficient phosphorescent emission from organic electroluminescent devices*, Nature, 1998. **395**(6698): p. 151-154.

12 Baldo, M. A., M. E. Thompson, and S. R. Forrest, *High-efficiency fluorescent organic light-emitting devices using a phosphorescent sensitizer*, Nature, 2000. **403**(6771): p. 750-753.

13 Sandee, A. J., C. K. Williams, N. R. Evans, J. E. Davies, C. E. Boothby, A. Kohler, R. H. Friend, A. B. Holmes, *Solution-Processible Conjugated Electrophosphorescent Polymers*, Journal of American Chemical Society, 2004. **126**(22): p. 7041-7048.

14 Köhler A., J. S. Wilson, R. H. Friend, M. K. Al-Suti, M. S. Khan, A. Gerhard, H. Bassler, *The singlet-triplet energy gap in organic and Pt-containing phenylene ethynylene polymers and monomers*, Journal of Chemical Physics, 2002. **116**(21): p. 9457-9463.

15 Laquindanum, J. G., H. E. Katz, A. Dodabalapur, and A. J. Lovinger, *n-Channel Organic Transistor Materials Based on Naphthalene Frameworks*, Journal of American Chemical Society, 1996. **118**(45): p.11331-11332.

16 Bernards, D. A., G. G. Malliaras, G. E. S. Toombes, S. M. Gruner, *Gating of an organic transistor through a bilayer lipid membrane with ion channels*, Applied Physics Letters, 2006. **89**(5): p. 053505.

17 Gao J., G. Yu, A. J. Heeger, *Polymer p-i-n Junction Photovoltaic Cells,* Advanced Materials, 1998. **10**(9): p. 692-685.

18 Shi, C., Y. Yao, Y. Yang, Q. Pei, *Regioregular Copolymers of 3-Alkoxythiophene and Their Photovoltaic Application,* Journal of American Chemical Society, 2006. **128**(27): p. 8980-8986.

19 He, J., L.Ma, J. Wu, Y. Yang. *Three-terminal organic memory devices,* Journal of Applied Physics, 2005. **97**(6): p. 064507.

20 Ouyang, J., C.-W. Chu; C. R. Szmanda, L. Ma, and Y. Yang, *Programmable polymer thin film and non-volatile memory device*, Nature Materials, 2004. **3**(12): p. 918-922.

21 Nilsson, D., T. Kugler, P. -O. Svensson, and M. Berggren, *An all-organic sensor–transistor based on a novel electrochemical transducer concept printed electrochemical sensors on paper*, Sensors and Actuators, B: Chemical, 2002. **B86**(2-3): p. 193-197.

22 Brütting, W., E. Buchwald, G. Egerer, M. Meier, K. Zuleeg, and M. Schwoerer, *Charge Carrier Injection and Transport in PPV Light Emitting Devices*. Synthetic Metals, 1997. **84**(1-3): p. 677-678.

23 Rikken, G. L. J. A., D. Braun, E. G. J. Staring, and R. Demandt, *Schottky Effect at a Metal-Polymer Interface*, Applied Physics Letters, **65**(2): p.219-221.

24 Sze, S. M., *Physics of Semiconductor Devices*, Wiley, New York, 1981.

25 Campbell, A. J., D. D. C. Bradley, and D. G. Lidzey, *Space-charge limited conduction with trips in poly(phenylene vinylene) light emitting diodes*. Journal of Applied Physics, **82**(12): p. 6326-6342.

26 Simmons, J. G., *Richardson-Schottky Effect in Solids*, Physical Review Letters, 1965. **15**(25): p. 967-968

27 Marks, R. N., D. D. C. Bradley, R. W. Jackson, P. L. Burn, and A. B. Holms, *Charge injection and transport in poly(p-phenylene vinylene) light emitting diodes*. Synthetic Metals, 1993. **57**(1): p. 4128-4133.

28 Parker, I. D., *Carrier tunneling and device characteristics in polymer light emitting diodes.* Journal of Applied Physics, **75**(3): p. 1656-1666

29 Davids, P. S., S. M. Kogan, I. D. Parker, and D. L. Smith, *Charge injection in organic light-emitting diodes: Tunneling into low mobility materials*, Applied Physics Letters, 1996. **69**(15):2270.

30 Gmeiner, J., S. Karg, M. Meier, W. Rieβ, P. Strohriegl, and M. Schwoerer, *Synthesis, electrical conductivity and electroluminescence of poly(p-phenylene vinylene) prepared by the precursor route*, Acta Polymerica, 1993. 44(4): p. 201-205.

31 Grüner, J. , P. J. Hamer, R. H. Friend, H.-J. Huber, U. Scherf, A. B. Holmes, *A high efficiency blue-light-emitting diode based on novel ladder poly(p-phenylene)s*, Advanced Materials, 2004. 6(10): p. 748 – 752.

32 Lagally, M. G., *Silicon Nanomembranes*, MRS Bulletin, 2007. **32**(1): p. 57-63

33 Kasap, S. O., *Principle of electronic materials and devices*, second edition, New York, 2001

34 Lampert, M. A., P. Mark, *Current injection in solids*, Academic Press, New York, 1970.

35 Blom, P. W. M. and M. C. J. M. Vissenberg, *Charge Transport in poly(p-phenylene vinylene) light-emitting diodes*, Materials Science and Engineering R-Report, 2000. **27**(3-4): p. 53-94.

36 Moliton A. and R. C. Hiorns, *Review of electronic and optical properties of semiconducting π-conjugated polymers: applications in optoelectronics*, Polymer International, 2004. **53**(10): p. 1397- 1412.

37 Hutchison, G. R., M. A. Ratner, and T. J. Marks, *Hopping transport in conductive heterocyclic oligomers: Reorganization energies and substituent effects*, Journal of the American Chemical Society, 2005. **127**(7): p. 2339-2350.

38 Burrows, P. E., Z. Shen, V. Bulovic, D. M. McCarty, S. R. Forrest, J. A. Cronin, and M. E. Thompson, *Relationship between electroluminescence and current transport in organic heterojunction light emitting devices*, Journal of Applied Physics, 1996. **79**(10): p. 7991-8006.

39 Ma, D., I. A. Hummelgen, B. Hu, F. E. Karasz, X. Jing, L. Wang, and F. Wang, *Determination of electron mobility in a blue-emitting alternating block copolymer by space-charge-limited current measurements*, Solid States Communications, 1999. **112**(5): p. 251-254.

40 Mott N. F. and R. W. Gurney, *Electronic Processes in Ionic Crystals*, Oxford University Press, Oxford, second edition, 1948.

41 Pitarch, Á., G. Garcia-Belmonte, J. Bisquert, and H. J. Bolink, *Impedance of space-charge-limited currents in organic light-emitting diodes with double injection and strong recombination*, Journal of Applied Physics, 2006. **100**(8): p. 084502(5).

42 Poplavskyy, D. and F. So, *Bipolar carrier transport in a conjugated polymer by complex admittance spectroscopy*, Journal of Applied Physics, 2005. **99**(3): p. 033707(9).

43 Malliaras, G. G., J. R. Salem, P. J. Brock, and C. Scott, *Electrical characteristics and efficiency of single-layer organic light-emitting diodes*, Physics Review B, 1998. **58**(20): p. R13411-R13414.

44 Baughman, R. H., J. L. Brédas, R. R. Chance, R. L. Elsenbaumer, and L. W. Shacklette, *Structural basis for semiconducting and metallic polymer dopant systems*, Chemical Reviews, 1982. **82**(2): 209-222.

45 Brédes J. L. and G. B. Street, *Polaron, Bipolaron, and Solitons in Conducting Polymers*. Accouts of Chemical Research, 1985. **18**(10): 309-315.

46 Turro, N. J., *Modern Molecular Photochemistry*, the Benjamin/Cummings Publishing Co., Inc.,1978.

47 Kaufman, J. H. and N. Colaneri, *evolution of polaron states into bipolaron in polypyrrole*, Physical Review Letters, 1984. **53**(10): p. 1005-1008.

48 Scott, J. C., P. Pfluger, M.T. Krounbi, and G. B. Street, *Electron-spin-resonance studies of pyrrole polymer: evidence for bipolarons*, Physical Review B, 1983. **28**(4): p.2140-2145.

49 Scott, J. C., J. L. Bredas, K. Yakushi, P. Pfluger, and G. B. Street, *The evidence for bipolarons in Pyrrole Polymers*, Synthetic Metals, 1984. **9**(2): p.165-172.

50 Yakushi, K., L. J. Lauchlan, T. C. Clarke, and G. B. Street, *Optical study of polypyrrole perchlorate,* Journal of Chemical Physics, 1983. **79**(10): p. 4774-4778.

51 Fesser, K., A. R. Bishop, and D. K. Campbell, *Optical absorption from polarons in a model of polyacetylene*, Physical Review B, 1983. **27**(8): p. 4804-4825.

52 X. Wei and Z. V. Vardeny, N. S. Sariciftci and A. J. Heeger, *Absorption-detected magnetic-resonance studies of photoexcitations in conjugated-polymer/C60 composites*, Physics Review B, 1996. 53(5): p. 2187-2190.

53 Qiu, Y., Z. An, and C. Q. Wu, *Dynamics of polaron formation in a polymer/metal structure*, Synthetic Metals, 2003. **135**(1-3): p. 503-504.

54 Takeda, N., S. Asaoka, and J. R. Miller, *Nature and Energies of Electrons and Holes in a Conjugated Polymer, Polyfluorene***,** Journal of the American Chemcial. Society, 2006. **128**(50): p. 16073 – 16082.

55 Kobrak, M. N. and E. R. Bittner, *Quantum molecular dynamics study of polaron recombination in conjugated polymers*, Physical Review B, 2000. **62**(17): p. 11473-11486.

56 Wilson, J. S., A. S. Dhoot, A. J. A. B. Seeley, M. S. Khan, A. Köhler, R. H. Friend, *Spin-dependent exciton formation in pi-conjugated compounds*, Nature, 2001. **413**(6858): p. 828-831.

57 Köhler, A., J. S. Wilson, and R. H. Friend, *Fluorescence and Phosphoresence in Organic Materials*, Advanced Materials, 2002. **14**(10): p.701-707.

58 Beljonne, D., Z. Shuai, J. Cornil, J. Ph. Calbert , J. L. Brédas, *On the luminescence efficiency of polymer light-emitting diodes: a quantum-chemical investigation*, Journal of Photochemistry and Photobiology A: Chemistry, 2001. **144** (1): p. 57–62.

59 Soo, Z. G. and S. Ramasesha, *Valence bond theory of linear Hubbard and Pariser-Parr-Pople models*, Physical Review B, 1984. **29**(10): p. 5410-5422.

60 Wohlgenannt, M., K. Tandon, S. Mazumdar, S. Ramasesha, and Z. V. Vardeny, *Formation cross-sections of singlet and triplet excitons in π conjugated polymers*, Nature, 2001. **409**(6819): p. 494-496.

61 Cao, Y., I. D. Parker, G. Yu, C. Zhang, and A. J. Heeger, *Improved quantum efficiency for electroluminescence in semiconducting polymers*, Nature, 1999. **397**(6718): p.414-417.

62 Shuai, Z., D. Beljonne, R. J. Silbey, and J. L. Brédas, *Singlet and Triplet exciton Formation Rates in Conjugated Polymer Light-Emitting Diodes*, Physical Review Letters, 2000. **84**(1): p. 131-134.

63 Burin, A. L. and M. A. Ratner, *Spin effects on the luminescence yield of organic light emitting diodes*, Journal of Chemical Physics, 1998. **109**(14): p. 6092-6102.

64 Tanaka, I. and S. Tokito, Phosphorescent-sentitized triplet-triplet annihilation in tris(8-hydroxyquinoline) aluminum, Journal of Applied Physics, 2005. **97**(11): p. 113532(4).

65 Taliani, C., V. Dediu, F. Biscarini, M. Cavallini, M. Murgia, G. Ruani, and P. Nozar, *Organic-inorganic hybrid spin-valve: A novel approach to spintronics*, Phase Transitions, 2002. **75**(7-8): p. 1049-1058.

66 Xiong, Z. H., D. Wu, Z. V. Vardeny, and J. Shi, *Giant magnetoresistance in organic spin-valves*, Nature, 2004. **427**(6977): p. 821-824.

67 Xie, S. J., K. H. Ahn, D. L. Smith, A. R. Bishop, and A. Saxena, *Ground-state properties of ferromagnetic metal/conjugated polymer interfaces*, Physical Review B, 2003. **67**(12): p. 125202(7).

68 Tsymbal, E. Y., V. M. Burlakov, and I. I. Oleinik, *Spin injection into amorphous semiconductors*, Physical Review B, 2002. **66**(7): p. 073201(4).

69 Fiederling, R., P. Grabs, W. Ossau, G. Schmidt, and L. W. Molenkamp, *Detection of electrical spin injection by light-emitting diodes in top- and side-emission configurations*, Applied Physics Letters, 2003. **82**(13): p. 2160-2162.

70 Merryfield, R. E., *Theory of Magnetic Field Effects on the Mutual Annihilation of Triplet Excitons*, Journal of Chemical Physics, 1968. **48**(9): p. 4318-4319.

71 Johnson, R. C., R. E. Merrifield, P. Avakian, and R. B. Flippen, *Effects of Magnetic Fields on the Mutual Annihilation of Triplet Excitons in Molecular Crystals*, Physics Review Letters, 1967. **19**(6): p. 285-287.

72 Tolstov, I. V., A. V. Belov, M. G. Kaplunov, I. K. Yakuschenko, N. G. Spitsina, M. M. Triebel, and E. L. Frankevich, *On the role of magnetic field spin effect in photoconductivity of composite films of MEH-PPV and nanosized particles of PbS*, Journal of Luminescence, 2005. **112**(1-4): p. 368-371.

73 Davis A. H. and K. Bussmann, *Large magnetic field effects in organic light emitting diodes based on tris(8-hydroxyquinoline aluminum)(Alq3)/N,N'-di(naphthalene-1-yl)-N,N' diphenyl-benzidine (NPB) bilayers*, Journal of Vacuum Science and Technology A, 2004. **22**(4): p. 1885 -1891.

74 Belaid, R., T. Barhoumi, L. Hachani, L. Hassine, and H. Bouchriha, *Magnetic field effect on recombination light in anthracene crystal*, Synthetic. Metals. **131**(1-3), 23-30 (2002).

75 Kalinowski, J., M,Cocchi, D. Virgili, V. Fattori, and P. Di Marco, *Magnetic field effects on organic electrophosphorescence*, Physical Review B, 2004. **70**(20): p. 205303(7).

76 Wilkinson, J., A. H. Davis, K. Bussmann, and J. P. Long, *Evidence for charge-carrier mediated magnetic-field modulation of electroluminescence in organic light-emitting diodes*, Applied Physics Letters, 2005. **86**(11): p. 111109(3).

77 Salis, G., S. F. Alvarado, M. Tschudy, T. Brunschwiler, and R. Allenspah, *Hysteretic electroluminescence in organic light-emitting diodes for spin injection*, Physical Review B, 2004. **70**(8): p. 085203(6).

78 Kalinowski, J., M. Cocchi, D. Virgili, P. Di Marco, and V. Fattori, *Magnetic field effects on emission and current in Alq3-based electroluminescent diodes*, Chemical Physics Letters, 2003. **380**(5-6): p. 710-715.

79 Mermer, Ö., G. Veeraraghavan, T. L. Francis, and M. Wohlgenannt, *Large magnetoresistance at room-temperature in small-molecular-weight organic semiconductor sandwich devices*, Solid State Communications, 2005. **134**(9): p. 631-636.

80 Francis, T. L., Ö. Mermer, G. Veeraraghavan, and M. Wohlgenannt, *Large magnetoresistance at room temperature in semiconducting polymer sandwich devices*, New Journal of Physics, 2004. **6**: p. 185(8).

81 Gärditz, C., A. G. Mückl, and M. Cölle, *Influence of anexternal magnetic field on the singlet and triplet emissions of tris-(8-hydroxyquinoline) aluminum (III) (Alq3)*, Journal of Applied Physics, 2005. **98**(10): p. 104507.

82 Frankevich, E. L., *On mechanisms of population of spin substates of polaron pairs*, Chemical Physics, 2004. **297**(1-3): P. 315-322.

83 Wohlgenannt M. and Z. V. Vardeny, *Spin-dependent exciton formation rates in π-conjugated materials*, Journal of Physics. Condensed Matter, 2003. **15**(3): p. R83-R107.

84 Baldo, M. A. and S. R. Forrest, *Transient analysis of organic electrophosphorescence: I. Transient analysis of triplet energy transfer*, Physical Review B, 2002. **62**(16), 10958(9).

85 Reufer, M., M. J. Walter, P. G. Lagoudaskis, A. B. Hummel, J. S. Kolb, H. G. Roskos, U. Scherf, and J. M. Lupton, *Spin-conserving carrier recombination in conjugated polymers*, Nature Materials, 2005. **4**(4): p. 340-346.

86 Steiner U. E. and T. Ulrich, *Magnetic field effects in chemical kinetics and related phenomena*, Chemical Reviews, 1989. **89**(1): p. 51-147.

87 Mermer, Ö., G. Veeraraghavan, T. L. Francis, y. Sheng, D. T. Nguyen, M. Wohlgenannt, A. Kohler, M. K. Al-Suti, and M. S. Khan, *Large magnetoresistance in nonmagnetic π-conjugated semiconductor thin film devices*, Physical Review B, 2005. **72**(20): p. 205202(12).

88 Yoshida, Y., A. Fujii, M. Ozaki, K. Yoshino, and E. L. Frankevich, *Magnetic field effect as a test for effectiveness of the light emission at the recombination of injected charge carriers in polymeric semiconductors*, Molecular Crystals Liquid Crystalline, 2005. **426**(1): p. 19-24.

89 Odaka, H., Y. Okimoto, T. Yamada, H. Okamoto, M. Kawasaki, and Y. Tokura, *Control of magnetic-field effect on electroluminescence in Alq(3)-based organic light emitting diodes*. Applied Physics Letters, 2006. **88**(12): p. 123501(3)

90 Kilså, K., J. Kajanus, S. Larsson, A. N. Macpherson, J. Mårtensson, and B. Albinsson, *Enhanced Intersystem Crossing in Donor/Acceptor Systems Based on Zinc/Iron or Free-Base/Iron Porphyrins*, Chemistry, 2001. **7**(10): p. 2122 – 2133.

91 Kalinowski, J., J. Szmytkowski, and W. Stampor, *Magnetic hyperfine modulation of charge photogeneration in solid films of Alq3*, Chemical Physcis Letters, 2003. **378**(3-4): p. 380-387.

92 Dhoot, A. S., D. S. Ginger, D. Beljonne, Z. Shai, N. C. Greenham, *Triplet formation and decay in conjugated polymer devices*, Chemical Physics Letters, 2002. **360**(3-4): p. 195-201.

93 Wittmer M. and I. Zschokke-Gränacher, *Exciton–charge carrier interactions in the electroluminescence of crystalline anthracene*, Journal of Chemical Physics, 1975. **63**(15): p. 4187-4194.

94 Romanova, Z. S., K. Deshayes, P. Piotrowiak, *Remote Intermolecular "Heavy-Atom Effect": Spin-Orbit Coupling Across the Wall of a Hemicarcerand*, Journal of American Chemical Society, 2001. **123**(10): p. 2444-2445.

95 Wilson, J. S., N. Chawdhury, A. Kohler, R. H. Friend, M. R. A. Al-Mandhary, M. S. Khan, M. Younus, P. R. Raithby, *The Energy Gap Law for Triplet States in Pt-Containing Conjugated Polymers and Monomers*, Journal of American Chemical Society, 2001. **123**(38): p. 9412-9417.

96 Xu, Z. H., Y. Wu, B. Hu , *Dissociation processes of singlet and triplet excitons in organic photovoltaic cells*, Applied Physics Letters, 2006. **89**(13): p. 131116(6).

97 Greenwald, Y., X. Xu, M.Fourmigué, G. Srdanov, C. Koss, F. Wudl, and A. J. Heeger, Polymer-polymer rectifying heterojunction based on poly(3,4-dicyanothiophene) and MEH-PPV, Journal of Polymer Science. Part A, Polymer Chemistry, 1998. **36**(17): p. 3115-3120.

98 Hu, B. and F. E. Karasz, *Interfacial effects in polymer LEDs*, Chemical Physics, 1998. **227**(1-2): p. 263-270.

99 Finkenzeller W. J. and H. Yersin, *Emission of Ir(ppy)3. Temperature dependence, decay dynamics, and magnetic field properties*, Chemical Physics Letters, 2003. **377**(3-4): p. 299-305.

100 Birks, J. B., *Organic Molecular Photophysics*, Wiley, London, 1975.

101 Wu, Y., B. Hu, and J. Howe, *Morphology-dependent exciton emission and energy transfer in fluorene-polymer-related fluorescent and phosphorescent composite films spin cast from a mixture of two dissimilar organic solvents*, Journal of Applied Physics, 2005. **98**(10): p. 103510.

102 IUPAC compendium of Chemical Terminology 2nd Edition (1997)

103 Lee, C-L., K. B. Lee, and J-J Kim, *Polymer phosphorescent light-emitting devices doped with tris(2-phenylpyridine) iridium as a triplet emitter*, Applied Physics Letters, 2000. **77**(15): p. 2280-2282.

104 Vaeth, K. M. and C. W. Tang, *Light-emitting diodes based on phosphorescent guest/polymeric host systems*, Journal of Applied Physics, 2002. **92**(7): p. 3447-3453.

105 Zhu, W., W. Mo, M. Yuan, W. Yang, and Y. Cao, *Highly efficient electrophosphorescent devices based on conjugated polymers doped with iridium complexes*, Applied Physics Letters, 2002. **80**(12): p. 2045-2047. (2002).

106 Wu, Y. and B. Hu, *Metal electrode effects on spin-orbital coupling and magnetoresistance in organic semiconductor devices*, Applied Physics Letters, 2006. **89**(20): p. 203510(3).

107 Prigodin, V. N., J. D. Bergeson, D. M. Lincoln, and A. J. Epstein, *Anomalous room temperature magnetoresistance in organic semiconductors*, Synthetic. Metals, 2006. **156**(9-10):p. 757-761.

108 Ito, F., T. Ikoma, K. Akiyama, A. Watanabe, S. Tero-Kubota, *Carrier Generation Process on Photoconductive Polymer Films as Studied by Magnetic Field Effects on the Charge-Transfer Fluorescence and Photocurrent*, Journal of Physical Chemistry B, 2005. **109**(18): p. 8707-8717.

109 Xu, Z., Y. Wu, and B. Hu, *Dissociation processes of singlet and triplet excitons in organic photovoltaic cells*, Applied Physics Letters, 2006. **89**(13): p. 131116(3).

110 Berthelot, L., J. Tardy, M. Garrigues, P. Cremillieu, J. Joseph and B. Masenelli, *ITO/PVK/Alq/metal LEDs: influence of PVK doping with DCM and of passivation with sputtered Si_3N_4*, Optical Materials, 1999. 12(2-3): p. 261-266.

111 Kim, Y., W. B. Im, *Effect of hole-blocking layer doped with electron-transport molecules on the performance of blue organic light-emitting device*, Physica Status Solidi (a), 2004. **201**(9): p. 2148 – 2153.

112 Koch, N., A. Kahn, J. Ghijsen, J.-J. Pireaux, J. Schwartz, R. L. Johnson, and A. Elschner, *Conjugated organic molecules on metal versus polymer electrodes: Demonstration of a key energy level alignment mechanism*, Appl. Phys. Lett. **82**(1): p. 70-72 (2003).

113 Hagen, J. A., W. Li, A. J. Steckl, and J. G. Grote, *Enhanced emission efficiency in organic light-emitting diodes using deoxyribonucleic acid complex as an electron blocking layer*, Applied Physics Letters, 2006. **88**(17): p. 171109 (2006).

114 Kido, J., H. Shionoya, and K. Nagai, *Single-layer white light-emitting organic electroluminescent devices based on dye-dispersed poly(N-vinylcarbazole)*, Applied Physics Letters, 1995. **67**(16): p. 2281-2283.

115 Chen, S. H., H. L. Chou, and A. C. Su, and S. A. Chen, *Molecular Packing in Crystalline Poly(9,9-di-n-octyl-2,7-fluorene)*, Macromolecules, 2004. **37**(18): p. 6833-6838.

116 Chen, S. H., A. C. Su, and S. A. Chen, *Noncrystalline Phases in Poly(9,9-di-n-octyl-2,7-fluorene)*, Journal of Physical Chemistry B, 2005. **109**(20): p. 10067-10072.

117 Misaki, M., Y. Ueda, S. Nagamatsu, Y. Yoshida, N. Tanigaki, and K. Yase, *Formation of Single-Crystal-like Poly(9,9-dioctylfluorene) Thin Film by the Friction-Transfer Technique with Subsequent Thermal Treatments*, Macromolecules, 2004. **37**(18): p. 6926-6931.

118 Arias, A. C., N. Corcoran, M. Banach, R. H. Friend, J. D. MacKenzie, and W. T. S. Huck, *Vertically segregated polymer-blend photovoltaic thin-film structures through surface-mediated solution processing*, Applied Physics Letters, 2002. **80**(10): p. 1695-1697.

119 Grell, M. and D. D. C. Bradley, *Polarized Luminescence from Oriented Molecular Materials*, Advanced Materials (Weinheim, Germany), 1999. **11**(11): p. 895-905.

120 Grell, M., D. D. C. Bradley, X. Long, T. Chamberlain, M. Inbasekaran, E. P. Woo, and M. Soliman, *Chain geometry, solution aggregation and enhanced dichroism in*

the liquidcrystalline conjugated polymer poly(9,9-dioctylfluorene), Acta Polymerica, 1998. **49**(8): p. 439-444.

121 Ariu, M., D. G. Lidzey, M. Lavrentiev, D. D. C. Bradley, M. Jandke, and P. Strohriegl, *A study of the different structural phases of the polymer poly(9,9'-dioctyl fluorene) using Raman spectroscopy*, Synthetic Metals, 2001. **116**(1-3): p. 217-221.

122 Khan, A. L. T., P. Sreearunothai, L. M. Herz, M. J. Banach, and A. Köhler, *Morphology-dependent energy transfer within polyfluorene thin films*, Physical Review B, 2004. **69**(8): p. 085201(8).

123 Grell, M., D. D. C. Bradley, G. Ungar, G. Hill, and K. S. Whitehead, *Interplay of Physical Structure and Photophysics for a Liquid Crystalline Polyfluorene*, Macromolecules, 1999. **32**(18): p. 5810-5817.

124 Schartel, B., V. Wachtendorf, M. Grell, D. D. C. Bradley, and M. Hennecke, *Polarized fluorescence and orientational order parameters of a liquid-crystalline conjugated polymer*, Physical Review B, 1999. **60**(1): 277-283.

125 Lin, W.-J., W.-C. Chen, W.-C. Wu, Y.-H. Niu, and A. K.-Y. Jen, *Synthesis and Optoelectronic Properties of Starlike Polyfluorenes with a Silsesquioxane Core*, Macromolecules, 2004. **37**(7): p. 2335-2341.

126 Hu, B. and F. E. Karasz, *Comparison of electroluminescent quantum efficiencies of PPV and a PPV-related alternating block copolymer*, Synthetic Metals, 1998. **92**(2): p. 157-160.

127 Ariu, M., M. Sims, M. D. Rahn, J. Hill, A. M. Fox, D. G. Lidzey, M. Oda, J. C. Gonzalez, and D. D. C. Bradley, *Exciton migration in β-phase poly(9,9-dioctylfluorene)*, Physical Review B, 2003. **67**(19): p. 195333(11).

128 Cadby, A. J., P. A. Lane, H. Mellor, S. J. Martin, M. Grell, C. Giebeler, D. D. C. Bradley, M. Wohlgenannt, C. An, and Z. V. Vardeny, *Film morphology and photophysics of polyfluorene*, Physical Review B, 2000. **62**(23): p. 15604 (6).

129 Ariu, M., D. G. Lidzey, M. Sims, A. J. Cadby, P. A. Lane, D. D. C. Bradley, *The effect of morphology on the temperature-dependent photoluminescence quantum efficiency of the conjugated polymer poly(9, 9-dioctylfluorene)*, Journal of Physics. Condensed Matter, 2002. **14**(28): p. 9975-9986.

VITA

Yue Wu was born in Yangzhou, Jiangsu Province, People's Republic of China (P.R. China) on July 26, 1975. He went to Nanjing University of Science and Technology, Jiangsu, China, in September 1993 and got his Bachelor's Degree from the Department of Polymer Science and Engineering of this university in July 1997. He was the recipient of outstanding graduates of that year.

After graduation with his Bachelor's degree in polymer engineering, Yue Wu continued his graduate study in East China University of Science and Technology, Shanghai, China. He obtained his Master's Degree in the Department of Materials Science and Engineering in 2000. His research focused on the surface modification of Ultra-High Molecular Weight Polyethylene (UHMWPE) fibers.

From September 2000 to December 2002, he worked as an engineer in Key Laboratory for Ultra-fine Materials of the Ministry of Education, Shanghai, China. The main work was to fabricate polymer/nano-particle composites

On January 2003, Yue Wu went to USA and has been studying light-emitting polymers in the Department of Materials Science and Engineering, College of Engineering, the University of Tennessee, Knoxville, for his Ph. D degree since then.